Uniwersytet Śląski
Wydział Matematyki, Fizyki i Chemii,
Instytut Fizyki im. Augusta Chełkowskiego
Zakład Biofizyki i Fizyki Molekularnej

Rozprawa doktorska

Badanie kinetyki rekrystalizacji oraz dynamiki molekularnej w kontekście stabilności fizycznej amorficznych związków farmaceutycznie czynnych

w formie spójnego tematycznie cyklu artykułów opublikowanych
w czasopismach naukowych

Autor:

mgr Karolina Kołodziejczyk-Jaszczak

Promotor:

prof. zw. dr hab. Marian Paluch

Promotor pomocniczy:

dr Katarzyna Grzybowska

Katowice 2016

PODZIĘKOWANIA

Składam serdecznie podziękowania
Panu prof. zw. dr. hab. Marianowi Paluchowi
za cenne wskazówki, wszechstronną
pomoc i poświęcony czas.

Składam również podziękowania
Pani dr Katarzynie Grzybowskiej
za opiekę i wiedzę, którą mi przekazała.

Dziękuję również wszystkim Kolegom i Koleżankom
z Zakładu Biofizyki i Fizyki Molekularnej za pomoc
oraz stworzenie przyjaznej i twórczej atmosfery.

Do powstania niniejszej rozprawy doktorskiej w znaczącym stopniu przyczyniło się stypendium, otrzymane przeze mnie w ramach programu „DoktoRIS - Program stypendialny na rzecz innowacyjnego Śląska" współfinansowanego przez Unię Europejską w ramach Europejskiego Funduszu Społecznego.

KAPITAŁ LUDZKI
NARODOWA STRATEGIA SPÓJNOŚCI

Śląskie.
Pozytywna energia

UNIWERSYTET ŚLĄSKI
W KATOWICACH

UNIA EUROPEJSKA
EUROPEJSKI
FUNDUSZ SPOŁECZNY

Projekt współfinansowany przez Unię Europejską w ramach Europejskiego Funduszu Społecznego

SPIS TREŚCI

LISTA PUBLIKACJI STANOWIĄCYCH PODSTAWĘ ROZPRAWY DOKTORSKIEJ

Wykaz publikacji włączonych do rozprawy doktorskiej:

1) K. Kolodziejczyk, M. Paluch, K. Grzybowska, A. Grzybowski, Z. Wojnarowska, L. Hawelek, J. D. Ziolo; *Relaxation Dynamics and Crystallization Study of Sildenafil in the Liquid and Glassy States*, Mol. Pharmaceutics, 2013, 10 (6), pp 2270–2282 (IF=4.384, punkty MNiSW=40)
2) K. Kolodziejczyk, K. Grzybowska, Z. Wojnarowska, M. Dulski, L. Hawelek, M. Paluch; *Isothermal Cold Crystallization Kinetics Study of Sildenafil*, Crystal Growth & Design, 2014, 14 (7), pp 3199-3209 (IF= 4.891, punkty MNiSW=40)
3) K. Kołodziejczyk, M. Tarnacka, E. Kamińska, M. Dulski, K. Kamiński, M. Paluch, *The Crystallization's Kinetic Under Confinement. Manipulation of the Crystalline Form of Salol by Varying Pore Diameter*; Crystal Growth & Design, Publication Date (Web): January 13, 2016 (IF=4.891, punkty MNiSW=40)

Wykaz publikacji związanych z tematem, lecz nie włączonych do rozprawy doktorskiej:

4) K. Grzybowska, M. Paluch, A. Grzybowski, Z. Wojnarowska, L. Hawelek, K. Kolodziejczyk, K. L. Ngai; *Molecular Dynamics and Physical Stability of Amorphous Anti-Inflammatory Drug: Celecoxib;* J. Phys. Chem. B 2010, 114 (40), pp 12792–12801 (IF=3.302, punkty MNiSW=30)
5) Z. Wojnarowska, C. M. Roland, K. Kolodziejczyk, A. Swiety-Pospiech, K. Grzybowska, M. Paluch; *Quantifying the Structural Dynamics of Pharmaceuticals in the Glassy State,* J. Phys. Chem. Lett., 2012, 3 (10), pp 1238–1241 (IF=7.458, punkty MNiSW=45)
6) A. Grzybowski, K. Kolodziejczyk, K. Koperwas, K. Grzybowska, M. Paluch, *Effects of lowering temperature and raising pressure on the spatially heterogeneous dynamics of glass-forming van der Waals liquids,* Physical Review B, 2012, 85, 220201 (IF=3.736, punkty MNiSW=35)
7) Z. Wojnarowska, K. Kołodziejczyk, K. J. Paluch, L. Tajber, K. Grzybowska, K. L. Ngai, M. Paluch; *Decoupling of conductivity relaxation from structural relaxation in protic ionic*

liquids and general properties, Phys. Chem. Chem. Phys., 2013, 15, pp 9205-9211 (IF=4.493, punkty MNiSW=35)

8) E. Kaminska, K. Adrjanowicz, K. Kaminski, P. Wlodarczyk, L. Hawelek, K. Kolodziejczyk, M. Tarnacka, D. Zakowiecki, I. Kaczmarczyk-Sedlak, J. Pilch, M. Paluch; *A New Way of Stabilization of Furosemide upon Cryogenic Grinding by Using Acylated Saccharides Matrices. The Role of Hydrogen Bonds in Decomposition Mechanism*, Mol. Pharmaceutics, 2013, *10* (5), pp 1824–1835 (IF=4.384, punkty MNiSW=40)
9) M. Tarnacka, K. Adrjanowicz, E. Kamińska, K. Kamiski, K, Grzybowska, K. Kołodziejczyk, P. Włodarczyk, Ł. Hawełek, A. Kocot, M. Paluch; *Molecular dynamics of itraconazole at ambient and high pressure,* Phys. Chem. Chem. Phys**.** 2013, 15, pp 20742-20752 (IF=4.493, punkty MNiSW=35)
10) A. Grzybowski, K. Koperwas, K. Kolodziejczyk, K. Grzybowska, M. Paluch*, Spatially Heterogeneous Dynamics in the Density Scaling Regime: Time and Length Scales of Molecular Dynamics near the Glass Transition;* J. Phys. Chem. Lett., 2013, 4 (24), pp 4273–4278 (IF=7.458, punkty MNiSW=45)
11) E. Kaminska, K Adrjanowicz, M. Tarnacka, K. Kolodziejczyk, M. Dulski, E. U. Mapesa, D. Zakowiecki, L Hawelek, I. Kaczmarczyk-Sedlak, K. Kaminsk*; Impact of Inter- and Intramolecular Interactions on the Physical Stability of Indomethacin Dispersed in Acetylated Saccharides;* Mol. Pharmaceutics 2014 4, 11 (8), pp 2935-47 (IF=4.384, punkty MNiSW=40)
12) K. Adrjanowicz, M. Paluch, K. Kaminski, S. Jurga, M. Jarek, M. Dulski, L. Hawelek, K. Kołodziejczyk, G. Bartkowiak, M. Jasiurkowska-Delaporte*; The Dynamic Glass Transition and Electrical Conductivity Behavior Dominated by Proton Hopping Mechanism Studied in the Family of Hyperbranched bis-MPA Polyesters;* Macromol. 2014, 47, 16, pp 5798-5807 (IF=5.8, punkty MNiSW=45)
13) E. Kaminska, M. Tarnacka, K. Kolodziejczyk, M. Dulski, D. Zakowiecki, L. Hawelek, K. Adrjanowicz, M. Zych, G. Garbacz; K. Kaminski, *Impact of low molecular weight excipient octaacetylmaltose on the liquid crystalline ordering and molecular dynamics in the supercooled liquid and glassy state of itraconazole;* Eur. J. Pharm. and Biopharm., 2014, 88, 3, pp 1094–1104 (IF=3.383, punkty MNiSW=35)
14) K. Adrjanowicz, K. Kolodziejczyk, W. K. Kipnusu; M. Tarnacka; E. U. Mapesal E. Kaminska, S. Pawlus, K. Kaminski, M. Paluch; *Decoupling between the Interfacial and Core Molecular Dynamics of Salol in 2D Confinement;* J. Phys. Chem. C*,* 2015, 119 (25), pp 14366–14374 (IF=4.772, punkty MNiSW=35)

15) E. Kaminska, M. Tarnacka, P. Wlodarczyk, K. Jurkiewicz, K. Kolodziejczyk, M. Dulski, D. Haznar-Garbacz, L. Hawelek, K. Kaminski, A. Wlodarczyk M. Paluch , *Studying the Impact of Modified Saccharides on the Molecular Dynamics and Crystallization Tendencies of Model API Nifedipine;* Mol. Pharmaceutics, 2015, 12(8), pp 3007-3019 (IF=4.384, punkty MNiSW=40)

Rozdział I

1 OGÓLNY CEL PRACY

Wśród dostępnych na rynku leków możemy wyróżnić farmaceutyki występujące w różnych formach – stałej (tabletki, proszki), płynnej (roztwory, syropy) i gazowej (aerozole). Statystyki pokazują, że ponad 80 % leków przyjmowanych doustnie występuje w formie stałej, z czego prawie połowa z nich okazuje się być słabo rozruszana w wodzie [1]. Stała postać leku zawiera w sobie substancję aktywną farmaceutycznie (ang. *active pharmaceutical ingredient,* API), która zazwyczaj występuje w formie krystalicznej oraz substancje pomocnicze. Krystaliczna forma API jest bardzo „wygodna", ponieważ jest ona stabilna termodynamicznie, a jej właściwości fizykochemiczne nie ulegają zmianie podczas produkcji oraz z czasem przechowywania. Jednakże badania pokazują, że w większości przypadków to właśnie krystaliczna forma API jest uważana za główną przyczynę słabej rozpuszczalności, a co za tym idzie - za słabe przyswajanie leków przez ludzki organizm (słabą biodostępność).

Jednym z najbardziej obiecujących sposobów poprawy rozpuszczalności leków jest przygotowanie substancji aktywnych farmaceutycznie (API) w formie amorficznej. Jak pokazują liczne prace badawcze, rozpuszczalność oraz szybkość rozpuszczania amorficznej formy API jest w wielu przypadkach nawet wielokrotnie - większa w porównaniu do odpowiadającej formy krystalicznej [2,3,4]. Warto także wspomnieć, że amorficzna forma API może ułatwić proces formulacji tabletek [5].

Niestety amorfizacja substancji farmaceutycznie czynnych ma też swoje słabe strony. Jest to spowodowane tym, iż faza amorficzna jest stanem termodynamicznie niestabilnym i w trakcie przechowywania czy produkcji może powrócić do swojej macierzystej formy [6,7].

Chcąc wprowadzić na rynek substancje lecznicze z amorficznymi substancjami czynnymi farmaceutycznie, przemysł farmaceutyczny od kilkunastu lat intensywnie bada przyczyny rekrystalizacji oraz poszukuje skutecznych sposobów na zahamowanie procesu rekrystalizacji materiałów amorficznych. Okazuje się, że prawdopodobnie kluczem

do zrozumienia niestabilności fizycznej stanu amorficznego jest poznanie ruchliwości molekuł zarówno powyżej jak i poniżej T_g.

Dlatego też głównym celem przeprowadzonych badań, których wyniki zostały opisane w publikacjach 1 – 3 było sformułowanie relacji pomiędzy kinetyką krystalizacji oraz dynamiką molekularną a stabilnością substancji amorficznej. Dodatkowo podjęto również próby stabilizacji amorficznych układów za pomocą sacharydów oraz porowatych matryc wykonanych z tlenku glinu (membrany AAO).

Przedmiotem badań były aktywne substancje farmaceutyczne, tj. sildenafil oraz salol. Sildenafil jest substancją stosowaną w leczeniu zaburzeń erekcji oraz pierwotnego nadciśnienia płucnego, a z kolei salol (salicylan fenylu) jest popularnym związkiem chemicznym używanym w lekach stosowanych do odkażania przewodu pokarmowego i dróg moczowych.

Do otrzymania amorficznej postaci wymienionych powyżej substancji aktywnych farmaceutycznie zastosowano witryfikację.

Badania wykonane zostały przy użyciu wielu metod eksperymentalnych, tj. szerokopasmowej spektroskopii dielektrycznej (BDS), różnicowej kalorymetrii skaningowej (DSC), spektroskopii w podczerwieni (FTIR), rentgenografii strukturalnej (XRD) oraz mikroskopii optycznej (OM).

Rozdział II

2 KRÓTKI KOMENTARZ DO UZYSKANYCH WYNIKÓW

2.1 REKRYSTALIZACJA AMORFICZNYCH SUBSTANCJI FARMACEUTYCZNYCH

W celu znalezienia sposobu uniknięcia rekrystalizacji leków amorficznych konieczna jest znajomość czynników wpływających na nukleację i wzrost kryształu. Badania tego procesu mogą być prowadzone zarówno w warunkach izotermicznych jak i nieizotermicznych. Prowadzenie badań w różnych warunkach termodynamicznych jest niezwykle istotne, ponieważ warunki produkcji i przechowywania gotowych już substancji amorficznych mają znaczący wpływ na ich właściwości i trwałość. Istnieje wiele metod eksperymentalnych, które monitorują proces rekrystalizacji amorficznych farmaceutyków. Są to przede wszystkim techniki rentgenowskie, kalorymetryczne, mikroskopowe, a także spektroskopowe – spektroskopia w podczernieni oraz dielektryczna. Wyniki otrzymane z każdej metody badawczej pozwalają na znalezienie parametrów charakteryzujących proces krystalizacji.

Analiza kinetyki krystalizacji sildenafilu stanowi podstawę artykułów 1 i 2. W pracach przeanalizowałam dane eksperymentalne uzyskane z pomiarów prowadzonych w warunkach izotermicznych (BDS, DSC, XRD, OM) oraz nieizotermicznych (DSC). Badania krystalizacji sildenafilu były prowadzone zarówno w cieczy przechłodzonej jak i w stanie szklistym (T_g=330 K). W celu analizy danych kinetyki krystalizacji, posłużyłam się opisanymi w literaturze dwoma modelami (i) modelem Avramiego [8,9] i Avramiego-Avramova [10] dla pomiarów izotermicznych oraz (ii) modelem Ozawy [11] przeznaczonym do opisu danych eksperymentalnych uzyskiwanych z pomiarów prowadzonych w warunkach nieizotermicznych. Dodatkowo, aby oszacować energię aktywacji procesu krystalizacji z pomiarów nieizotermicznych, zastosowałam równania Kissingera [12] oraz Augisa i Bennetta [13]. W rezultacie otrzymałam bardzo podobne wyniki mechanizmu kinetyki krystalizacji dla

każdego z warunków pomiarowych. Jak pokazują rezultaty analiz, sildenafil na początku procesu krystalizacji tworzy trójwymiarowe krystality z natychmiastowym i sporadycznym zarodkowaniem (wykładnik Avramiego, *n*=2.6-3.6), a wartość stałej szybkości krystalizacji *k* rośnie wraz ze wzrostem temperatury, co sugeruje, że proces rekrystalizacji jest zdominowany przez dyfuzję cząsteczek, a nie przez zarodkowanie krystalitów. Ponadto oszacowałam wartość bariery aktywacji niezbędnej do zapoczątkowania procesu rekrystalizacji. Warto tutaj podkreślić, że wartość energii aktywacji jest różna w zależności od warunków eksperymentu (warunki izotermiczne i nieizotermiczne), co prawdopodobnie spowodowane jest specyfiką prowadzonych pomiarów.

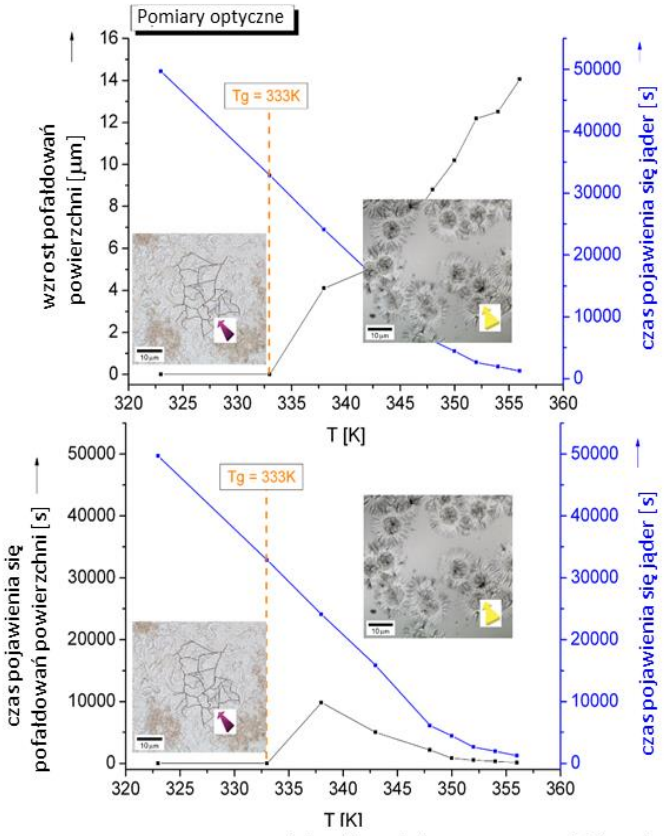

Rys. 1 Temperaturowa zależność wzrostu pofałdowań powierzchni sildenafilu i pojawienia się jąder kryształów

Dodatkowo wykonałam obserwacje mikroskopowe, dzięki którym możliwe było prześledzenie całego procesu rekrystalizacji oraz zaobserwowanie zewnętrznego kształtu (morfologii) kryształu sildenafilu. Badania te ujawniły zaskakującą i dość skomplikowaną naturę procesu rekrystalizacji tej substancji. Okazuje się, że pojawienie się zarodka krystalizacji oraz jego wzrost poprzedzają tworzące się na powierzchni cieczy przechłodzonej deformacje, których kształt zależy od temperatury prowadzenia eksperymentu. Deformacje te są dwojakiego rodzaju - pierwsze obserwowane w *T*<333 K, mają charakter niewielkich „zmarszczek" układających się w pewne obszary, nazwane przeze mnie domenami. Z kolei drugi rodzaj deformacji zauważalny jest w temperaturach wyższych niż 333 K i cechuje się wzrastającym pofałdowaniem powierzchni cieczy, wewnątrz którego pojawiają się zarodki kryształów (Rys. 1). Szybkość pojawienia się pofałdowań, wzrostu oraz częstotliwość ich występowania zależy od temperatury prowadzenia obserwacji. Warto także podkreślić, iż początkowe zniekształcenia powierzchni mają charakter amorficzny, a temperatura pojawienia

się deformacji drugiego rodzaju dość dobrze koresponduje z wartością temperatury zeszklenia sildenafilu, T_g=330 K.

W celu wyjaśnienia nietypowego zachowania poprzedzającego krystalizację, wykonałam dodatkowe badania przy użyciu spektroskopii w podczerwieni oraz posłużyłam się obliczeniami teoretycznymi. Przewidywania teoretyczne wskazały możliwość tworzenia międzycząsteczkowych wiązań wodorowych pomiędzy grupą amidową jednej molekuły, a grupą aminową drugiej cząsteczki sildenafilu. Z obliczeń tych wynika, że długość tego wiązania w cieczy przechłodzonej ulega skróceniu w porównaniu do występującego w krysztale sildenafilu. Potwierdzenie kalkulacji widoczne jest w widmach podczerwonych jako spadek intensywności dwóch pasm pochodzących od grup aminowej i amidowej, a także jako przesunięcie tych pasm w kierunku wyższej liczby falowej. Dlatego też zasugerowałam, że obserwowane pofałdowania powierzchni cieczy przechłodzonej mogą mieć związek z reorganizacją cząsteczek i formowaniem wiązań wodorowych w badanym układzie.

Ponadto obserwacje mikroskopowe pokazały, że czas potrzebny na uformowanie się zarodka krystalizacji jest w przybliżeniu podobny do czasu indukcji t_0, szacowanego na podstawie modelu Avramiego-Avramova, a uformowane kryształy sildenafilu mają pokrój igiełkowy.

Podobną analizę procesu rekrystalizacji przeprowadzałam również w artykule 3. W pracy tej głównym tematem było porównanie kinetyki krystalizacji salolu „w masie" (ang. *bulk)* oraz „układach zamkniętych" (ang. *confinement).* „Układy zamknięte" tworzył salol umieszczony w membranach wykonanych z tlenku glinu (AAO), których średnica *d* wynosiła: 150, 100, 73 oraz 13 nm. Analizę porównawczą kinetyki krystalizacji przeprowadziłam na danych eksperymentalnych uzyskanych z pomiarów izotermicznych (BDS i DSC). W celu oszacowania parametrów krystalizacji zastosowałam wspomniane już wcześniej dwa modele - model Avramiego i Avramiego-Avramova. Z przeprowadzonej przeze mnie analizy wynika, że wymiarowość powstających kryształów próbki makroskopowej („w masie") jest w przybliżeniu równa 3, podczas gdy dla salolu umieszczonego w membranach n~2. Wynik ten jest zgodny z oczekiwaniami, ponieważ ograniczenie przestrzeni przez ścianki porów uniemożliwia wzrost kryształu salolu w trzech wymiarach. Z drugiej strony, analiza stałej szybkości procesu krystalizacji dostarczyła wyników, które początkowo wydawały się niezgodne z intuicją. Okazuje się bowiem, że krystalizacja układu salol-membrana AAO, w którym średnica porów wynosi 150 nm zachodzi znacznie szybciej niż w próbce makroskopowej w tych samych warunkach (T_c=245 K), a następnie przy d=100 nm zwalnia,

aż wreszcie zostaje całkowicie zahamowana, gdy średnica porów wynosi *d*=73 i 13nm. Przyspieszenie procesu krystalizacji w membranie o największej średnicy (*d*=150 nm) jest najprawdopodobniej związane z odmiennym rodzajem mechanizmu krystalizacji.

2.2 DYNAMIKA MOLEKULARNA A REKRYSTALIZACJA

Powszechnie uważa się, że kluczowym czynnikiem, który kontroluje proces rekrystalizacji ze stanu amorficznego jest ruchliwość molekularna. Monitorowanie dynamiki molekularnej w szerokim zakresie temperatur i częstotliwości możliwe jest za pomocą spektroskopii dielektrycznej. Metoda ta pozwala na scharakteryzowanie procesów relaksacyjnych obserwowanych w stanie szklistym oraz w cieczy przechłodzonej. W fazie cieczy przechłodzonej relaksacja α (strukturalna) jest procesem dominującym, który związany jest z kooperatywnym ruchem cząsteczek. Proces ten jest odpowiedzialny za zjawisko powstawania fazy amorficznej substancji. Podczas przejścia ciesz-szkło czasy relaksacji strukturalnej stają się zbyt długie, by można je było wyznaczyć eksperymentalnie. Wówczas w widmie dielektrycznym zaczynają dominować znacznie szybsze procesy drugorzędowe (oznaczane odpowiednio β, γ, δ itd.), które odzwierciedlają szybkie, lokalne ruchy wewnątrzcząsteczkowe lub małokątowe rotacje całych molekuł. W literaturze zostało pokazane, że zarówno strukturalna relaksacja i lokalna ruchliwość molekuł może mieć wpływ na zapoczątkowanie rekrystalizacji [14,15].

W artykule 1 skupiłam się na znalezieniu możliwych korelacji pomiędzy dynamiką molekularną a tendencją do rekrystalizacji. W tym celu zostały przeprowadzone badania dynamiki molekularnej sildenafilu w szerokim zakresie temperatur. Z analizy widm deliktycznych wynika, że w cieczy przechłodzonej dominujący jest pierwszorzędowy proces relaksacyjny, natomiast w szkle obserwowana jest jedynie drugorzędowa relaksacja β. Jednym z ważniejszych parametrów opisujących relaksację strukturalną jest parametr kruchości (m_p). Wielkość ta jest bardzo często używana do przewidywania tendencji do krystalizacji. Wykazano, że ciecze kruche (gdzie $m_p \geq 100$), w przypadku których dynamika molekularna zmienia się gwałtownie wraz ze zmianą temperatury w pobliżu przejścia szklistego, często charakteryzują się także silną tendencją do krystalizacji. Na podstawie danych otrzymanych z pomiarów dielektrycznych oszacowałam, że m_p dla sildenafilu wynosi 85 (w τ_α = 100 s,

T_g=328 K), co klasyfikuje go jako ciecz średniokruchą i potwierdza jego dość dużą tendencję do rekrystalizacji w fazie cieczy przechłodzonej.

Dodatkowo, szczegółowa analiza czasów relaksacji strukturalnej sildenafilu pozwoliła mi na sprawdzenie związku między czasami relaksacji α-procesu (τ_α) a czasem krystalizacji τ_{cr} oszacowanym z modelu Avramiego-Avramova. Obliczenie stosunku energii aktywacji τ_α i τ_{cr} pozwoliło wyznaczyć tzw. współczynnik sprzężenia *S* (ang. *coupling coefficient*). Współczynnik ten definiuje nachylenie prostej na wykresie zależności log τ_{cr} (log τ_α), a jego wartość określa wpływ dyfuzji rotacyjnej na kinetykę krystalizacji (*S*=1). W przypadku sildenafilu oszacowana wartość *S*=0.49 wskazuje na to, iż krystalizacja nie jest kontrolowana wyłącznie przez dyfuzję rotacyjną. Ponadto relacja pomiędzy mechanizmem krystalizacji, zjawiskiem dyfuzji a czasami relaksacji strukturalnej może być bardziej skomplikowana niż podają to równania Debey'a-Stokesa i Stokesa-Einsteina.

Teoretyczne obliczenia i symulacje dynamiki molekularnej pokazują także, że możliwy jest związek między dynamiczną heterogenicznością a pojawieniem się zarodków krystalizacji [16, 17]. Miarą dynamicznej heterogeniczności układów ciecz-szkło jest czteropunktowa czasowo-przestrzenna funkcja korelacji (dynamiczna podatność $\chi_4(t)$). Niestety bezpośredni pomiar $\chi_4(t)$ jest praktycznie niemożliwy za pomocą tradycyjnych metod eksperymentalnych. Dlatego też oszacowałam wartość $\chi_4^{\max}$ utożsamianą z rozmiarem regionów wewnątrz, których ruchy molekuł są zależne od siebie i przyrównałam ją do średniej liczby dynamicznie skorelowanych cząsteczek N_c. W tym celu skorzystałam z zaproponowanego przez L. Berthiera i jego współpracowników [18, 19] przybliżenia: $N_c = \chi_4^{\max} \approx \frac{k_B}{\Delta C_p}\left(\frac{\beta_{KWW}}{e}\right)^2\left(\frac{\partial \ln \tau}{\partial \ln T}\right)^2$.

W rozważaniach tych skupiłam się na wykazaniu zależności pomiędzy czasem indukcji t_0, czasem krystalizacji τ_{cr} a liczbą dynamicznie skorelowanych molekuł. Na podstawie danych eksperymentalnych dowiodłam, że występuje silna liniowa korelacja zarówno pomiędzy N_c a t_0 jak i N_c a τ_{cr}. Wynik ten sugeruje, że wzrost dynamicznej heterogeniczności powoduje spowolnienie dyfuzji, a co za tym idzie - proces krystalizacji staje się wolniejszy.

Rozważając rekrystalizację w stanie szklistym należy także rozpatrzeć znaczenie procesów drugorzędowych. Jak już wspomniałam, sildenafil w stanie szklistym wykazuje tylko jeden dobrze widoczny proces β, co sugerowałoby stosunkowo wysoką stabilność fizyczną. Warto również wspomnieć, że drugorzędowe relaksacje odzwierciedlające ruchy całych cząsteczek – zwane relaksacjami Johari'ego-Goldsteina (JG) – są uważane jako prekursor kooperatywnej ruchliwości cząsteczek czyli α-relaksacji. Dlatego też w celu określenia natury

procesu drugorzędowego posłużyłam się rozszerzonym modelem sprzężeniowym (ang. *extended coupling model (CM)*) [20,21]. Model ten klasyfikuje proces drugorzędowy jako JG, gdy czas relaksacji τ_{JG} odpowiada tzw. czasowi prymitywnej relaksacji τ_p wyznaczonemu z równania $\tau_p = t_c^{1-\beta_{KWW}} \tau_\alpha^{\beta_{KWW}}$. Oszacowane przeze mnie czasy relaksacji prymitywnej znacznie odbiegają od czasów β-relaksacji sildenafilu. Oznacza to, że proces β obserwowany w sildenafilu nie jest klasyfikowany jako proces JG i nie wykazuje międzycząsteczkowego charakteru. Wynik ten wyklucza relaksację drugorzędową jako przyczynę rekrystalizacji.

2.3 STABILNOŚĆ FIZYCZNA – PRZEWIDYWANIA TEORETYCZNE ORAZ DANE EKSPERYMENTALNE

Wprowadzenie nowego produktu farmaceutycznego na rynek jest wyjątkowo długim i kosztownym procesem. Etap badawczo-rozwojowy nowego leku obejmuje wiele badań. Jednym z nich są właśnie badania stabilności, będące podstawą określenia okresu ważności leku, warunków przechowywania, a także uwalniania. Badania te są konieczne, by w całym swoim okresie trwałości lek pozostawał skuteczny i bezpieczny dla pacjentów. Analizy stabilności leku opierają się w pierwszym etapie na sprawdzeniu i poznaniu trwałości substancji aktywnej (API) w fazie stałej i/lub w roztworach, a w następnej kolejności na poznaniu trwałości gotowej postaci tego leku [22]. W celu określenia trwałości fizycznej powszechnie stosuje się wiele metod badawczych – techniki optyczne, spektroskopia w podczerwieni oraz metody termiczne. Jednakże w przypadku badania stabilności substancji amorficznych jedną z najszybszych i najprostszych w zastosowaniu technik jest dyfrakcja rentgenowska.

Stąd też w pracy 1 w celu oszacowania stabilności fizycznej sildenafilu w fazie szklistej posłużyłam się zarówno teoretycznymi obliczeniami jaki i badaniami eksperymentalnymi tj. analizą strukturalną (XRD). Chcąc odzwierciedlić warunki przechowywania leku, badania eksperymentalne oraz teoretyczne obliczenia stabilności fizycznej sildenafilu wykonywane były w temperaturze pokojowej. Uzyskane wyniki pokazują, że sildenafil w fazie szklistej charakteryzuje się stosunkowo dużą stabilnością fizyczną, czego dowodzą badania rentgenowskie. Eksperymentalnie stwierdzono, że „czas życia" formy amorficznej wynosi 6 miesięcy (w temperaturze pokojowej $T=T_g$-30 K), a po upływie tego czasu następuje rekrystalizacja sildenafilu.

Wykonane przeze mnie teoretyczne przewidywania stabilności sildenafilu w fazie szklistej oparte zostały na analizie dynamiki molekularnej. Jak wiadomo, ruchliwość molekuł w szkle w znacznym stopniu zmniejsza się, a czasy relaksacji strukturalnej (opisujące kooperatywne ruchy cząsteczek) stają się zbyt długie, by mogły być monitorowane eksperymentalnie. Dlatego też możliwe jest jedynie oszacowanie czasów α-relaksacji poniżej temperatury zeszklenia. Aby tego dokonać posłużyłam się tzw. rozszerzonym modelem Adama – Gibbsa [23,24,25], który łączy w sobie parametry funkcji VFT i termodynamiczny parametr γ_{Cp}. Na podstawie wykreślonej zależności log τ_α (1000/T) oszacowałam, iż w warunkach przechowywania tj. w temperaturze pokojowej, czas τ_α~10^9 s, co w przybliżeniu wynosi około 32 lata. Wynik ten sugeruje, że ruchy molekuł są na tyle powolne, że sildenafil w stanie szkła nie powinien ulegać rekrystalizacji w tym okresie. Rezultat ten nie jest co prawda zgodny z wynikiem eksperymentalnym otrzymanym z pomiarów XRD (gdzie stabilność sildenafilu wynosi 6 miesięcy), ale jest spodziewany ze względu na zaobserwowaną dość znaczną różnicę w wartościach energii aktywacji dla relaksacji strukturalnej i procesu krystalizacji.

2.4 METODY STABILIZACJI ORAZ KONTROLOWANIA REKRYSTALIZACJI

Jednym z możliwych sposobów stabilizacji form amorficznych jest odpowiednie zmniejszenie ruchliwości molekularnej danej substancji. Powszechnie uważa się, że przechowywanie substancji amorficznych 50 °C poniżej temperatury zeszklenia jest wystarczające by nie została zapoczątkowana rekrystalizacja [26]. Strategia ta ma bardzo ograniczone zastosowanie, ponieważ określa jedynie warunki przechowywania. Niestety w wielu przypadkach nawet znaczne obniżenie temperatury przechowywania nie jest wystarczające by zapobiec rekrystalizacji [27].

Spowolnienie ruchliwości molekuł można również osiągnąć przez dodanie do amorficznej formy API odpowiednich substancji pomocniczych - stabilizujących, którymi są nieaktywne składniki organiczne takie jak sacharydy (inulina, glukoza, maltoza, pochodne celulozy, itp.) czy polimery (poliwinylipirolidon (PVP), glikol polietylenowy (PEG), polimetylomatakarylan (PMMA)). Substancje stabilizujące znacząco wpływają na temperaturę zeszklenia układu (zazwyczaj podnoszą T_g), a także mogą utworzyć specyficzny rodzaj oddziaływań z amorficzną API, co w rezultacie uniemożliwia rekrystalizację. W literaturze opisano wiele wyników prac badawczych, które pokazują, iż czasami niewielki dodatek

polimeru lub sacharydu może spowodować znaczne opóźnienie lub nawet całkowite zahamowanie procesu rekrystalizacji [28]. Warto tutaj wspomnieć, że w publikacjach 8, 11, 13 i 15, których jestem współautorką, tematyka ta została dokładniej przedyskutowana.

W ostatnich latach obserwuje się również, że używane powszechnie w biomedycynie, elektronice, technologii chemicznej materiały nanoporowate mogą pełnić rolę matryc stabilizujących amorficzne substancje. W początkach lat 90 ubiegłego wieku, Park i McKenna [29] na przykładzie orto-terfenylu (OTP) i polistyrenu (PS) umieszczonych w szklanych porach (ang. *controlled pore glasses*, CPG's) pokazali, że możliwe jest spowolnienie, a nawet zahamowanie krystalizacji, przy czym efekt ten zależny jest od średnicy porów. Dodatkowo zauważono również, iż modyfikacji ulegają wielkości dynamiczne (czasy relaksacji) i termodynamiczne (T_g, T_m, ΔH_m, C_p) badanych substancji zamkniętych w matrycach porowatych, a zmiany te są ściśle związane z rozmiarem (d) porów.

Analiza wpływu wielkości porów na proces rekrystalizacji oraz zmiany T_m, ΔH_m stanowi tematykę publikacji 3. Jak już wcześniej wspomniałam, salol umieszczony w membranach AAO, w których średnica porów była mniejsza niż 73 nm nie ulegał krystalizacji.

Ponadto przeprowadziłam analizę temperatury oraz entalpii topnienia kryształów uformowanych w membranach o średnicach porów 150 nm i 100 nm. Liczne badania pokazują, że obniżenie T_m oraz ΔH_m następuje wraz ze zmniejszeniem średnicy porów. Relacja ta opisywana jest za pomocą termodynamicznego równania Gibbsa-Thomsona [30,31]. Analizując temperaturę topnienia kryształów salolu w membranach, zauważyłam, że $T_{m\ conf}$ różni się od $T_{m\ bulk}$ salolu, ale nie jest spełniona liniowa relacja Gibbsa-Thomsona, ponieważ T_{m150nm}=300 K, a T_{m100nm}=312 K. Rozważając wartości temperatur topnienia salolu w matrycach AAO dopatrzyłam się pewnych podobieństw z T_m próbki makroskopowej. Salol „w masie" może występować w dwóch odmianach polimorficznych - stabilnej, której T_m^I =315 K i metastabilnej - T_m^{II} =302 K. Stąd też porównując wartości temperatur topnienia dla układów zamkniętych z T_m makroskopowej próbki salolu wywnioskowałam, że w porach o średnicy 150 nm pojawia się metastabilna forma salolu, a w porach, gdzie d=100 nm - stabilna. W celu potwierdzenia występowania dwóch odmian polimorficznych w membranach AAO oszacowałam energię aktywacji na podstawie danych z pomiarów izotermicznej i nieizotermicznej krystalizacji. Ponadto przeprowadziłam również badania za pomocą spektroskopii w podczerwieni, które wykazały różnice w liczbie wiązań, szerokości oraz intensywności pasm absorpcyjnych obu form polimorficznych.

Otrzymane wyniki pokazują, że zaproponowany sposób stabilizacji amorficznego salolu za pomocą matryc AAO jest skuteczny, a także daje możliwość kontrolowania wzrostu kryształu oraz tworzenia form polimorficznych charakteryzujących się pożądanymi właściwościami fizykochemicznymi.

Próby stabilizacji fizycznej podjęłam również w przypadku sildenafilu. W tym celu posłużyłam się sacharydami jako inhibitorami krystalizacji oraz użyłam membran AAO. Niestety zastosowanie zarówno mono- (glukozy) jaki i disacharydów (sacharozy, maltozy) oraz ich acetylowanych pochodnych dodawanych nawet w dużym nadmiarze (4:1 w/w) okazało się niewystarczające, by zahamować rekrystalizację tej substancji. Z kolei w celu stworzenia układów zamkniętych sildenafil-membrana AAO konieczne było opracowanie odpowiedniej technologii wprowadzenia tej substancji do wnętrza matrycy. Standardowa technika napełniania matryc AAO polega na umieszczeniu membrany AAO w stopionej substancji, a następnie utrzymywanie całego układu w temperaturze topnienia substancji przez kilka godzin (w p=10^2 bara). W przypadku sildenafilu długotrwałe utrzymywanie go w T_m grozi degradacją substancji. Dlatego też podjęłam próby przygotowania roztworów sildenafilu z różnymi rozpuszczalnikami, w których umieszczałam matryce AAO. Jako rozpuszczalnika użyłam (i) acetonu oraz (ii) etanolu. Przygotowane w ten sposób układy umieszczałam w piecu w celu odparowania rozpuszczalnika. Niestety ilość sildenafilu, która została umieszczona w membranach AAO okazała się zbyt mała, by możliwe były pomiary eksperymentalne.

Rozdział III

3 WYNIKI BADAŃ

3.1 PUBLIKACJA I

BADANIE DYNAMIKI MOLEKULARNEJ ORAZ KRYSTALIZACJI SILDENAFILU W STANIE CIECZY PRZECHŁODZONEJ ORAZ W SZKLE.

Autorzy:

K. Kolodziejczyk, M. Paluch, K. Grzybowska, A. Grzybowski, Z. Wojnarowska, L. Hawelek, J. D. Ziolo;

Referencje:

Molecular Pharmaceutics, 2013, 10 (6), pp 2270–2282

Skrót:

W pracy tej przedstawiony został temat stabilności fizycznej oraz dynamiki molekularnej sildenafilu przygotowanego w fazie przechłodzonej oraz szklistej (T_g=330 K). Wykazaliśmy, że sildenafil w formie szkła nie ulega krystalizacji w temperaturze pokojowej przez okres 6 miesięcy ($T<T_g$), jednakże w cieczy przechłodzonej substancja ta z łatwością rekrystalizuje. W celu określenia mechanizmu krystalizacji przeprowadziliśmy badania w warunkach izotermicznych oraz nieizotermicznych, które dowiodły, że obie metody dają te same wyniki, co oznacza niewystępowanie odmian polimorficznych.

molecular pharmaceutics

Article

pubs.acs.org/molecularpharmaceutics

Relaxation Dynamics and Crystallization Study of Sildenafil in the Liquid and Glassy States

K. Kolodziejczyk,[†] M. Paluch,[†] K. Grzybowska,*[,†] A. Grzybowski,[†] Z. Wojnarowska,[†] and L. Hawelek[†,‡]

[†]Institute of Physics, University of Silesia, ul. Uniwersytecka 4, 40-007 Katowice, Poland

[‡]Institute of Non Ferrous Metals, ul. Sowinskiego 5, 44-100 Gliwice, Poland

J. D. Ziolo

Poznan University of Medical Sciences, Faculty of Medicine I, Fredry 10, 61-701 Poznan, Poland

ABSTRACT: In this paper, the physical stability and molecular dynamics of amorphous sildenafil are investigated in both the liquid and glassy states. We have established that the amorphous sildenafil is resistant to recrystallization at temperatures below the glass transition temperature T_g during the experimental period of its storage (i.e., above 6 months), however, it easily undergoes cold crystallization at $T > T_g$. To determine the crystallization mechanism, the isothermal and non-isothermal studies of the cold crystallization kinetics of the drug are performed by using the broadband dielectric spectroscopy (BDS) and the differential scanning calorimetry (DSC), respectively. The cold crystallization mechanism has been found to be similar in both the isothermal and non-isothermal cases. This mechanism has been analyzed from the point of view of the molecular mobility of sildenafil investigated in the supercooled liquid and glassy states by using the BDS measurements in the wide temperature range. This analysis has been enriched with a new approach based on a recently reported measure of dynamic heterogeneity given by a four-point dynamic susceptibility function. No tendency to recrystallization of glassy sildenafil at $T < T_g$ is also discussed in relation to molecular dynamics of sildenafil in the glassy state. The relatively small molecular mobility reflected in one secondary relaxation as well as the predicted large time scale of structural relaxation of glassy sildenafil suggests that amorphous sildenafil should not recrystallize during its long-term storage at room temperature.

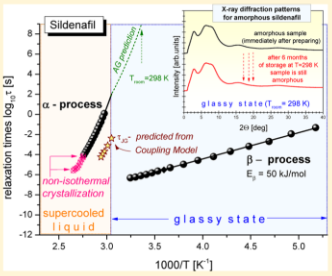

KEYWORDS: *sildenafil, viagra, amorphous drug, physical stability, isothermal crystallization, non-isothermal crystallization, molecular mobility, dielectric relaxation*

■ INTRODUCTION

Many drugs are prepared in the crystalline form because it is the most thermodynamically stable solid state. Consequently, their physicochemical properties do not change even during long-term storage. However, the drugs in the crystalline form are usually poorly water-soluble, and then their bioavailability is strongly limited.

In recent years, there is a great interest in studies on amorphous drugs and their physicochemical properties such as dissolution rate, solubility, physical and chemical stability, and mechanical effects. It has been observed that drugs prepared in the amorphous form are characterized by a better bioavailability than their crystalline counterparts.[1−4] This enables patients to take smaller doses of the drugs. Unfortunately, the amorphous pharmaceuticals are usually thermodynamically unstable and quickly return to their crystalline form.[5,6] Therefore, to develop stable amorphous drugs it is crucial to determine factors that govern the recrystallization process in both their supercooled and glassy states.

In general, crystallization mechanisms are explored by exploiting isothermal and non-isothermal experimental techniques. A very useful technique employed to the isothermal crystallization kinetics study is broadband dielectric spectroscopy (BDS).[6−8] In the isothermal cold crystallization experiment the amorphous sample is annealed above its glass transition temperature T_g and a reduction in the amorphous fraction of the system is reflected in a corresponding drop in the dielectric strength $\Delta\varepsilon_\alpha$ of the structural relaxation process, which is monitored during the BDS measurement. This behavior is typical for the crystallization process, because the decrease in the value of $\Delta\varepsilon_\alpha$ is related to the decreasing number of relaxing molecules participating in the structural process during the increasing degree of crystallinity. The widely used method to investigate both isothermal and non-isothermal crystallization kinetics is the differential scanning calorimetry (DSC). In the isothermal DSC experiment the amorphous sample is quickly heated to a temperature above T_g, and then

Received: August 29, 2012
Revised: March 25, 2013
Accepted: April 17, 2013
Published: April 17, 2013

the heat flow changes at constant temperature are recorded as a time function during the crystallization process. However, in the non-isothermal cold crystallization kinetics measured by DSC, the amorphous sample is heated at a fixed rate ϕ and the changes in the heat flow are detected as a temperature or time function. The study of crystallization kinetics provides information on nucleation and crystal growth mechanisms by using characteristic parameters of the crystallization kinetics (such as the kinetic exponent n, the crystallization rate k, the characteristic crystallization time τ_{cr}, the induction time t_0 for crystallization, and the activation energy for crystallization E_a) determined from different models of crystallization kinetics.[9−14]

It should be emphasized that a molecular mobility factor is considered to play a key role in crystallization phenomena. It is expected that a better understanding of nucleation and crystal growth mechanisms investigated by experiments of crystallization kinetics can be gained on the molecular level by finding correlations between molecular mobility and crystallization. Over an extremely large time scale (even 12 decades), the molecular mobility can be monitored in single measurements by using the BDS technique. Therefore, BDS is a very useful tool to investigate molecular dynamics of pharmaceuticals in the wide temperature range both in the supercooled liquid and glassy states, which are characterized by relaxation processes of different nature. In the supercooled liquid, the structural α-relaxation is a dominant process that reflects cooperative motions of many molecules and is responsible for the liquid−glass transition. In the glassy state, the α-relaxation process becomes very slow and usually only secondary relaxations are experimentally observed, which reflect fast local motions that have an inter- or intramolecular origin and can be investigated by BDS measurements. It is still fervently debated which kind of molecular mobility, reflected in the structural relaxation or rather in secondary processes, is responsible for crystallization of amorphous drugs.[2,5,7,15−18] Recently, a comparative analysis of the time scales of relaxation processes and characteristic crystallization times has been suggested to supplement the study of relations between the length scale of heterogeneity and the tendency of amorphous materials toward crystallization.[19,20] The latest theoretical investigations[21−23] show that a four-point dynamic susceptibility function is a proper measure of the dynamic heterogeneity of glass-forming liquids. Although it is difficult to determine the four-point correlation function, because it requires performing complex nonlinear measurements, some approximated methods have been proposed to evaluate an average number of dynamically correlated molecules N_c based for instance on standard linear dielectric spectroscopy and heat capacity measurements.[21−26] This way to evaluate the degree of dynamic heterogeneity constitutes a very promising course of investigations of molecular dynamics. Therefore, it becomes important to establish correlations between characteristic parameters of the crystallization kinetics and the dynamic heterogeneity of amorphous drugs.

In this paper, we study the physical stability and molecular dynamics of amorphous sildenafil (a popular drug used in the treatment of erectile dysfunction and pulmonary arterial hypertension) in both the liquid and glassy states. To find the crystallization mechanism of sildenafil we investigate the isothermal and non-isothermal cold crystallization kinetics of the drug by using BDS and DSC techniques, respectively. Moreover, by exploiting the broadband dielectric spectroscopy we investigate the sildenafil relaxation dynamics in the wide temperature range to establish relations between the molecular mobility and the tendency of the amorphous sildenafil to crystallization.

EXPERIMENTAL METHODS

Materials. The investigated drug, sildenafil ($C_{22}H_{30}N_6O_4S$, M_w = 474,57 g/mol, IUPAC name: 5-[2-ethoxy-5-(4-methylpiperazin-1-yl)sulfonylphenyl]-1-methyl-3-propyl-4*H*-pyrazolo-[4,3-*d*]pyrimidin-7-one) was delivered from Polpharma in Starogard Gdanski as a white crystalline powder. This drug is used in the treatment of erectile dysfunction and pulmonary arterial hypertension. The chemical structure of studied substance is presented in Figure 1. Amorphous samples were prepared by quench-cooling of the melt of the crystalline form of sildenafil.

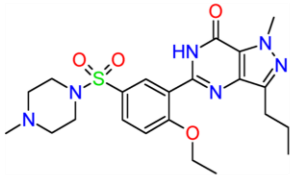

Figure 1. Chemical structure of sildenafil.

Methods. *X-ray Diffraction (XRD).* The isothermal X-ray diffraction measurements for sildenafil were carried out at room temperature (T = 298 K) on the laboratory Rigaku-Denki D/MAX RAPID II-R diffractometer attached with a rotating anode Ag Kα tube (λ = 0.5608 Å), an incident beam (0 0 2) graphite monochromator and an image plate in the Debye−Scherrer geometry. The pixel size was 100 μm × 100 μm. Crystalline and amorphous samples of sildenafil were placed inside Lindemann glass capillaries (1.5 mm in diameter). Measurements were performed for the sample filled and empty capillaries, and the intensity for the empty capillary was then subtracted. The beam width at the sample was 0.1 mm. The two-dimensional diffraction patterns were converted into the one-dimensional intensity data using suitable software.

Broadband Dielectric Spectroscopy (BDS). Isobaric measurements of the complex dielectric permittivity $\varepsilon^*(\omega) = \varepsilon'(\omega) - i\varepsilon''(\omega)$ were carried out using the Novo-Control Alpha dielectric spectrometer over the frequency range from 3×10^{-3} to 3×10^6 Hz at ambient pressure. The temperature stability controlled by the Quatro System using a nitrogen gas cryostat was better than 0.1 K. Dielectric measurements of sildenafil were performed in a parallel-plate cell (diameter, 20 mm; gap, 0.1 mm) immediately after preparation of the amorphous sample.

Non-isothermal dielectric measurements were performed in the temperature range 133−357 K, whereas isothermal dielectric measurements of sildenafil crystallization were carried out above the glass transition temperature at the following crystallization temperatures: 348, 350, 353, 356, and 358 K. At each crystallization temperature dielectric spectra were recorded every 900 s.

Differential Scanning Calorimetry (DSC). Calorimetric measurements of the non-isothermal cold crystallization of sildenafil were carried out by Mettler-Toledo DSC apparatus equipped with a liquid nitrogen cooling accessory and an HSS8 ceramic sensor (heat flux sensor with 120 thermocouples).

Temperature and enthalpy calibrations were performed by using indium and zinc standards.

The amorphous form of the sildenafil was prepared in an open aluminum crucible (40 μL) outside the DSC apparatus. First, the crystalline sample was melted in the crucible on the heating plate (CAT M 17.5), and next the melt was immediately cooled to vitrify the sample. Crucibles with such prepared glassy samples have been sealed with the top with one puncture. Amorphous samples were scanned at various heating rates 10, 20, 30, 40, and 50 K/min over a temperature range of 303 K to well above the respective melting points.

Each measurement at a given heating rate was repeated 3 times. For each experiment a new amorphous sample was prepared.

To obtain accurate temperature dependences of heat capacity $C_p(T)$ for crystalline and amorphous sildenafil a stochastic temperature-modulated differential scanning calorimetry (TMDSC) technique implemented by Mettler-Toledo TOPEM has been exploited. The quenched sample was heated at a rate of 0.5 K/min. In the experiment, a temperature amplitude of the pulses of 0.5 K was selected with a switching time range with minimum and maximum values of 15 and 30 s, respectively. To achieve higher accuracy of the heat capacity we adjusted our evaluations using a sapphire reference curve. The glass transition temperature T_g was determined as the temperature of the half step height of the temperature dependences of the quasi-static heat capacity $C_p(T)$.

RESULTS AND DISCUSSION

Isothermal Study of Amorphous Sildenafil Recrystallization below T_g (XRD). It is a well-known observation that the physical stability of amorphous drugs is greatly affected by their thermal history. Amorphous pharmaceuticals can recrystallize during their storage under isothermal conditions below their glass transition temperature T_g as well as they can undergo a cold crystallization process on heating from the amorphous state to the supercooled region, i.e., in the temperature range between T_g and the melting temperature T_m. To get a full picture of the tendency of amorphous sildenafil toward recrystallization, we performed thorough investigations of the crystallization process of the drug in both the glassy and supercooled liquid states under isothermal and non-isothermal conditions.

Using the X-ray diffraction (XRD) technique, we performed long-term isothermal studies of the tendency of amorphous sildenafil toward recrystallization during its storage in normal conditions, i.e., at room temperature T_{room} = 298 K, atmospheric pressure, and the quasi-constant humidity RH ≈ 10%. It should be noted that the temperature of the storage of glassy sildenafil, T_{room}, is lower by 30 K than the glass transition temperature T_g of this drug. The X-ray diffraction pattern of the sample measured immediately after vitrification of sildenafil (see Figure 2b) is characterized by a very broad amorphous halo in contrast to that for the initial crystalline sample (see Figure 2a) for which numerous sharp Bragg peaks can be observed. It confirms that the sample prepared by quench-cooling of the melt of the crystalline form of sildenafil has indeed an amorphous structure. This amorphous sample was stored in the measuring capillary in normal conditions, and X-ray diffraction measurements have been carried out at specified time intervals to check whether the recrystallization process from the glassy state is begun. We found that diffraction patterns of amorphous sildenafil remain unchanged for all the planned time of our investigation, i.e., the system has been still fully amorphous even after 6 months of storage at T = 298 K (see Figure 2c). Therefore, we can claim that amorphous sildenafil is resistant to recrystallization during its storage at $T < T_g - 30$ K. This is for example in contrast to highly unstable amorphous celecoxib for which the degree of recrystallization from the glassy state exceeded 10% only after 2 days of that sample storage at room temperature $T_{room} = T_g - 30$ K.[5] This result is optimistic from the point of view of implementation of the amorphous sildenafil to therapy.

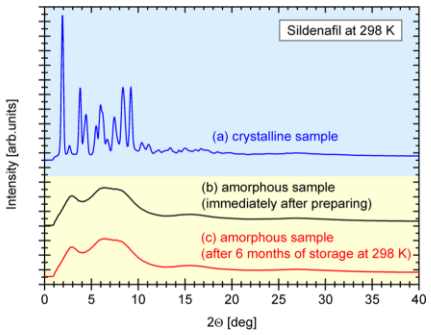

Figure 2. X-ray diffraction patterns for solid sildenafil performed at room temperature T = 298 K (30 K below its T_g): (a) the initial crystalline form of sildenafil; (b) amorphous sildenafil measured immediately after its preparation by quench-cooling of the melt of crystal (a); (c) amorphous sildenafil after 6 months of its storage at 298 K.

Isothermal Cold Crystallization Kinetics Study (above T_g) by BDS. Although we have detected no tendency of the amorphous sildenafil toward recrystallization during its long-term storage at $T < T_g - 30$ K, we have found that it easily undergoes cold crystallization when it is heated from its amorphous state ($T < T_g$) to the supercooled liquid ($T_g < T < T_m$). To describe the recrystallization processes above T_g we performed the analysis of cold crystallization kinetics in both isothermal and non-isothermal conditions.

The isothermal cold crystallization kinetics of sildenafil was studied by broadband dielectric spectroscopy (BDS), which is a very sensitive method to investigate changes in molecular dynamics during the crystallization process in terms of a reduction of molecular mobility reflected in the structural relaxation. The isothermal cold crystallization of sildenafil has been investigated at selected temperatures in the range of supercooled liquids, i.e., at the following crystallization temperatures: 348, 350, 353, 356, and 358 K. For each measurement, a new amorphous sample was prepared by fast cooling of the melted sildenafil on the capacitor plate. Immediately after amorphization, spectra of the complex dielectric permittivity $\varepsilon^*(\omega) = \varepsilon'(\omega) - i\varepsilon''(\omega)$ were recorded under isothermal conditions at specified time intervals throughout the crystallization process. The representative frequency dependences of the real (ε') and imaginary (ε'') parts of complex dielectric permittivity measured during the course of crystallization at 350 K are presented in Figure 3. It is clearly visible that both the static dielectric permittivity and amplitudes of structural relaxation loss peaks begin to rapidly decrease with time after an induction time of crystallization at which the changes in the spectra are not observed. Such a

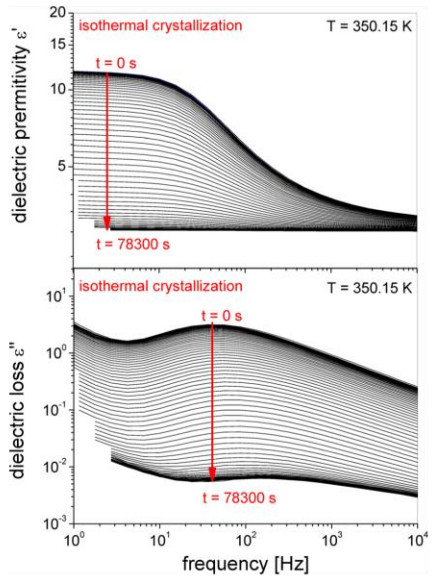

Figure 3. Dielectric spectra of the real (upper panel) and imaginary (lower panel) parts of the complex dielectric permittivity collected during an isothermal crystallization at T = 350 K.

dramatic drop in the dielectric strength of the structural relaxation $\Delta\varepsilon_\alpha$ is typical for the crystallization process because an increase in the crystalline volume fraction leads to a reduction in the number of reorienting dipoles contributing to the α-relaxation. The increase in the crystallization degree with time can be analyzed from the normalized real permittivity ε'_n by using the following formula:

$$\varepsilon'_n(t) = \frac{\varepsilon'(0) - \varepsilon'(t)}{\varepsilon'(0) - \varepsilon'(\infty)} \quad (1)$$

where $\varepsilon'(0)$ is the static dielectric permittivity at the beginning of the crystallization, $\varepsilon'(\infty)$ is the long-time limiting value, and $\varepsilon'(t)$ is the value at a given time of crystallization, t. Figure 4 presents the plot of ε'_n as a function of time at each crystallization temperature.

The kinetics of isothermal crystallization of sildenafil have been analyzed by using the Avrami and Avramov models.

Avrami Model of Crystallization. The Avrami model[9,10] is most frequently used to describe the crystallization kinetics under isothermal conditions. We analyzed the time dependences of ε'_n for sildenafil by using the following modified Avrami equation:

$$\varepsilon'_n(t) = 1 - \exp(-K(t)^n) \quad (2)$$

where $K = k^n$ is a crystallization rate constant, which depends on the crystallization temperature and geometry of the sample, n is the Avrami exponent that is related to the time dependence of the nucleation rate and to the dimensionality of the crystallization, and t_0 is the induction time of crystallization.

To establish values of the Avrami parameters it is convenient to prepare the so-called Avrami plot, which is based on the formula

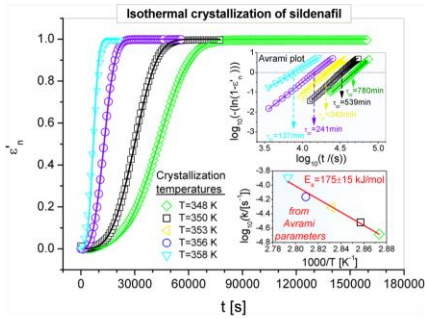

Figure 4. Time dependence of normalized real permittivity ε'_n. Solid lines represent Avrami fits in terms of eq 2. The upper inset shows the Avrami plots in terms of eq 3 for each crystallization temperature in the time ranges in which the dependences are linear. The crystallization times τ_{cr} graphically determined at $\log(-\ln(1 - \varepsilon'_n)) = 0$, which corresponds to $\varepsilon'_n = (\varepsilon'_n)'_{max} = 0.63$ according to the Avramov model, are the same as those calculated from the Avrami parameters K and n (see Table 1). The lower inset presents the temperature dependence of the logarithm of the crystallization rate k related to the Avrami parameters as follows: $k = K^{1/n}$. The solid line in the lower inset denotes the linear fit to eq 4.

$$\log(-\ln(1 - \varepsilon'_n)) = \log K + n \log(t) \quad (3)$$

The above equation shows that values of n and $\log K$ can be determined respectively as the slope and the intercept of the plot of $\log(-\ln(1 - \varepsilon'_n))$ vs $\log(t)$ if the dependence is linear. As can be seen in the upper inset in Figure 4, the Avrami plots are constructed for each temperature of crystallization in the time ranges in which the linear character of the obtained dependences is maintained. The values of Avrami parameters, n and K collected in Table 1, obtained from the Avrami plots we use to describe entire time dependences of ε'_n (see the main panel of Figure 4). The value of Avrami exponent n changes (from 2.6 to 3.5) with various crystallization temperatures. This result suggests that sildenafil can form coexistent rather three-dimensional crystallites from instantaneous and sporadic nucleation.[27,28] Moreover, we found that the crystallization rate constant K increases with increasing crystallization temperature, which can indicate that the crystallization process is dominated by the diffusion of molecules and not by the nucleation of crystallites for which the dependence $K(T)$ is a decreasing function.[29]

To find the activation energy for crystallization E_a of sildenafil we applied the Arrhenius law:

$$\log k = \log k_0 - \frac{E_a}{RT} \log e \quad (4)$$

where k is the crystallization rate expressed in inverse time units, which is related to the Avrami parameters as follows: $k = K^{1/n}$, and R is the gas constant, whereas k_0 and E_a are fitting parameters. As can be seen in the lower inset to Figure 4 the found dependence $\log k$ vs $1000/T$ is linear in the crystallization temperature range and the activation energy of sildenafil isothermal crystallization E_a established from the slope of the plot equals 175 ± 15 kJ/mol.

Avramov Model of Crystallization. Since the Avrami plot does not hold the linear character for entire time range, we additionally analyzed the isothermal crystallization kinetics of

Table 1. Comparison of Isothermal Cold Crystallization Kinetics Parameters of Sildenafil Obtained from the Avramov and Avrami Analyses

	Avrami model			Avramov model			
crystn temp [K]	n	t_0 [s]	log(K [s^{-n}])	N	t_0 [min]	τ_{cr} [min] at $(\varepsilon_n')'_{max}$	$\tau_{cr} = K^{-1/n}$ [min] from Avrami params
348	3.47 ± 0.02	50	−16.21 ± 0.11	3.60 ± 0.02	30.2 ± 2.0	785 ± 3	780 ± 4
350	3.48 ± 0.05	0	−15.72 ± 0.15	3.48 ± 0.03	19.4 ± 1.8	531 ± 4	539 ± 6
353	3.30 ± 0.04	0	−14.23 ± 0.13	3.32 ± 0.03	10.0 ± 1.7	336 ± 3	343 ± 4
356	3.06 ± 0.03	0	−12.74 ± 0.13	3.03 ± 0.02	6.9 ± 1.0	239 ± 2	241 ± 2
358	2.60 ± 0.03	0	−10.15 ± 0.11	2.57 ± 0.02	5.8 ± 0.8	137 ± 2	134 ± 2

sildenafil by using the approach recently proposed by Avramov et al.[11]

$$\varepsilon_n'(t) = 1 - \exp\left(-\left(\frac{t - t_0}{\tau_{cr}}\right)^n\right) \quad (5)$$

where τ_{cr} is a characteristic time for the isothermal overall crystallization. The parameters n and t_0 have the same meaning as those in the Avrami model (eq 2), whereas τ_{cr} is related to the Avrami parameters as follows: $\tau_{cr} = K^{-1/n}$. This method allows us to avoid measurement errors caused by the thermal instability at the beginning of the experiment and enables us to estimate correctly the crystallization induction time t_0.

To determine the Avramov parameters we construct the so-called Avrami−Avramov plot for each crystallization temperature (as an example see Figure 5 for T = 350 K). The Avrami−Avramov plot includes the dependence of the normalized real permittivity ε_n' on ln t as well as the first derivative of the normalized real permittivity $d\varepsilon_n'/d(\ln t)$ versus ln t, which is usually exploited in the analysis based on the Avramov model instead of the following exact equation:

$$\frac{d\varepsilon_n'(t)}{d(\ln(t - t_0))} = n\left(\frac{t - t_0}{\tau_{cr}}\right)^n \exp\left(-\left(\frac{t - t_0}{\tau_{cr}}\right)^n\right) \quad (6)$$

The function defined by eq 6 achieves the maximum value $(\varepsilon_n')'_{max} = n/e$ at $t - t_0 = \tau_{cr}$. Thus, preliminarily assuming that $t_0 = 0$, we can easily find ln τ_{cr} for $(\varepsilon_n')'_{max}$ from the Avrami−Avramov plot and the parameter n can be simply calculated as follows:

$$n = \frac{(\varepsilon_n')'_{max}}{0.368} \quad (7)$$

It should be noted that $\varepsilon_n'(\tau_{cr}) = 1 - 1/e \approx 0.63$ according to eq 6. However, we usually obtain from experimental dependences $\varepsilon_n'(t)$ that $\varepsilon_n'(\tau_{cr}) < 0.63$. It means that the induction time $t_0 > 0$. In this case, we can estimate the proper value of t_0 by finding t from the condition $\varepsilon_n' = 0.63$ and then calculating $t_0 = t - \tau_{cr}$. The values of Avramov parameters obtained from the Avrami−Avramov plots, n, τ_{cr}, and t_0, are collected in Table 1. We have established that the values of the Avramov parameters can be successfully used to describe the dependence $\varepsilon_n'(\ln t)$ (an example is presented in Figure 5). We also calculated the values of crystallization time τ_{cr} from the Avrami parameters K and n. As can be seen from Table 1, both the Avrami and Avramov methods yield similar values of the parameters n and τ_{cr}, whereas the crystallization induction time t_0 is estimated more reliably from the Avramov model, which provides times t_0 longer than those obtained by using the Avrami equation.

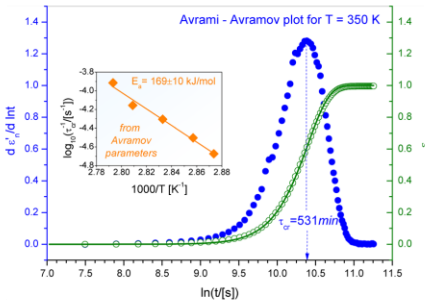

Figure 5. Avrami−Avramov plot: time evolution of normalized real permittivity ε_n' (open green circles) and its first derivative toward the natural logarithm of the time (closed blue circles). The solid line is the best fit to eq 5 by using the Avramov parameters collected in Table 1. The inset presents the temperature dependence of the logarithm of the inverse crystallization time from the Avramov model. The solid line in the inset denotes the linear fit to eq 4 with $k = 1/\tau_{cr}$.

Since the rate of crystallization $k = 1/\tau_{cr}$, the temperature dependence of the crystallization time τ_{cr} can be used to determine the activation energy of overall isothermal crystallization in terms of eq 4. We have performed this analysis by using τ_{cr} found from the Avramov model (see the inset to Figure 5), obtaining E_a = 169 ± 10 kJ/mol, which is in accord with the value of the activation energy established from the Avrami parameters.

Non-Isothermal Cold Crystallization Kinetics Study (above T_g) by DSC. To thoroughly recognize a tendency to recrystallization of the amorphous sildenafil under various conditions we also investigate the non-isothermal cold crystallization of the drug. We have studied the kinetics of non-isothermal crystallization by the DSC technique, employing a series of experiments carried out at different heating rates, ϕ. Sildenafil in the amorphous form was heated at various rates, 10, 20, 30, 40, and 50 K/min, immediately after its vitrification. As can be seen in Figure 6, the cold crystallization occurs on heating the amorphous form between the glass transition temperature T_g and the melting temperature T_m.

It can be observed that the glass transition and the exothermic peak of crystallization shift toward higher temperatures with increasing heating rate. The values of the glass transition temperature T_g and the characteristic temperatures of crystallization, i.e., the onset temperature of crystallization T_o and the peak temperature of crystallization T_p (the temperature at the maximum crystallization rate), found at the various heating rates ϕ are collected in Table 2.

The parameters T_o, T_p, and ϕ are useful to determine the activation energy of non-isothermal crystallization E_c, which is established herein by exploiting two methods proposed by

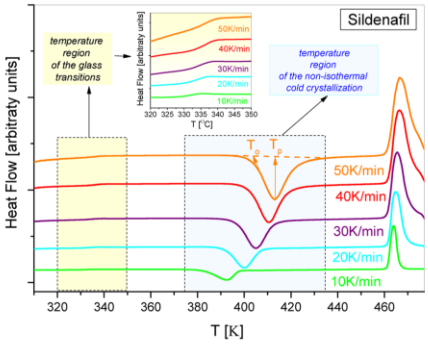

Figure 6. DSC thermograms of the sildenafil measured at different heating rates.

Table 2. Characteristic Temperatures of the Glass Transition and the Crystallization Process Determined from DSC Thermograms Measured at Different Heating Rates[a]

heating rate ϕ [K/min]	glass transition temp T_g [K]	temp of crystn [K]	
		onset T_o	peak T_p
10	330.3 ± 0.1	378.2 ± 0.1	392.0 ± 0.1
20	333.5 ± 0.1	391.0 ± 0.1	400.4 ± 0.1
30	334.5 ± 0.1	396.3 ± 0.1	405.6 ± 0.1
40	335.9 ± 0.1	401.3 ± 0.1	411.0 ± 0.1
50	336.9 ± 0.1	404.2 ± 0.1	413.8 ± 0.1

[a]See Figure 6.

Kissinger[13] and by Augiss and Bennett.[14,30] According to the Kissinger approach to the evaluation of E_c, it is sufficient to consider only the variation of the peak temperature of crystallization T_p with the heating rate ϕ by using the following equation:

$$\ln\left(\frac{\varphi}{T_p^2}\right) = C_K - \frac{E_c}{RT_p} \tag{8}$$

where C_K is a fitting parameter.

However, additionally taking into account the onset temperature of crystallization T_o, Augiss and Bennett suggested a more accurate method that relies on the formula

$$\ln\left(\frac{\varphi}{T_p - T_o}\right) = C_{AB} - \frac{E_c}{RT_p} \tag{9}$$

where C_{AB} is a fitting parameter.

The analysis of the activation energy of non-isothermal crystallization in terms of eqs 8 and 9 is performed in Figure 7. As a result, we obtained the activation energy value, E_c = 100 ± 10 kJ/mol, from the Kissinger equation, which is in accord with E_c = 120 ± 15 kJ/mol found from the Augiss and Bennett method. Thus, the activation energy of non-isothermal cold crystallization of sildenafil is slightly less (by about 35%) than the activation energy for the isothermal cold crystallization.

To study the mechanism of the non-isothermal cold crystallization of sildenafil we rather cannot use the classical Avrami model (eq 2) which assumes that crystallization occurs under isothermal conditions. Ozawa[12] extended the Avrami

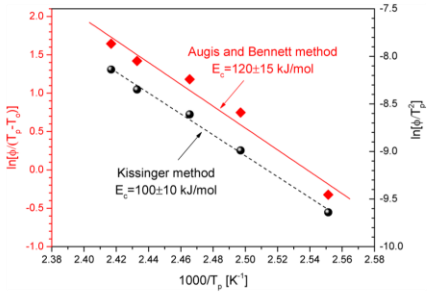

Figure 7. Kissinger (black circles) and Augiss and Bennett (red diamonds) plots for exothermic crystallization peaks for sildenafil characterized by temperatures collected in Table 2. The solid lines indicate the linear fits to eqs 8 and 9, respectively.

equation to describe the non-isothermal crystallization analysis by assuming that the non-isothermal crystallization process consists of innumerable isothermal crystallization processes. On this assumption, the Ozawa equation can be obtained by replacing the time variable t in the Avrami model with the quotient of temperature and heating rate T/ϕ for instance in the following form:

$$\log(-\ln(1 - D_c)) = \log Z(T) - n_O \log(\varphi) \tag{10}$$

where D_c is the relative degree of the non-isothermal crystallization, n_O is the Ozawa exponent, and $Z(T)$ is the Ozawa crystallization rate constant. It is worth noting that the Ozawa kinetic parameters hold physical meaning similar to those of the Avrami parameters.[31]

The relative degree of the non-isothermal crystallization D_c for each heating rate can be determined as a temperature function from DSC thermograms presented in Figure 6 by integration of the exothermic peak during the heating process:

$$D_c(T) = \frac{\int_{T_0}^{T}\left(\frac{dH_c}{dT}\right)dT}{\int_{T_0}^{T_\infty}\left(\frac{dH_c}{dT}\right)dT} \tag{11}$$

where T_0 and T_∞ are temperatures at which the crystallization process begins and ends, respectively, whereas dH_c/dT represents the heat flow at a given T. The obtained temperature dependences of D_c are shown in Figure 8, which are used to construct the Ozawa plots of $\log(-\ln(1 - D_c))$ versus $\log(\phi)$ for a few chosen temperatures (see the inset to Figure 8). Since performed Ozawa plots are linear, it is justified to apply eq 10 to determine the Ozawa kinetic parameters. As a result (see Table 3), we found that the values of the Ozawa exponent n_O for non-isothermal cold crystallization of sildenafil changed from 3.3 to 3.5, which are within the range of the values of the exponent n established from the Avrami and Avramov analyses for isothermal cold crystallization of the drug. Moreover, it has turned out that the Ozawa crystallization rate constant $Z(T)$ increases with increasing temperature.[31,32] It suggests that the non-isothermal crystallization occurs in the diffusion-controlled region similarly to the isothermal crystallization of sildenafil. Therefore, one can expect that the mechanisms of the isothermal and non-isothermal cold crystallizations of sildenafil are similar.

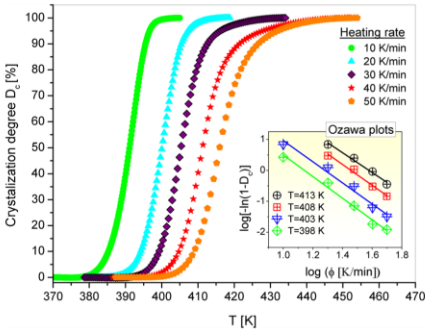

Figure 8. Temperature dependences of the crystallization degree $D_c(T)$ determined from eq 11 at different heating rates. The inset shows the Ozawa plots constructed from the non-isothermal crystallization data for sildenafil. Solid lines in the inset denote the linear fits to eq 10.

Table 3. Non-Isothermal Cold Crystallization Kinetics Parameters of Sildenafil Obtained from the Ozawa Analyzes According to Eq 10

	Ozawa model	
crystn temp [K]	n_O	log (Z [(K/min)^{n_O}])
398.15	3.50 ± 0.23	4.00 ± 0.32
403.15	3.42 ± 0.30	4.38 ± 0.43
408.15	3.37 ± 0.28	4.92 ± 0.43
413.15	3.21 ± 0.27	5.06 ± 0.42

Molecular Dynamics of Sildenafil in the Liquid and Glassy States. From investigations of physical stability of sildenafil, we have established that amorphous form of this drug reveals a high resistance for recrystallization during its storage at normal conditions, i.e., at atmospheric pressure and T_{room} = 298 K (which corresponds to T_g − 30 K) whereas above T_g sildenafil is characterized by strong tendency toward crystallization. Now, we intend to study the relation between molecular mobility and physical stability of sildenafil in both the liquid and glassy states by using broadband dielectric spectroscopy.

Figures 9 and 10 present dielectric spectra for sildenafil obtained on heating the sample from the glassy state (Figure 9) to the liquid state (Figure 10) at atmospheric pressure.

In the glassy state, where structural relaxation times are too long to be observed in the experimental frequency window, only secondary relaxation processes can be detected, which reflect some small angle reorientations of entire molecules or intramolecular motions. As can be seen in Figure 9 we can distinguish only one secondary β-process for amorphous sildenafil below T_g, which shifts toward higher frequencies with increasing temperature. During further heating of the sample, the structural α-relaxation process emerges above T_g (see Figure 10). The α-relaxation is much more pronounced in the spectra than the secondary process. The structural process reflects cooperative reorientational movements of entire molecules and provides a main characterization for relaxation dynamics of supercooled liquids as well as the glass transition. In addition, in the imaginary part of the complex permittivity ε'' (see Figure 10a), the conductivity contribution, related to translational motions of ions in the sample, is observed.

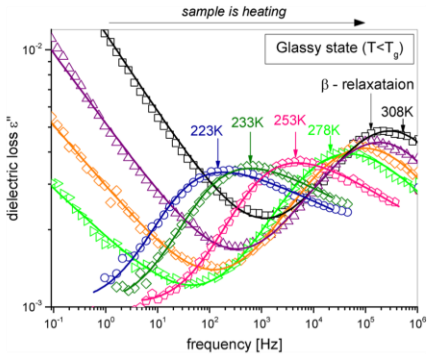

Figure 9. The dielectric loss spectra of sildenafil at different temperatures at $T < T_g$.

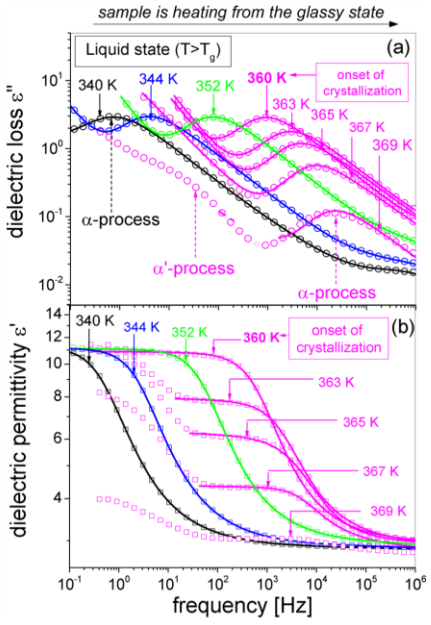

Figure 10. The imaginary (a) and real (b) parts of the complex dielectric permittivity of sildenafil at different temperatures at $T > T_g$.

By analyzing the structural relaxation we can also detect cold crystallization of sildenafil under non-isothermal condition. As can be seen in Figure 10a, the α-process peaks move toward higher frequencies on heating up to T_{cryst} = 360 K, which indicates the increase in molecular mobility of the system. At T > 360 K, both amplitudes of structural relaxation loss peaks (Figure 10a) and static dielectric permittivity of the α-process (Figure 10b) begin rapidly decreasing with increasing temperature. Such a sudden drop in the dielectric strength of the α-process is caused by the onset of the sample recrystallization on heating and reflects the increasing degree of crystallinity. It is worth noting that a new relaxation process (α') emerges in the

low frequency flank of the α-peak at high crystallization degrees of sildenafil. This α'-relaxation can be attributed to conformational mobility originating from the remaining amorphous fraction adjacent to the crystal surfaces.[33]

To determine relaxation times of α- and β-processes at various temperatures for sildenafil, we fitted the entire dielectric spectra using the following Havriliak–Negami[34] (HN) formula supplemented with the dc conductivity contribution term:

$$\varepsilon^*(\omega) = \varepsilon'(\omega) - i\varepsilon''(\omega) = \varepsilon_\infty + \sum_k \frac{\Delta\varepsilon_k}{[1 + (i\omega\tau_k)^{\xi_k}]^{\delta_k}} - i\frac{\sigma_0}{\varepsilon_0\omega} \quad (12)$$

where ε_∞ is the high frequency limit permittivity and k stands for either the primary or the secondary processes, $\Delta\varepsilon_k$ is the relaxation strength, τ_k is the HN relaxation time, and ξ_k and δ_k are the HN exponents of the relaxation processes, whereas σ_0 is the dc electrical conductivity and ε_0 is the dielectric permittivity of the vacuum.

From the best fits of dielectric spectra shown in Figures 9 and 10 we found the temperature dependences of α- and β-relaxation times (see Figure 11).

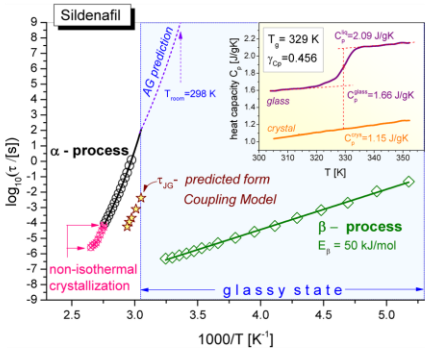

Figure 11. The relaxation map of sildenafil. Temperature dependence of structural relaxation times (open black circles) was fitted to the VFT equation given by eq 13 (solid black line). Crossed pink circles show α-relaxation times above T_g in the crystallization range. Temperature dependence of the secondary β-relaxation was fitted to the Arrhenius equation given by eq 20 (solid green line). Stars are the primitive relaxation times of the coupling model calculated with $\beta_{KWW} = 0.68$ at temperatures $T \approx T_g$. The dashed blue line is a prediction of temperature dependence of structural relaxation times in the glassy state from the extended AG model (eq 17) using $\gamma_{Cp} = 0.456$. The inset shows temperature dependences of heat capacity for crystalline and amorphous sildenafil established from TOPEM measurements near T_g.

Supercooled Liquid Dynamics. To describe the temperature dependence of the structural α-relaxation times τ_α, we used the Vogel–Fulcher–Tammann (VFT) equation:[35−37]

$$\tau_\alpha(T) = \tau_\infty \exp\left(\frac{A}{T - T_{VFT}}\right) \quad (13)$$

where τ_∞, T_{VFT}, and A are fitting parameters. The values of the VFT parameters for sildenafil, which have been established only by exploiting the α-relaxation times nonaffected by non-isothermal crystallization (see black circle points in Figure 11), are collected in Table 4.

One of the important parameters that characterize the structural relaxation is the fragility parameter, m_p, defined as

$$m_p \equiv \left.\frac{d\log\tau_\alpha}{d(T_g/T)}\right|_{T=T_g} \quad (14)$$

This parameter is often used to predict the tendency of glass-forming liquids toward crystallization. The values of m_p typically range between $m_p = 16$ and about 200 for various materials. The liquids characterized by small values of m_p are classified as *strong* systems, whereas large values of m_p are a feature of *fragile* materials. Molecular mobility in fragile liquids changes rapidly with temperature near T_g, which can be associated with a weak thermodynamic stability and a larger tendency toward crystallization of amorphous systems. Based on the values of the VFT parameters, we estimated that $m_p = 85$ at $\tau_\alpha = 100$ s, which classifies sildenafil as a *medium fragile* liquid. It is worth noting that the dynamic fragility found from dielectric α-relaxation times in terms of eq 14 is identical to the thermodynamic fragility calculated from the relation proposed by Wang and Angell[38,39]

$$m_p = 56\frac{T_g\Delta C_p(T_g)}{\Delta H_m} \quad (15)$$

where the jump in the heat capacity $\Delta C_p(T_g) = 0.43$ J/(g K) at $T_g = 329$ K (see the inset to Figure 11) and the enthalpy of fusion $\Delta H_m = 93.60$ J/g (evaluated from the thermogram for heating rate of 10 K/min presented in Figure 6).

A moderately big value of m_p obtained for sildenafil well corresponds to the low physical stability of this drug in the supercooled liquid state. This conclusion corresponds also to the Tanaka concept of frustration against crystallization.[40,20] According to this two-order-parameter (TOP) model a supercooled liquid near the glass transition tends to order into the equilibrium crystal (long-range ordering). However a liquid does not crystallize because of frustration that is a locally favored short-range ordering. The frustration effects increase the free-energy barrier for nucleation and act as impurities against crystallization. Therefore, a fragile system more easily crystallizes than a strong glass-former, because the frustration

Table 4. Comparison of the Glass Transition Temperatures T_g and the Fragility Parameters m_p Determined from the Dielectric Structural Relaxation Analysis and TOPEM Measurements

BDS measurements						
VFT params for α-process					DSC (TOPEM measurement)	
$\log(\tau_\infty/(s))$	T_{VFT} [K]	A [K]	T_g [K] at $\tau_\alpha = 100$ s	m_p at $\tau_\alpha = 100$ s[a]	T_g [K]	m_p[b]
−17.05 ± 0.50	254 ± 3	3230 ± 240	328 ± 0.1	85 ± 2	329 ± 0.1	85 ± 1

[a]From eq 14. [b]From eq 15.

against crystallization in fragile liquids is weaker. Consequently, a higher fragility implies a higher nucleation rate.[41]

Time Scales of Crystallization and Structural Relaxation. A general issue that should be addressed in crystallization studies is to discuss a possible relation between molecular mobility and crystallization kinetics. As already mentioned, the molecular dynamics of supercooled sildenafil monitored by broadband dielectric spectroscopy is characterized by α-relaxation. Therefore, we investigate whether molecular motions reflected in the structural relaxation control the cold crystallization of supercooled sildenafil. It should be pointed out that our analyses of isothermal and non-isothermal crystallization kinetics resulted in the conclusion that the mechanism of the cold crystallization of sildenafil is dominated by the diffusion of molecules. To find a possible correlation between α-relaxation dynamics and isothermal cold crystallization kinetics for sildenafil, we compare the characteristic isothermal crystallization times τ_{cr} found from the Avramov model of crystallization kinetics with the corresponding structural relaxation times τ_α at the temperatures at which the isothermal crystallization were performed. As can be seen in Figure 12, there is a large difference in the time scales of the

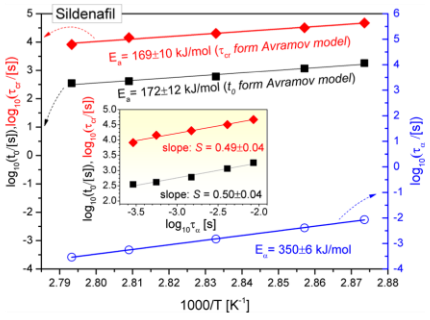

Figure 12. Comparison of temperature dependences of the characteristic isothermal crystallization times τ_{cr} found from the Avramov model of crystallization kinetics (red diamonds), the induction times t_0 determined from the Avramov model (black squares), and structural relaxation times τ_α (open blue circles) at the temperatures at which the isothermal crystallization were performed. The solid lines indicate linear fits to the Arrhenius law. The inset shows log−log plots τ_{cr} and t_0 vs τ_α within the crystallization temperatures range. The solid lines in the inset denote linear fits.

isothermal crystallization and structural relaxation. Nevertheless, this simple observation should be supplemented with the analysis of the activation energies, which shows that the activation energy of isothermal cold crystallization (E_a = 169 kJ/mol) found from the Arrhenius law is less than the activation energy of the structural relaxation (E_α = 350 kJ/mol) that also can be established from the Arrhenius law in the considered crystallization temperature range (see Figure 12). The obtained ratio of the activation energies, that is equal to S = 0.49 for sildenafil, defines the slope of the plot of the dependence of log τ_{cr} on log τ_α (see the inset to Figure 12). This slope S called a coupling coefficient is regarded as a measure of correlation between τ_{cr} and τ_α, and it has been recently investigated[7,42] to answer the question whether the molecular mobility reflected in the structural relaxation can be straightforwardly exploited to explain the diffusion controlled mechanism of crystallization kinetics. The coupling coefficient S = 1 is interpreted to indicate that the crystallization is controlled by diffusion on the assumption that diffusivity and viscosity (or structural relaxation time) are inversely proportional according to the Stokes−Einstein equation. In the case of sildenafil, the value of S is considerably less than 1. It suggests that the crystallization of the drug is not controlled solely by diffusion or the relation between diffusivity and dielectric structural relaxation time is more complex than that given by the simple Debye−Stokes and Stokes−Einstein equations. It should be noted that an analogous coupling analysis has been earlier suggested for the crystallization onset time and the dielectric relaxation time to investigate whether the crystallization process is controlled by the molecular mobility reflected in the relaxation processes.[43−45]Using the lag time for nucleation estimated as the induction time t_0 determined from the Avramov model, we examine the correlation between t_0 and the structural relaxation time τ_α to determine the corresponding coupling coefficient S. As a result (see Figure 12), we find nearly the same values of the activation energy (E_a = 172 kJ/mol) and the coupling coefficient S = 0.50 for the induction time to those established for the characteristic crystallization time τ_{cr}. It confirms that the diffusion seems not to be a dominant factor that controls the crystallization of sildenafil. Moreover, it is worth noting that the linear dependences of log τ_{cr} and log t_0 vs inverse temperature can be superimposed by vertical shifting, which is a consequence of the very similar values of the activation energies found from these dependences. It means that τ_{cr} is linearly proportional to t_0 in the case of sildenafil. A similar proportionality has been also established by Avramov et al. for other materials.[11]

Dynamic Heterogeneity. The latest theoretical and simulation investigations suggest that there is a relationship between the glass formation, dynamic heterogeneity, and crystal nucleation.[46,47] As already mentioned, it has been also argued that a liquid near the glass transition tends to order into the equilibrium crystal, but frustration effects of locally favored short-range ordering on long-range ordering prevent crystallization and help vitrification, because the frustration effects increase the free-energy barrier for nucleation.[20,40] It suggests that the correlation length scale of dynamic heterogeneity can be used as an indicator of the tendency to nucleation. In this context, it is interesting to find how the induction time t_0 depends on the degree of the dynamic heterogeneity of the drug. Moreover, since we have established a very good linear proportionality of τ_{cr} to t_0, an important question arises whether the average number of dynamically correlated molecules of the system correlates with its characteristic crystallization time τ_{cr}.

Recently, a four-point time dependent correlation function $\chi_4(t)$ has been considered to be sensitive to dynamic heterogeneities, because it contains information on both spatial and temporal correlations. The height of the peak in the dynamic susceptibility has been assumed to directly yield the number of dynamically correlated molecules, N_c.[22] Although the relation $N_c = \chi_4^{max}$ is still under discussion and it has been pointed out that N_c can be only proportional to χ_4^{max} in the case of some systems, e.g., the confined ones,[48] it can be applied to bulk samples examined in our study of sildenafil as a good estimator of the average number of dynamically correlated molecules. Since direct experimental investigations that would result in determining the four-point correlation function are difficult due to the necessity of measurements that monitor the system nonlinear response, the function $\chi_4(t)$ is estimated by

using a derivative analysis of the two-point correlation function, $\Phi(t)$. According to the approach proposed by Berthier et al.,[22,21] the dynamic susceptibility of real molecular systems can be expressed in the following approximate way: $\chi_4(t) \approx (k_B/\Delta C_p)T^2[\partial\Phi(t)/\partial T]^2$, where k_B is the Boltzmann constant and ΔC_p is the change in the heat capacity between liquid and glassy states. Exploiting the Kohlrausch−Williams−Watts (KWW) function to parametrize the two-point correlation function, $\Phi(t) = \exp[-(t/\tau_\alpha)^{\beta_{KWW}}]$, where β_{KWW} is the stretch parameter and τ_α is the structural relaxation times, it has been suggested[49,22,21,25] that the maximal dynamic susceptibility of real glass formers can be predicted as follows:

$$N_c = \chi_4^{max} \approx \frac{k_B}{\Delta C_p}\left(\frac{\beta_{KWW}}{e}\right)^2\left(\frac{\partial \ln \tau}{\partial \ln T}\right)^2 \quad (16)$$

Assuming that ΔC_p is a linear temperature function at ambient pressure, we have found the slope and the intercept of the linear dependence $\Delta C_p(T)$ from DSC measurements (see inset to Figure 11) according to the earlier reported procedure[26] that omits the change in the heat capacity of the glassy state with temperature. Moreover, we have established that the stretch parameter of the KWW function, β_{KWW}, does not change for sildenafil within the considered range of crystallization temperatures and $\beta_{KWW} = 0.68$. As a result, we have estimated the number of dynamically correlated molecules N_c by using eq 16 at each crystallization temperature.

From Figure 13, one can see that the time scales of the isothermal crystallization expressed by the logarithms of the

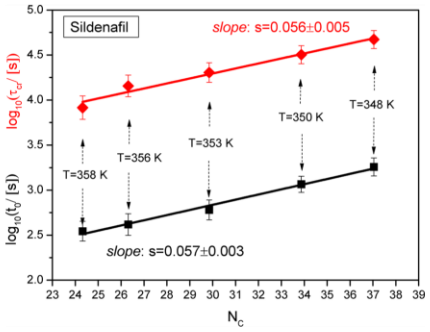

Figure 13. Dependences of the characteristic isothermal crystallization time τ_{cr} (red diamonds) and the induction time t_0 (black squares) both found from the Avramov model of crystallization kinetics on the average number of dynamically correlated molecules N_c calculated from eq 16 at crystallization temperatures. The solid lines denote linear fits.

induction time and the crystallization time, log t_0 and log τ_{cr}, determined from the Avramov model at different crystallization temperatures, are strongly correlated with the number of dynamically correlated molecules. These correlations are linear in the considered crystallization temperature range and characterized by nearly the same slope, which indicates that the increase in N_c by 10 molecules of sildenafil results in a half decade increase in both the crystallization and induction times. It means that the change in N_c by 10 molecules causes a relatively large change in τ_{cr} by about 8.5 h in the considered range of characteristic crystallization times, whereas t_0 changes by about 18.5 min in the considered range of induction times. This finding suggests that the increase in the dynamic heterogeneity causes a slowdown in diffusion, and consequently the crystallization of sildenafil becomes slower. Since the dynamic heterogeneity seems to strongly influence the diffusivity, one can expect that the study of the dynamic heterogeneity of drugs should give us a better insight into our understanding of crystallization process and methods for controlling the physical stability of amorphous drugs. This conclusion is also supported by our latest studies of crystallization under high pressure,[50] which indicate that the number of dynamically correlated molecules N_c determines the crystallization rate rather than the structural relaxation time. It results from our observation that the crystallization rate of indomethacin does not change with pressure if N_c = const under compression of the drug, however, the crystallization rate varies with pressure in isochronal conditions, i.e., at τ_α = const. Nevertheless, one should remember that the methods for estimating N_c are still under discussion as already mentioned. For instance, complex measurements of higher-order nonlinear susceptibilities, which are still very rarely carried out, are required in the future to verify the values of χ_4^{max} estimated in terms of eq 16. Then, we will be able to straightforwardly apply the method based on the simple relation, $N_c = \chi_4^{max}$, to estimate the average number of dynamically correlated molecules. Moreover, the suggested correlations of both the induction time and the crystallization time with the average number of dynamically correlated molecules require further studies on different materials in wide temperature ranges and also under high pressure. If the correlations are consequently confirmed as general rules, their contributions to the enhancement of our understanding of crystallization phenomena are expected to be meaningful.

Glass Dynamics. Exploiting different experimental techniques we have established that supercooled sildenafil is highly unstable and easily recrystallizes, but the amorphous sildenafil is resistant to recrystallization during all periods of isothermal experiment, i.e., even after 6 months of storage at $T < T_g - 30$ K. By analyzing molecular mobility of sildenafil in the glassy state, one can predict whether the physical stability of the amorphous drug is expected to be actually permanent or not. As already mentioned molecular dynamics in the glassy state extremely slows down and the structural relaxation times (that characterize cooperative motions of many entire molecules) become very large. Therefore, they are rarely gathered directly from dielectric measurements that are possible only in the limited range of α-relaxation times below T_g. In this situation, the time scale of α-relaxation in the glassy state is usually only predicted. A commonly used method for evaluating τ_α below T_g is based on the Adam and Gibbs (AG) model[51] extended[52−54] into the glassy state. According to the extended AG approach, the temperature dependence of structural relaxation times can be evaluated from the following formula:

$$\tau_\alpha(T, T_f) = \tau_\infty \exp\left(\frac{A}{T(1 - T_{VFT}/T_f)}\right) \quad (17)$$

where τ_∞, A, T_{VFT} are the fitting parameters found from the VFT (eq 13) in the liquid state. T_f in eq 17 is the fictive temperature that can be estimated by using the following equation:

$$\frac{1}{T_f} = \frac{\gamma_{Cp}}{T_g} + \frac{1-\gamma_{Cp}}{T} \tag{18}$$

where γ_{Cp} is a thermodynamic parameter defined as follows[52,53]

$$\gamma_{Cp} = \left.\frac{C_p^{liq} - C_p^{glass}}{C_p^{liq} - C_p^{cryst}}\right|_{T=T_g} = \left.\frac{\Delta C_p}{C_{p_{conf}}}\right|_{T=T_g} \tag{19}$$

The value of γ_{Cp} can vary between 0 (for extremely fragile systems) and 1 (for extremely strong materials).

Using the values of the VFT parameters collected in Table 4 and the value of the thermodynamic parameter γ_{Cp} = 0.456, which has been calculated from the jump in the heat capacity $\Delta C_p(T_g)$ = 0.43 J/(g K) and the configurational heat capacity $C_{p_{conf}}(T_g)$ = 0.94 J/(g K) at T_g = 329 K (see the inset to Figure 11), we have generated the dependence log $\tau_\alpha(T^{-1})$ in the glassy state from eq 17 (see the blue line in Figure 11). The predicted time scale of the structural relaxation rapidly increases with decreasing temperature in the glassy state. For instance, in normal conditions of drug storage, i.e., at room temperature T_{room} = 298 K, $\tau_\alpha \approx 10^9$ s, which equals about 32.5 years. This result suggests that such extremely slow molecular motions reflected in the structural relaxation should not lead to recrystallization of the glassy sildenafil during its storage at $T \leq T_{room}$ for a very long time.

However, if we consider the potential recrystallization of the glass, we cannot omit the reported role of the secondary relaxations in the crystallization process. As already mentioned, sildenafil in the glassy state reveals only one well-distinguished secondary β-process. The temperature dependence of the secondary β-relaxation times τ_β (presented in Figure 11) obeys the Arrhenius law:

$$\tau_\beta(T) = \tau_\infty \exp\left(\frac{E_\beta}{kT}\right) \tag{20}$$

where the values of the fitting parameters for sildenafil are as follows: the preexponential factor $\tau_\infty = 10^{-14.9}$ s, and the activation energy of the β-process E_β = 50 kJ/mol.

By comparison with other materials that often exhibit two or even three secondary relaxations, the molecular mobility of sildenafil in the glassy state is relatively small. This feature of molecular dynamics of the glassy sildenafil can make a decisive impact on the tendency of the drug toward recrystallization. Recently, we have investigated the tendency of an anti-inflammatory drug, celecoxib, toward crystallization,[5] which has been established to be considerable in both the liquid and glassy states. Later, we found that the physical stability of the glassy celecoxib can be enhanced by mixing with octaacetylmaltose.[2] Based on dielectric measurements and quantum mechanical calculations, we suggested that this stabilizing effect of adding octaacetylmaltose to celecoxib could be explained by suppressing two of three secondary processes of celecoxib. Thus, one can suspect that the high physical stability of sildenafil in the glassy state strongly correlates with the low degree of molecular mobility.

In addition, it is worth noting that among different secondary relaxations those reflecting motions of the whole molecule (intermolecular secondary relaxations also called Johari–Goldstein (JG) relaxations) are considered to be of particular interest from the point of view of crystallization studies, because the JG process is regarded as a precursor of the molecular mobility of the cooperative α-relaxation. Therefore, it is interesting to verify whether the secondary β-relaxation observed for sildenafil in the glassy state can be classified as the JG process or not by using the criteria of Ngai and Paluch[55] based on the extended coupling model (CM).[56] The genuine JG relaxation is the precursor of structural relaxation (a local molecular motion which leads to the α-relaxation), therefore its relaxation time τ_{JG} should correspond well to the primitive relaxation time τ_0 of the CM, i.e., $\tau_{JG} \approx \tau_0$.

The CM relates the primitive relaxation time τ_0 to the structural relaxation time τ_α, at any temperature T and pressure P, by the following equation:

$$\tau_0 = (t_c)^{1-\beta_{KWW}}(\tau_\alpha)^{\beta_{KWW}} \tag{21}$$

where β_{KWW} is the stretch parameter of the KWW function used to fit the α-loss peak, and t_c is equal to 2 ps for small molecular and polymeric glass formers. From eq 21 with the previously determined parameter β_{KWW} = 0.68 and structural relaxation times τ_α from the VFT fit, we calculated the values of primitive relaxation time τ_0 at several temperatures near T_g for sildenafil, which are denoted in Figure 11 by the star symbols. As can be seen the obtained values of τ_0 are considerably different from β-relaxation times τ_β if we extrapolate the latter to higher temperatures (i.e., $\tau_0 \gg \tau_\beta$ at T close to T_g). It means that β-relaxation observed in sildenafil cannot be classified as the JG process. Consequently, the β-relaxation of sildenafil does not have any intermolecular character which is often expected to play a potential role in devitrification, but it originates from intramolecular motions of smaller parts of the sildenafil molecules. Therefore, their influence on physical stability of amorphous sildenafil seems to be not significant.

As a conclusion, we can state that there is no molecular mobility of sildenafil in the glassy state, which can be straightforwardly suspected of resulting in a potential recrystallization of sildenafil.

■ CONCLUSIONS

In this paper, we investigated the physical stability of sildenafil in the liquid and glassy states. By using different experimental techniques (XRD, BDS, and DSC), we established that supercooled sildenafil is highly unstable and easily recrystallizes, but the amorphous sildenafil does not show any tendency toward recrystallization during all periods of the isothermal experiment, i.e., even after 6 months of storage at room temperature T = 298 K (which is the temperature less than the glass transition temperature T_g by 30 K.

We examined isothermal and non-isothermal cold crystallization kinetics of sildenafil by means of BDS and DSC techniques, respectively. As a result, we concluded that the mechanisms of the isothermal and non-isothermal cold crystallization of sildenafil seem to be similar, i.e., (i) sildenafil can form coexistent three-dimensional crystallites from instantaneous and sporadic nucleation (the values of the exponents in Avrami, Avramov, and Ozawa models range from 2.6 to 3.6), and (ii) the crystallization process is dominated by the diffusion of molecules and not by the nucleation of crystallites (crystallization rate constants found from Avrami, Avramov, and Ozawa models increase with increasing crystallization temperature). However, it should be noted that the activation energy of non-isothermal cold crystallization of

sildenafil is less by about 35% than the activation energy for the isothermal cold crystallization.

Moreover, we studied the relation between the molecular mobility and the physical stability of sildenafil in both the liquid and glassy states. We found that the fragility parameter (which is often considered to correlate with the nucleation rate) calculated from both its dynamic and thermodynamic definitions is relatively high (m_p = 85), which well corresponds to the low physical stability of this drug in the supercooled liquid. We analyzed the coupling between dielectric structural relaxation time and characteristic crystallization time for sildenafil, determining its measure given by the coupling coefficient S. We evaluated that S = 0.48 for the drug. It suggests that the crystallization of the drug is not controlled solely by diffusion or the relation between diffusivity and dielectric structural relaxation time is more complex than the inverse proportionality following from the simple Debye−Stokes and Stokes−Einstein equations.

Since the important role of dynamic heterogeneities in crystallization has been recently reported, we examined how the change in the number of dynamically correlated molecules influences both the induction time t_0 and the characteristic crystallization time τ_{cr}, which have been determined from the analysis of isothermal cold crystallization in terms of the Avramov model. We established that there are strong linear correlations between log t_0 and the number of dynamically correlated molecules N_c as well as between log τ_{cr} and N_c in the considered crystallization temperature range. It can be interpreted that a slowdown in diffusion is caused by the increase in the average number of dynamically correlated molecules, which results in a slower crystallization process. This finding confirms that the study of the effect of the length scale of spatially heterogeneous dynamics on crystallization can give us a better insight into the mechanism of crystallization kinetics, which is expected to make improvements to methods for controlling the physical stability of amorphous drugs. However, it requires further studies on a series of various pharmaceuticals.

The found resistance to recrystallization of amorphous sildenafil during our long-term storage experiment (6 months at $T = T_g - 30$ K) correlates with results of our investigations of molecular mobility of sildenafil in the glassy state. This study suggests that neither molecular motions reflected in structural dielectric relaxation times nor molecular mobility related to only one intramolecular secondary dielectric β-relaxation seems to cause the drug recrystallization during a much longer period than that experimentally verified. This result is promising from the point of view of the application of amorphous sildenafil to therapy. However, it should be confirmed by further long-term studies of the amorphous drug stability.

■ AUTHOR INFORMATION

Corresponding Author

*E-mail: katarzyna.grzybowska@us.edu.pl.

Notes

The authors declare no competing financial interest.

■ ACKNOWLEDGMENTS

K.K., K.G., and A.G. are thankful for the financial support from the Polish National Science Centre within the program MAESTRO2 (decision no. DEC-2012/04/A/ST3/00337). M.P. and Z.W. are grateful for the financial support from the Polish National Science Centre within the program OPUS3 (decision no. DEC-2012/05/B/NZ7/03233). Z.W. acknowledges the financial assistance from FNP START (2013).

■ REFERENCES

(1) Adrjanowicz, K.; Kaminski, K.; Paluch, M.; Wlodarczyk, P.; Grzybowska, K.; Wojnarowska, Z.; Hawelek, L.; Sawicki, W.; Lepek, P.; Lunio, R. Dielectric relaxation studies and dissolution behavior of amorphous verapamil hydrochloride. *J. Pharm. Sci.* **2010**, *99*, 828−839.

(2) Grzybowska, K.; Paluch, M.; Wlodarczyk, P.; Grzybowski, A.; Kaminski, K.; Hawelek, L.; Zakowiecki, D.; Kasprzycka, A.; Jankowska-Sumara, I. Enhancement of amorphous celecoxib stability by mixing it with octaacetylmaltose: the molecular dynamics study. *Mol. Pharmaceutics* **2012**, *9* (4), 894−904.

(3) Adrjanowicz, K.; Grzybowska, K.; Kaminski, K.; Hawelek, L.; Paluch, M.; Zakowiecki, D. Comprehensive studies on physical and chemical stability in liquid and glassy states of telmisartan (TEL): solubility advantages given by cryomilled and quenched material. *Philos. Mag.* **2011**, *91*, 1926−1948.

(4) Kaminski, K.; Adrjanowicz, K.; Wojnarowska, Z.; Grzybowska, K.; Hawelek, L.; Paluch, M.; Zakowiecki, D.; Mazgalski, J. Molecular dynamics of the cryomilled base and hydrochloride ziprasidones by means of dielectric spectroscopy. *J. Pharm. Sci.* **2011**, 2642−2657.

(5) Grzybowska, K.; Paluch, M.; Grzybowski, A.; Wojnarowska, Z.; Hawelek, L.; Kolodziejczyk, K.; Ngai, K. L. Molecular Dynamics and Physical Stability of Amorphous Anti-Inflammatory Drug: Celecoxib. *J. Phys. Chem. B* **2010**, *114*, 12792−12801.

(6) Adrjanowicz, K.; Kaminski, K.; Wojnarowska, Z.; Dulski, M.; Hawelek, L.; Pawlus, S.; Paluch, M.; Sawicki, W. Dielectric relaxation and crystallization kinetics of ibuprofen at ambient and elevated pressure. *J. Phys. Chem. B* **2010**, *114*, 6579−6593.

(7) Dantuluri, A. K. R.; Amin, A.; Puri, V.; Arvind, A. K. Bansal. Role of α-relaxation on crystallization of amorphous celecoxib above T_g probed by dielectric spectroscopy. *Mol. Pharmaceutics* **2011**, *8*, 814−822.

(8) Alie, J.; Menegotto, J.; Cardon, P.; Duplaa, H.; Caron, A.; Lacabanne, C.; Bauer, M. Dielectric study of the molecular mobility and the isothermal crystallization kinetics of an amorphous pharmaceutical drug substance. *J. Pharm. Sci.* **2004**, *93*, 218−233.

(9) Avrami, M. Kinetics of Phase Change. I General Theory. *J. Chem. Phys.* **1939**, *7*, 1103.

(10) Avrami, M. Kinetics of Phase Change. II Transformation-Time Relations for Random Distribution of Nuclei. *J. Chem. Phys.* **1940**, *8*, 212.

(11) Avramov, I.; Avramova, K.; Russel, C. New Method to Analyze Data on Overall Crystallization Kinetics. *J. Cryst. Growth* **2005**, *285*, 394−399.

(12) Ozawa, T. Kinetics of non-isothermal crystallization. *Polymer* **1971**, *12*, 150.

(13) Kissinger, H. E. Variation of peak temperature with heating rate in differential thermal analysis. *J. Res. Natl. Bur. Stand.* **1956**, *57*, 217−221.

(14) Augis, J. A.; Bennett, J. E. Calculation of the Avrami parameters for heterogeneous solid state reactions using a modified the Kissinger method. *J. Therm. Anal.* **1978**, *13*, 283−292.

(15) Bhattacharya, S.; Suryanarayanan, R. Local mobility in amorphous pharmaceuticals—characterization and implications on stability. *J. Pharm. Sci.* **2009**, *98*, 2935−2953.

(16) Bhugra, C.; Pikal, M. J. Role of thermodynamic, molecular, and kinetic factors in crystallization from the amorphous state. *J. Pharm. Sci.* **2008**, *97*, 1329−1349.

(17) Johari, G. P.; Kim, S.; Shanker, R. M. Dielectric relaxation and crystallization of ultraviscous melt and glassy states of aspirin, ibuprofen, progesterone, and quinidine. *J. Pharm. Sci.* **2007**, *96*, 1159−1175.

(18) Wojnarowska, Z.; Grzybowska, K.; Adrjanowicz, K.; Kaminski, K.; Paluch, M.; Hawelek, L.; Wrzalik, R.; Dulski, M.; Sawicki, W.; Mazgalski, J.; Tukalska, A.; Bieg, T. Study of the Amorphous Glibenclamide Drug: Analysis of the Molecular Dynamics of

Quenched and Cryomilled Material. *Mol. Pharmaceutics* **2010**, *7*, 1692−1707.
(19) Vyazovkin, S.; Dranca, I. Physical stability and relaxation of amorphous indomethacin. *J. Phys. Chem. B* **2005**, *109*, 18637−18644.
(20) Shintani, H.; Tanaka, H. Frustration on the way to crystallization in glass. *Nat. Phys.* **2006**, *2*, 200−206.
(21) Berthier, L.; Biroli, G.; Bouchaud, J.-P.; Cipelletti, L.; El Masri, D.; L'Hôte, D.; Ladieu, F.; Pierno, M. Accompanying the Glass Transition Direct Experimental Evidence of a Growing Length Scale. *Science* **2005**, *310*, 1797−1800.
(22) Dalle-Ferrier, C.; Thibierge, C.; Alba-Simionesco, C.; Berthier, L.; Biroli, G.; Bouchaud, J.-P.; Ladieu, F.; L'Hôte, D.; Tarjus, G. Spatial correlations in the dynamics of glassforming liquids: Experimental determination of their temperature dependence. *Phys. Rev. E* **2007**, *76*, 041510-1−041510-15.
(23) Berthier, L. Dynamic heterogeneity in amorphous materials. *Physics* **2011**, *4*, 42-1−42-7.
(24) Roland, C. M.; Fragiadakis, D.; Coslovich, D.; Capaccioli, S.; Ngai, K. L. Correlation of nonexponentiality with dynamic heterogeneity from four-point dynamic susceptibility $\chi 4(t)$ and its approximation $\chi T(t)$. *J. Chem. Phys.* **2010**, *133*, 124507.
(25) Fragiadakis, D.; Casalini, R.; Roland, C. M. Comparing dynamic correlation lengths from an approximation to the four-point dynamic susceptibility and from the picosecond vibrational dynamics. *Phys. Rev. E* **2011**, *84*, 042501.
(26) Grzybowski, A.; Kolodziejczyk, K.; Koperwas, K.; Grzybowska, K.; Paluch, M. Effects of lowering temperature and raising pressure on the spatially heterogeneous dynamics of glass-forming van der Waals liquids. *Phys. Rev. B* **2012**, *85*, 220201(R).
(27) Shi, X. M.; Zhang, J.; Jin, J.; Chen, S. J. Non-isothermal crystallization and melting of ethylene-vinyl acetate copolymers with different vinyl acetate contents. *eXPRESS Polym. Lett.* **2008**, *2*, 623−629.
(28) Böhm, N.; Kulicke, W.-M. Rheological studies of barley (1→3)(1→4)-β-glucan in concentrated solution: mechanistic and kinetic investigation of the gel formation. *Carbohydr. Res.* **1999**, *315*, 302−311.
(29) Massalska-Arodz, M.; Williams, G.; Smith, I. K.; Conolly, C.; Aldridge, G. A.; Dabrowski, R. Molecular dynamics and crystallization behaviour of isopentyl cyanobiphenyl as studied by dielectric relaxation spectroscopy. *J. Chem. Soc., Faraday Trans.* **1998**, *94*, 387−394.
(30) Abu-Sehly, A. A. Study of the kinetics of non-isothermal crystallization in $Ge_{20}Te_{80}$ chalcogenide glass. *Physica B* **2003**, *325*, 372−379.
(31) Supaphol, P.; Apiwanthanakorn, N. Nonisothermal cold-crystallization kinetics of poly(trimethylene terephthalate). *J. Polym. Sci., B: Polym. Phys.* **2004**, *42* (22), 4151−4163.
(32) Zeng, J. B.; Srinivansan, M.; Li, S. L.; Narayan, R.; Wang, Y. Z. Nonisothermal and Isothermal Cold Crystallization Behaviors of Biodegradable Poly(p-dioxanone). *Ind. Eng. Chem. Res.* **2011**, *50*, 4471−4477.
(33) Viciosa, M. T.; Correia, N. T.; Salmerón Sanchez, M.; Carvalho, A. L.; Romão, M. J.; Gómez Ribelles, J. L.; Dionísio, M. Real-Time Monitoring of Molecular Dynamics of Ethylene Glycol Dimethacrylate Glass Former. *J. Phys. Chem. B* **2009**, *113*, 14209−14217.
(34) Havriliak, S.; Negami, S. *J. Polym. Sci. C* **1966**, *14*, 99.
(35) Vogel, H. Das Temperaturabhangigkeitgesetz der Viskosität von Flüssigkeiten. *J. Phys. Z.* **1921**, *22*, 645−646.
(36) Fulcher, G. S. Analysis of Recent Measurements of the Viscosity of Glasses. *J. Am. Ceram. Soc.* **1925**, *8*, 339−355.
(37) Tammann, G.; Hesse, W. Die Abhängigkeit der Viscosität von der Temperatur bie unterkühlten Flüssigkeiten. *Z. Anorg. Allg. Chem.* **1926**, *156*, 245−257.
(38) Wang, L.-M.; Velikov, V.; Angell, C. A. Direct determinetaion of kinetic fragility indicates of glassforming liquids by differentional scanning calorimetry: Kinetic versus thermodynamic fragilities. *J. Chem. Phys.* **2002**, *117*, 10184−10355.
(39) Wang, L.-M.; Angell, C. A. Response to "Comment on 'Direct determination of the fragility indexes of glassforming liquids by differential scanning calorimetry. Kinetic vs thermodynamic fragilities'". *J. Chem. Phys.* **2003**, *118*, 10353−10355.
(40) Tanaka, H. Relationship among glass-forming ability, fragility, and short-range bond ordering of liquids. *J. Non-Cryst. Solids* **2005**, *351*, 678−690.
(41) Sanz, A.; Nogales, A.; Ezquerra, T. A. Influence of Fragility on Polymer Cold Crystallization. *Macromolecules* **2010**, *43*, 29−32.
(42) Napolitano, S.; Wübbenhorst, M. Effect of a reduced mobility layer on the interplay between molecular relaxations and diffusion limited crystallization rate in ultrathin polymer films. *J. Phys. Chem. B* **2007**, *111*, 5775−5780.
(43) Caron, V.; Bhugra, C.; Pikal, M. J. Prediction Of Onset Of Crystallization In Amorphous Pharmaceutical Systems: Phenobarbital, Nifedipine/PVP, and Phenobarbital/PVP. *J. Pharm. Sci.* **2010**, *99*, 3887−3900.
(44) Korhonen, O.; Bhugra, C.; Pikal, M. J. Correlation between Molecular Mobility and Crystal Growth of Amorphous Phenobarbital and Phenobarbital with Polyvinylpyrrolidone and L-Proline. *J. Pharm. Sci.* **2008**, *97*, 3830−3841.
(45) Bhugra, C.; Shmeis, R.; Krill, S. L.; Pikal, M. J. Prediction of Onset of Crystallization from Experimental Relaxation Times. II. Comparison between Predicted and Experimental Onset Times. *J. Pharm. Sci.* **2008**, *97*, 455−472.
(46) Saika-Voivod, I.; Bowles, R. K.; Poole, P. H. Crystal Nucleation in a Supercooled Liquid with Glassy Dynamics. *Phys. Rev. Lett.* **2009**, 225701.
(47) Kawasaki, T.; Araki, T.; Tanaka, H. Correlation between Dynamic Heterogeneity and Medium-Range Order in Two-Dimensional Glass-Forming Liquids. *Phys. Rev. Lett.* **2007**, *99*, 215701.
(48) Abate, A. R.; Durian, D. J. Topological persistence and dynamical heterogeneities near jamming. *Phys. Rev. E* **2007**, *76*, 021306.
(49) S. Capaccioli, S.; Ruocco, G.; Zamponi, F. Dynamically correlated regions and configurational entropy in supercooled liquids. *J. Phys. Chem. B* **2008**, *112*, 10652−10658.
(50) Adrjanowicz, K.; Grzybowski, A.; Grzybowska, K.; Kolodziejczyk, K.; Kaminski, K.; Ziolo, J.; Paluch, M. From Heterogeneous to Homogeneous-Like Dynamics: Behavior of Dynamic Heterogeneity and Crystallization Tendency of Supercooled Indomethacin under Compression. (Submitted.)
(51) Adam, G.; Gibbs, J. H. On the temperature dependence of cooperative relaxation properties in glass forming liquids. *J. Chem. Phys.* **1965**, *43*, 139−146.
(52) Shamblin, S. L.; Tang, X.; Chang, L.; Hancock, B. C.; Pikal, M. J. Characterization of the time scales of molecular motion in pharmaceutically important glasses. *J. Phys. Chem. B* **1999**, *103*, 4113−4121.
(53) Hodge, I. M. Strong and fragile liquids—a brief critique. *J. Non-Cryst. Solids* **1996**, *202*, 164−172.
(54) Hancock, B. C.; Shamblin, S. L. Molecular mobility of amorphous pharmaceuticals determined using differential scanning calorimetry. *Thermochim. Acta* **2001**, *380*, 95−107.
(55) Ngai, K. L.; Paluch, M. Classification of secondary relaxation in glass-formers based on dynamic properties. *J. Chem. Phys.* **2004**, *120*, 857−873.
(56) Ngai, K. L. An extended coupling model description of the evolution of dynamics with time in supercooled liquids and ionic conductors. *J. Phys.: Condens. Matter* **2003**, *15*, S1107.

3.1.1 Oświadczenia współautorów publikacji I

prof. zw. dr hab. Marian Paluch
Uniwersytet Śląski
Instytut Fizyki im. Augusta Chełkowskiego
ul. Uniwersytecka 4
40-007 Katowice

Katowice, 24 lutego 2016 r.

OŚWIADCZENIE

Oświadczam, że w pracy K. Kolodziejczyk, M. Paluch, K. Grzybowska, A. Grzybowski, Z. Wojnarowska, L. Hawelek, J. D. Ziolo, *Molecular Pharmaceutics,* 2013, 10 (6), pp 2270–2282 zatytułowanej „*Relaxation Dynamics and Crystallization Study of Sildenafil in the Liquid and Glassy State“,* mój udział polegał na polegał na nadzorowaniu przeprowadzonych analiz, dyskusji otrzymanych wyników oraz korekcie tekstu manuskryptu.

dr Katarzyna Grzybowska
Uniwersytet Śląski
Instytut Fizyki im. Augusta Chełkowskiego
ul. Uniwersytecka 4
40-007 Katowice

Katowice, 24 lutego 2016 r.

OŚWIADCZENIE

Oświadczam, że w pracy K. Kolodziejczyk, M. Paluch, K. Grzybowska, A. Grzybowski, Z. Wojnarowska, L. Hawelek, J. D. Ziolo, *Molecular Pharmaceutics,* 2013, 10 (6), pp 2270–2282 zatytułowanej „*Relaxation Dynamics and Crystallization Study of Sildenafil in the Liquid and Glassy State",* mój udział polegał na nadzorowaniu przeprowadzonych analiz, dyskusji otrzymanych wyników oraz korekcji tekstu manuskryptu.

Katarzyna Grzybowska

dr hab. Andrzej Grzybowski
Uniwersytet Śląski
Instytut Fizyki im. Augusta Chełkowskiego
ul. Uniwersytecka 4
40-007 Katowice

Katowice, 24 lutego 2016 r.

OŚWIADCZENIE

Oświadczam, że w pracy K. Kolodziejczyk, M. Paluch, K. Grzybowska, A. Grzybowski, Z. Wojnarowska, L. Hawelek, J. D. Ziolo, *Molecular Pharmaceutics,* 2013, 10 (6), pp 2270–2282 zatytułowanej „*Relaxation Dynamics and Crystallization Study of Sildenafil in the Liquid and Glassy State",* mój udział polegał na konsultacji przedstawionej w artykule analizy korelacji między stopniem heterogeniczności dynamicznej sildenafilu a skalami czasowymi, charakteryzującymi kinetykę procesu krystalizacji tej substancji leczniczej.

dr Żaneta Wojnarowska
Uniwersytet Śląski
Instytut Fizyki im. Augusta Chełkowskiego
ul. Uniwersytecka 4
40-007 Katowice

Katowice, 24 lutego 2016 r.

OŚWIADCZENIE

Oświadczam, że w pracy K. Kolodziejczyk, M. Paluch, K. Grzybowska, A. Grzybowski, Z. Wojnarowska, L. Hawelek, J. D. Ziolo, *Molecular Pharmaceutics,* 2013, 10 (6), pp 2270–2282 zatytułowanej „*Relaxation Dynamics and Crystallization Study of Sildenafil in the Liquid and Glassy State",* mój udział polegał na pomocy podczas wykonywania pomiarów dielektrycznych oraz w analizie wyników.

dr Łukasz Hawełek
Instytut Metali Nieżelaznych
ul. Sowińskiego 5
44-100 Gliwice

Katowice, 7 stycznia 2016 r.

OŚWIADCZENIE

Oświadczam, że w pracy K. Kolodziejczyk, M. Paluch, K. Grzybowska, A. Grzybowski, Z. Wojnarowska, L. Hawelek, J. D. Ziolo, Molecular Pharmaceutics, 2013, 10 (6), pp 2270–2282 zatytułowanej „*Relaxation Dynamics and Crystallization Study of Sildenafil in the Liquid and Glassy State*“, mój udział polegał na pomiarach i analizie danych szerokokątowej dyfrakcji rentgenowskiej.

Jerzy Dawid Zioło
ul. Polanka 8c/10
61-131 Poznań

Katowice, 7 stycznia 2016 r.

OŚWIADCZENIE

Oświadczam, że w pracy K. Kolodziejczyk, M. Paluch, K. Grzybowska, A. Grzybowski, Z. Wojnarowska, L. Hawelek, J. D. Ziolo, Mol. Pharmaceutics, 2013, 10 (6), pp 2270–2282 zatytułowanej *„Relaxation Dynamics and Crystallization Study of Sildenafil in the Liquid and Glassy States”,* mój udział polegał na pomocy w rejestracji danych pomiarowych.

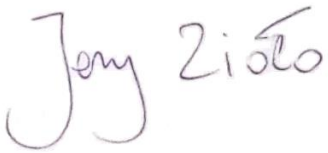

3.2 PUBLIKACJA II

BADANIE KINETYKI KRYSTALIZACJI SILDENAFILU W WARUNKACH IZOTERMICZNYCH

Autorzy:

K. Kolodziejczyk, K. Grzybowska, Z. Wojnarowska, M. Dulski, L. Hawelek, M. Paluch

Referencje:

Crystal Growth & Design, 2014, 14 (7), pp 3199-3209

Skrót:

W artykule opisaliśmy krystalizację sildenafilu w warunkach izotermicznych. Kinetykę krystalizacji badaliśmy za pomocą różnicowej kalorymetrii skaningowej (DSC), rentgenografii strukturalnej (XRD) oraz mikroskopii optycznej (OM). Do analizy otrzymanych danych wykorzystany została model Avramiego i Avramiego-Avramova. Modele te pozwoliły scharakteryzować parametry krystalizacji takie jak szybkość tego procesu, wymiarowość zarodków oraz energię aktywacji krystalizacji. Analiza wykazała, że model Avramiego i Avramiego-Avramova może być stosowany wymiennie do opisu kinetyki krystalizacji, ponieważ otrzymane parametry różnią się jedynie nieznacznie od siebie. Co więcej, pomiary optyczne pozwoliły na oszacowanie czasu potrzebnego na uformowanie się zarodków, ich rozmieszczenia (gęstości nukleacji) i wielkości krystalitów. Ponadto podczas obserwacji wzrostu kryształów zauważyliśmy pofałdowanie powierzchni próbki przed pojawieniem się jąder kryształów. Zachowanie to może być związane z formowaniem się wiązań wodorowych pomiędzy cząsteczkami sildenafilu, co potwierdzone zostało obliczeniami teoretycznymi.

CRYSTAL GROWTH & DESIGN

Article

pubs.acs.org/crystal

Isothermal Cold Crystallization Kinetics Study of Sildenafil

K. Kolodziejczyk,*[,†] K. Grzybowska,[†] Z. Wojnarowska,[†] M. Dulski,[†] L. Hawelek,[†,‡] and M. Paluch[†]

[†]Institute of Physics, University of Silesia, ul. Uniwersytecka 4, 40-007 Katowice, Poland

[‡]Institute of Non Ferrous Metals, ul. Sowinskiego 5, 44-100 Gliwice, Poland

ABSTRACT: Isothermal cold crystallization of sildenafil, which is used as API of Viagra, was investigated by differential scanning calorimetry, optical microscopy, and X-ray diffraction. To analyze the kinetics of crystallization Avrami and Avramov approaches were used. These two models enabled us to characterize basic parameters such as crystallization constant rate (k), dimensionality (n) and activation energy of the crystallization process. It was found that the value of parameter n only slightly changes with temperature, indicating the same mechanism of crystallization. Moreover, we found that the activation energies for the crystallization process obtained from the all applied methods are comparable. From the optical measurements, it was possible to estimate the time of the nuclei formation, the nucleation density, sizes of the forming embryos and crystals at each temperature as well as the crystal morphology and habit. Additionally, monitoring the crystallization process by optical microscopy, we observed unexpected corrugations of the sample surface before the nucleation begins. This behavior can be related to the phenomenon of H-bond formation between molecules of sildenafil.

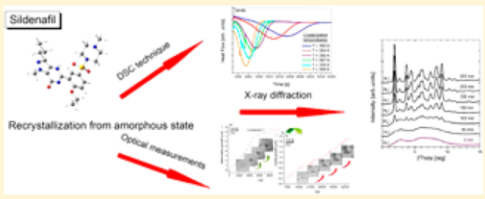

1. INTRODUCTION

There is still growing interest in the problem of nucleation and crystal growth both from theorists[1] and experimentalists[2−5,7−10] because a great importance of the crystallization phenomenon in various fields of science and technology. It is a well-known fact that crystallization process may play both positive and negative roles. In the pharmaceutical industry, on the one hand, it can be exploited for separation, purification, filtration, and drying during synthesis of active pharmaceutical ingredients[2,3] but, on the other hand, is undesired phenomenon in case of amorphous drugs. Physical instability of amorphous drugs and their ability to recrystallization become a serious problem in pharmacy that needs to be solved immediately.

In order to find a way how to avoid uncontrolled recrystallization of glassy (amorphous) materials, all key factors that influence on nucleation and the crystal growth[4] have to be recognized. Undoubtedly, the nucleation is the first and the most important stage of crystallization controlling the overall crystallization process. Therefore, the careful analysis and understanding the nucleation process along with the crystal growth can provide a valuable information which enable to create and produce drugs having desired physicochemical properties.

The investigations of the nucleation process may be carried out under nonisothermal and isothermal conditions. This is a key point, because conditions that occur during the process of production and storage have a significant impact on stability and properties of pharmaceuticals. In order to find the optimal conditions for industrial production and, consequently, to obtain amorphous drugs with better physical stability, it is necessary to study the crystallization process at nonisothermal conditions. On the other hand, the isothermal crystallization studies are essential to predict how long the drug will last in amorphous state during storage at given conditions.[5,6]

There is a number of experimental techniques widely used for investigation of crystallization process of amorphous pharmaceuticals, for example, X-ray techniques (XRD and SAXS)[7,8] differential scanning calorimetry,[9−11] dielectric spectroscopy,[12] and microscopic techniques (polarized light microscopy, SEM, AFM, TEM).[9,13,14] Each of these methods allows to determine characteristic parameters describing the crystallization process, that is, induction time, dimensionality of formed nucleus and the rate of crystal growth during crystallization, radius of the length crystals, morphology and crystal habit.

In this Article, we focus on a study of the kinetics of the crystallization process under isothermal conditions. From the experimental point of view, the most frequently used method to study the isothermal crystallization is a differential scanning calorimetry (DSC). When a material crystallizes, a measurable amount of heat is evolved, resulting in an exothermic peak in the DSC thermal curve. The shape of this peak is directly related to the kinetics of crystallization. Moreover, measurement of the isothermal crystallization makes possible to determine a half-lifetime ($t_{1/2}$), which can be used as a measure of crystallization speed. However, from DSC measurements it is not possible to separate activation barriers for the nucleation and the crystal growth.

Optical methods are employed to monitor temporary changes occurring on the surface of the sample, embryos

Received: September 12, 2013
Revised: May 8, 2014
Published: May 30, 2014

formation and to visually track the crystal growth. However, information derived from the optical measurements are limited to observation of the processes occurring on the surface of crystallites. Consequently, this knowledge might be not sufficient in many cases, because of inadequate information about the internal structure of formed embryo crystals.

However, to determine the internal structure of the formed crystallites, X-ray technique should be used. This method allows to identify and determine the crystal structures in the sample and quantify the degree of crystallinity of the sample.

The sample chosen for our studies was sildenafil, which is an active pharmaceutical ingredient (API) of Viagra, and is used in the treatment of erectile dysfunction, as well as pulmonary arterial hypertension. Amorphous form of sildenafil was obtained by quench-cooling of the melt. This API has already been the subject of our previous investigations,[15] which revealed that sildenafil has a strong tendency to recrystallization from the supercooled liquid state. In our previous paper, we focused on the study of relaxation dynamics and crystallization kinetics of supercooled sildenafil by means of broadband dielectric spectroscopy. The chief motivation of this work is to provide a complete description of the crystallization process of sildenafil by performing isothermal DSC, X-ray and optical measurements.

2. EXPERIMENTAL SECTION

2.1. Materials. The investigated drug, sildenafil (of 99,8% purity) ($C_{22}H_{30}N_6O_4S$, M_w = 474.57 g/mol, IUPAC name: 5-[2-ethoxy-5-(4-methylpiperazin-1-yl)sulfonylphenyl]-1-methyl-3-propyl-4H-pyrazolo[4,3-*d*] pyrimidin-7-one) was delivered from Polpharma in Starogard Gdanski as a white crystalline powder. This drug is used in the treatment of erectile dysfunction and pulmonary arterial hypertension.

Amorphous samples were prepared by quench-cooling technique; crystalline form of sildenafil has been heated to the melting point (T_m = 462 K) and then rapidly cooled. The glass transition temperature of the amorphous sildenafil is equal 329 K[15]

2.2. Methods. *2.2.1. Differential Scanning Calorimetry (DSC).* Measurements of the isothermal cold crystallization were carried out by Mettler-Toledo DSC apparatus equipped with a liquid nitrogen cooling accessory and a HSS8 ceramic sensor (heat flux sensor with 120 thermocouples). Temperature and enthalpy calibrations were performed by using indium and zinc standards. The amorphous form of sildenafil was prepare in open aluminum crucible (40 μL) outside DSC apparatus. First, the sample of crystalline sildenafil powder was packed into a DSC pan, heated on the heating plate (CAT M 17.S) to melting temperature and than quickly quench-cooled to vitrify the sample. Crucibles with such prepared glassy samples have been put into DSC apparatus and time dependence measurements of heat flow where performed at various temperatures: 352, 354, 356, 357, 358, and 359 K. The sample was heated from room temperature to crystallization temperatures at 20 K/min under nitrogen purge. For each experiment a new amorphous sample was prepared. Each measurement at given temperature was repeated 3 times. All DSC sample weights were in the range of 9.5−9.7 mg. Analysis of measurements curves were performed by using the software of the DSC instrument. Humidity during the isothermal crystallization done using DSC (in nitrogen atmosphere with the flow rate 60 mL/min) was close to 0%.

2.2.2. X-ray Diffraction (XRD). The X-ray diffraction measurements were carried out on the laboratory Rigaku-Denki D/MAX RAPID II-R diffractometer attached with a rotating anode Ag Kα tube (λ = 0.5608 Å), an incident beam (0 0 2) graphite monochromator and an image plate in the Debye-Scherrer geometry. The pixel size was 100 μm × 100 μm. Crystalline and amorphous samples of sildenafil were placed inside glass capillaries (1.5 mm in diameter). Measurements were performed for the sample filled and empty capillaries and the intensity for the empty capillary was then subtracted. The beam width at the sample was 0.1 mm. The two-dimensional diffraction patterns were converted into the one-dimensional intensity data using suitable software.

Examined sample was prepared in the following manner: crystalline sildenafil was placed in a glass capillary, then melted, and rapidly cooled. Capillary with vitrified sildenafil was placed in the diffractometer. During the study, first, the sample was heated to temperature of measurement (that is, in the supercooled liquid state), and then, it was observed a progress of the crystallization of amorphous sildenafil over the time. Sample remained in the X-ray diffractometer during entire experiment. Measurements were performed at various temperatures 348, 350, 352, and 356 K. Humidity during the isothermal crystallization done using PXRD (in closed capillary) was close to 0%. For each experiment, a new amorphous sample was prepared. Each measurement at given temperature was repeated 3 times.

2.2.3. Optical Measurements. The optical measurements were carried out by using Olympus BX51 polarized light microscope, equipped with an Olympus SC30 camera and a halogen source light. Optical figures were collected using Olympus Soft Imaging Solutions GmbH 5.1 (analysis CellÂ software) at UMPlanFI 10× and 50× objective and at 0.30 aperture. Additionally, whole stored microphotography were corrected by CellÂ and Adobe Photoshop 12 software. Amorphous sample of sildenafil was prepared on the glass slide. Measurements were preformed at several temperatures: 323, 333, 343, 348, 350, 352, 354, and 356 K. The temperature of the sample was stabilized with accuracy ±0.1 K by a temperature controller. In the first part of optical measurements microphotography were recorded from 1 to 14 min, whereas in the second part from 5 to 25 min depends on the temperature condition. For each experiment a new amorphous sample was prepared. Each measurement at given temperature was repeated twice.

2.2.4. Infrared Measurements (IR). Infrared measurements were performed using an Agilent Cary 660 FTIR spectrometer equipped with a standard source and a DTGS Peltier-cooled detector. The crystalline and glassy spectra of sildenafil have been collected using GladiATR diamond accessory (Pike Technologies) equipped with temperature controller in the range 4000−380 cm^{-1}. All spectra were accumulated with a spectral resolution of 2 cm^{-1}, and the interferograms were recorded by accumulating 16 scans. Isothermal infrared were also carried out with the temperature accuracy of ±0.1 K.

2.2.5. Theoretical Calculation. The geometries of the sildenafil have been fully optimized using Becke's hybrid exchange and correlated three-parameter with the Lee−Yang−Parr correlation functional (B3LYP)[16−18] and standard Gaussian basis sets 6-31G(d,p).[18] These calculations were carried out in the gas phase using density functional theory (DFT) calculations,[19−21] and the Gaussian09 software package.[21] The optimized molecules with the labeling system used

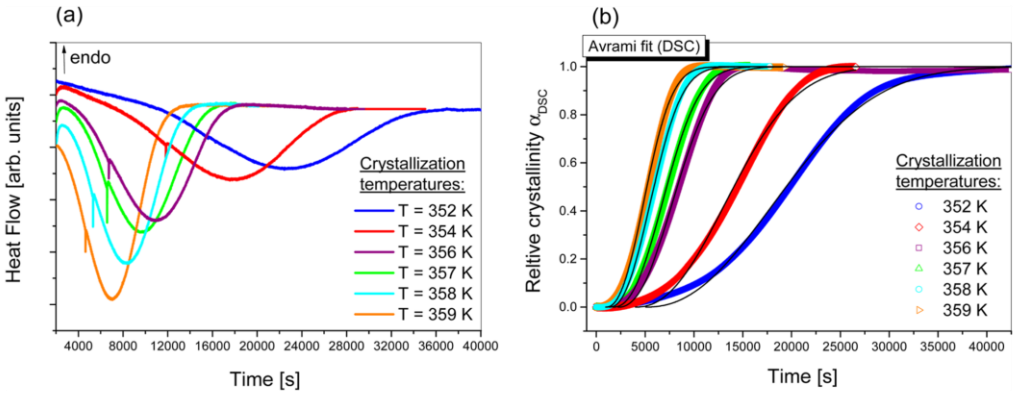

Figure 1. (a) Heat flow versus time during the isothermal crystallization of sildenafil at the different crystallization temperatures measured by DSC. (b) Plots of relative crystallinity α_{DSC} versus crystallization time (t) for sildenafil during isothermal crystallization. Solid line represent Avrami fits in terms of eq 2

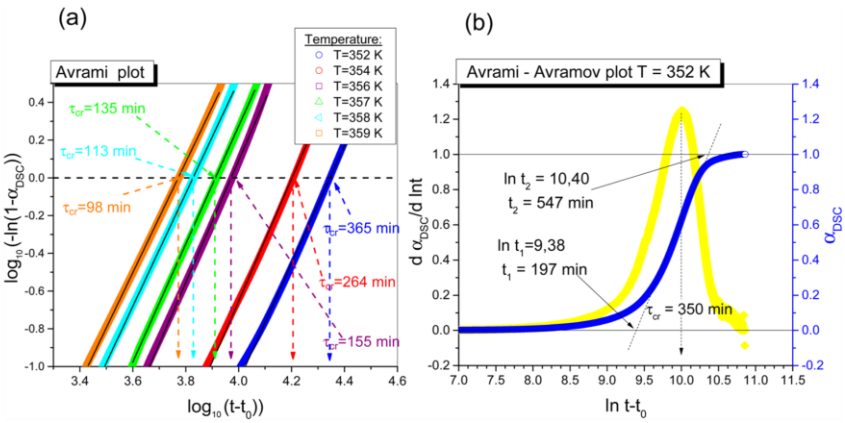

Figure 2. (a) Avrami plot: the plots of $\log[-\ln(1 - \alpha_{DSC}(t))]$ versus $\log_{10}$ $(t - t_0)$ at the labeled temperatures for each isothermal crystallization temperature in the linear range obtained from X-ray measurements. The crystallization time τ_{cr} was designated from $\log[-\ln(1 - \alpha_{DSC}(t))] = 0$. (b) Avrami–Avramov plot: Time evolution of the normalized degree of crystallization α_{DSC} and its first derivative with respect to the natural logarithm of the time in T_c = 352 K. All the parameters obtained from the Avrami plot and Avrami–Avramov plot were collected in Table 1

for the present calculations were visualized using GaussView 5.0.8 software. These optimized geometries structures were used as input files for vibrational harmonic calculation. On the basis of these calculations, all conformers have positive harmonic vibrations indicating a true energy minimum.[22]

3. RESULTS AND DISCUSSION

As previously mentioned, the main objective of this work is to investigate the crystallization process of amorphous sildenafil at isothermal conditions using three different experimental methods: DSC, XRD, and optical technique. The experimental results are analyzed in terms of the Avrami and Avramov models.

3.1. Differential Scanning Calorimetry (DSC). The isothermal cold crystallization kinetics of sildenafil was monitored by DSC at six different temperatures: 352, 354, 356, 357, 358, and 359 K.

Figure 1 shows the exothermic peaks of isothermal crystallization at labeled temperatures. It can be seen that the maximum of the exothermic peak in the DSC curve shifts toward a longer time values with lowering of the crystallization temperature (T_c), indicating that the T_c is an important factor affecting the crystallization time.

On the basis of the data obtained from DSC, it is possible to estimate the relative degree of crystallization α_{DSC}. In case of DSC measurements, this parameter is defined as follows:

$$\alpha_{DSC} = \frac{\int_{t_0}^{t} \frac{dH}{dt} dt}{\int_{t_0}^{t_\infty} \frac{dH}{dt} dt} = \frac{A_t}{A_\infty} \quad (1)$$

Table 1. Comparison of Parameters Estimated from Avrami and Avramov Models for Kinetisc of Isothermal Crystallization Obtained from DSC Measurements

	DSC measurements								
	Avrami[a]				Avramov model[b]				
T_c [K]	n	t_0 [min]	τ_{cr} [min]	k [s^{-1}]	n eq 5	n (eq 6)	t_0 [min]	τ_{cr} [min]	$k = 1/\tau_{cr}$ [s^{-1}]
352	3.13	84	365	4.55×10^{-5}	3.38	3.33	12	350	4.63×10^{-05}
354	3.23	66	264	6.20×10^{-5}	3.49	3.80	7	263	6.34×10^{-05}
356	3.29	37	155	1.24×10^{-4}	3.30	3.25	5	155	1.07×10^{-4}
357	3.12	28	135	1.20×10^{-4}	3.05	3.03	4	134	1.24×10^{-4}
358	2.99	21	113	1.47×10^{-4}	3.06	2.97	2	112	1.48×10^{-4}
359	2.92	15	98	1.67×10^{-4}	2.98	2.97	1	101	1.65×10^{-4}

[a] $E_a = 203 \pm 21$ kJ/mol. [b] $E_a = 211 \pm 8$ kJ/mol.

where dH/dt is the rate of heat evolution, t_0 and t_∞ is the time at which crystallization starts and ends, and A_t and A_∞ are areas under normalized DSC curve for the partially and fully crystalline material, respectively.

The time evolutions of the degree of crystallization α as determined from DSC measurements at different temperatures during isothermal crystallization are displayed in Figure 1b. The kinetics curves have been normalized by the maximal value of the parameter α_{DSC} measured after the crystallization is completed. Note that all curves have a characteristic sigmoidal shape. Moreover, the curves are shifted toward a shorter time with increasing T_c. This effect is due to the decrease in the crystallization time upon increasing temperature.

One of the most prominent models commonly used to describe the crystallization kinetics is one proposed by Avrami[23,24]

$$\alpha(t) = 1 - \exp(-K(t - t_0)^n) \tag{2}$$

where $\alpha(t)$ is a degree of crystallization, $K = k^n$ is a crystallization rate constant, which depends on a crystallization temperature and geometry of sample, n is the Avrami exponent that is related to the time dependence of the nucleation rate and to the dimensionality of the crystallization and t_0 is the induction time of crystallization. The time dependence of degree of crystallization obtained from DSC measurements were fitted by the Avrami function (eq 2) (see Figure 1b). However, because of not very good fitting of measuring points in the entire time range we applied a convenient and more accurate method to analyze the sildenafil crystallization kinetics based on the conversion of eq 2 to its logarithmic form

$$\log[-\ln(1 - \alpha(t))] = \log K + n \log(t - t_0) \tag{3}$$

The above equation suggests that the dependence of $\log[-\ln(1 - \alpha)]$ on $\log(t - t_0)$ should be a linear function. Consequently, one can estimate the values of n and $\log K$ by using a simple linear regression. In Figure 2a, the Avrami plot constructed based on eq 3 is presented for DSC data. The shown Avrami plots have been limited to their linear range at each temperature of crystallization. Therefore, parameters n and K can be easily determined for sildenafil as the slope and the intercept of these curves, receptively. From the Avrami plots, we also calculated the characteristic time of crystallization, τ_{cr} for each temperature. This time constant was evaluated from the condition $\log[-\ln(1 - \alpha(t))] = 0$

Since the Avrami plots in fact do not hold the linear character in the entire time range, which has been not shown in Figure 2, we additionally analyzed the isothermal crystallization kinetics of sildenafil by using the approach recently proposed by Avramov et al.[25]

$$\alpha(t) = 1 - \exp\left(-\left(\frac{t - t_0}{\tau_{cr}}\right)^n\right) \tag{4}$$

where τ_{cr} is a characteristic time for the isothermal overall crystallization, which is related to the Avrami parameters as follows: $\tau_{cr} = K^{-1/n}$. The parameters n and t_0 have the same meaning as the ones in the Avrami model (eq 2). All the parameters that characterize the crystallization process can be easily determined by plotting the first derivative of crystallization degree $d\alpha(t)/d(\ln(t - t_0))$ versus $\ln(t - t_0)$. To obtain n and τ_{cr} for the crystallization process, we need to superimpose the dependence $\alpha_{DSC}(\ln(t - t_0))$ at the same graph. Such a typical plot, constructed for DSC data, is shown in Figure 2b. It is worth noting that the first derivative of the Avramov function $\alpha'(t)$ possesses its maximum at the crystallization time, τ_{cr}. If we substitute $t - t_0 = \tau_{cr}$ in eq 4, we get the following relationship $\alpha(\tau_{cr}) = 1 - 1/e \approx 0.63$. However, we usually obtain that $\alpha(\tau_{cr}) < 0.63$ from experimental dependences $\alpha(t)$. It means that the induction time $t_0 > 0$. In this case, we can estimate the proper value of t_0 by finding t from the condition $\alpha = 0.63$ and then calculating $t_0 = t - \tau_{cr}$. The value of n can be estimated from the following equation

$$n = \frac{(\alpha(t))'_{max}}{0.368} \tag{5}$$

where $(\alpha(t))'_{max}$ is a maximum of the first derivative of the normalized degree of crystallization. There is an alternative way to evaluate the parameter n. One can draw (see Figure 2b) a tangent to the experimentally determined sigmoidal curve $\alpha_{DSC}(\ln(t - t_0))$ at $t - t_0 = \tau_{cr}$ and read abscissas $\ln t_1$ and $\ln t_2$ of the points of its intersection with the horizontal straight lines determined at the limit values of $\alpha_{DSC} = 0$ and 1, respectively. Then, the parameter n can be estimated from the following equation

$$n = \frac{e}{\ln t_2 - \ln t_1} \tag{6}$$

On the basis of the Avrami and Avramov models, we obtained parameters that characterize the crystallization kinetics of sildenafil. Results from DSC measurements were collected in Table 1. As can be seen, the values of the parameters n, k, t_0, and τ_{cr} are nearly independent of the choice of the model. Only the values of the parameter t_0 are slightly different. This discrepancy can be explained by the fact that the experimental data are not well described by the Avrami function (eq 2), as

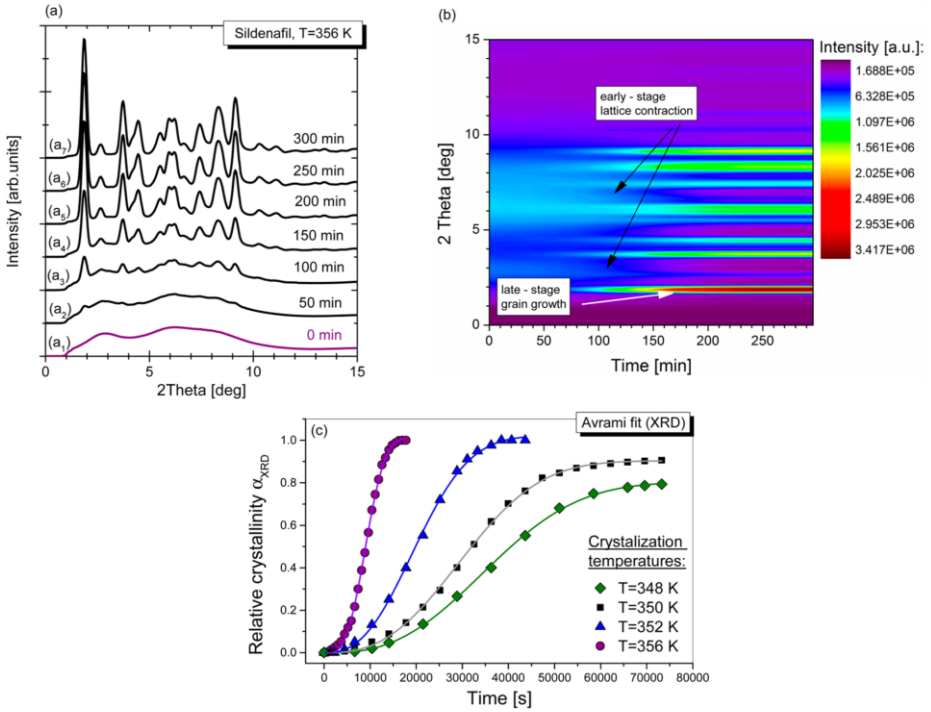

Figure 3. (a) X-ray diffraction patterns for sildenafil performed at temperature T_c =356 K: (a_1) initial amorphous form prepared by quench-cooling of the melt of crystal and (a_2–a_7) gradual increase Bragg's reflects indicating isothermal recrystallization of the amorphous form observed at time periods from 0 to 300 min. (b) Color map, from small local rearrangements cause a change in structure from liquid-like (violet/blue, low intensity) to crystal-like (red, high intensity). (c) Plots of relative crystallinity α versus crystallization time (t) for sildenafil during isothermal crystallization. Solid line represents Avrami fits in terms eq 8

shown in Figure 1b. Moreover, we found that the values of the parameter n oscillate around 3 in both the considered models, whereas the values of the crystallization rate k and the crystallization time τ_{cr} increase and decrease with increasing the temperature of crystallization, respectively.

3.2. X-ray Diffraction (XRD). The second method we applied to study the isothermal crystallization of sildenafil was X-ray diffraction. Figure 3 shows a time evolution of the XRD patterns characteristic for the crystallization process, which has been monitored during isothermal annealing of the sildenafil at T_c = 356 K. The diffraction pattern (a_1) was measured for the sample obtained immediately after vitrification. As can be seen in the diffraction pattern (a_1) in Figure 3a, the amorphous sample is characterized by a broad halo, and there is no the Bragg reflections characteristic for the crystalline structures. However, as crystallization proceeds a small diffraction peaks start to appear and their intensity increases with time (diffractions patterns a_2–a_7 in Figure 3). This behavior indicates the increase in the degree of crystallization of sample. In Figure 3b, the color intensity map is displayed. This map was created from a time sequence of XRD patterns as the snapshots taken during 300 min. The different stages of the crystallization process as well as the structural transformations (grain growth, lattice contraction, chemical ordering) can be identified as indicated by arrows. One can observe that a small local rearrangements cause a change in the structure from liquid-like (violet/blue) to crystal-like (red) state, without the changing of the local density but solely by increasing of the orientation order.

The same analysis was repeated for the data gathered at different temperatures. Analyzing XRD patterns we found that the diffraction peak with the highest intensity occurs at $2\theta \approx 2^\circ$ for each crystallization temperature. The time of appearance and growth of the diffraction peak is strongly dependent on the temperature, that is, the higher the temperature the earlier occurrence of the peak. Naturally, the position of the reflex is related to the symmetry and the unit cell size of formed crystal structure, while the intensity is associated with the distribution of atoms in the cell. On the other hand, the width of the peak in the diffractogram allows to specify the size of crystallites. The width and area of the peak depend on the diffraction pattern, i.e.: the wider peaks, the smaller will be crystals. Comparing the width of the diffraction peaks at each temperature, it appears that the smallest crystallites are formed at a temperature T_c = 348 K, while the largest ones at T_c = 356 K. We also found that the samples always recrystallize to the same, initial crystal form of sildenafil independently of the crystallization temperature.

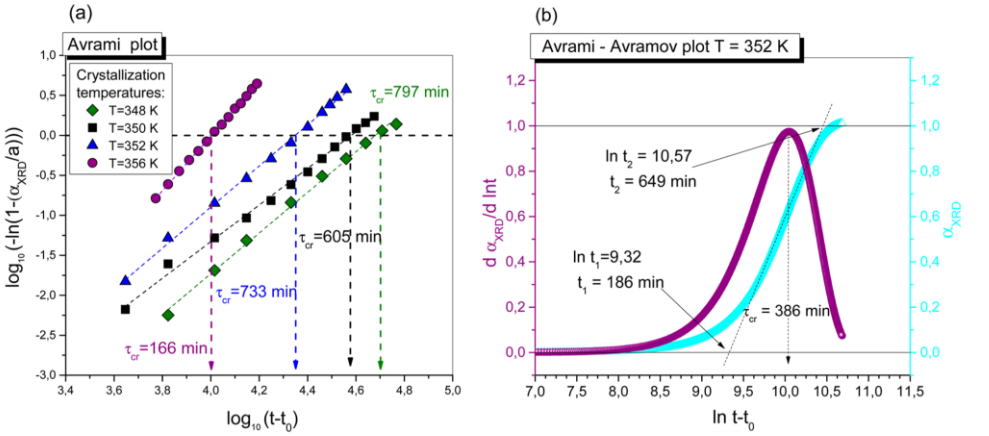

Figure 4. (a) Avrami plot: the plots of log $(-\ln (1 - (\alpha_{XRD}(t))/\alpha))$ versus $\log_{10}(t - t_0)$ at the labeled temperatures for each isothermal crystallization temperature in the linear range obtained from X-ray measurements. The crystallization time τ_{cr} was designated from log $(-\ln(1 - (\alpha_{XRD}(t))/\alpha)) = 0$. (b) Avrami–Avramov plot: Time evolution of the normalized degree of crystallization α_{XRD} and its first derivative toward the natural logarithm of the time in T_c = 352 K XRD method. Parameter a was omitted in this case because for this temperature is equal 1. All the parameters obtained from the Avrami plot and Avrami–Avramov plot were collected in Table 2

Table 2. Comparison of Isothermal Crystallization Parameters Obtained from X-ray Measurements[a]

	X-ray measurements									
	Avrami[b]					Avramov model[c]				
T_c [K]	a	n	t_0 [min]	τ_{cr} [min]	k [s^{-1}]	n (eq 5)	n (eq 6)	t_0 [min]	τ_{cr} [min]	$k = 1/\tau_{cr}$ [s^{-1}]
348	0.80	2.54	10.20	682	2.06×10^{-5}	3.33	2.60	37	682	2.44×10^{-5}
350	0.90	2.29	0	536	2.63×10^{-5}	2.98	2.43	20	581	2.87×10^{-5}
352	1.00	2.57	0	422	4.50×10^{-5}	2.65	2.16	7.7	386	4.31×10^{-5}
356	1.00	3.40	4.93	158	9.79×10^{-5}	3.22	2.65	6	170	9.81×10^{-5}

[a]Values of the X-ray measurements were estimated from Avramov and Avrami model. [b]E_a = 207 ± 15 kJ/mol. [c]E_a = 190 ± 26 kJ/mol.

To find the crystallization kinetics parameters, we determined the degree of crystallization of the samples from XRD measurements using the formula

$$\alpha_{XRD} = \frac{A_P}{A_T} \times 100\% \tag{7}$$

where A_P and A_T are areas of XRD peaks for a partially crystalline sample and a completely crystalline material, respectively. Figure 3c shows the time dependences of the degree of crystallization evaluated in this way at various temperatures. In contrast to the DSC data, sildenafil measured by means of the XRD technique at lower temperatures T_c = 348 and 350 K did not crystallize completely during the crystallization course. Therefore, to describe the curves of the time evolution of the crystallization, we have to use the modified Avrami equation[26]

$$\alpha(t) = a(1 - \exp(-K(t - t_0)^n)) \tag{8}$$

where a is the value for $\alpha(t)$ as t approaches infinity. This modification is related to the incomplete degree of crystallization of the sample. As can be seen in Figure 3c, the modified Avrami equation with the pre-exponential factor a describes the experimental data successfully.

For data obtained from XRD measurements, we also performed (see Figure 4) analyses of the crystallization kinetics using the Avrami plot and the Avramov model modified by the factor a

$$\log\left(-\ln\left(1 - \frac{\alpha_{XRD}(t)}{a}\right)\right) = \log K + n \log(t - t_0) \tag{9}$$

and

$$\alpha_{XRD}(t) = a\left(1 - \exp\left(-\left(\frac{t - t_0}{\tau_{cr}}\right)^n\right)\right) \tag{10}$$

Results for XRD measurements were collected in Table 2. On the basis of the analysis we found that the value of parameter n varies in the range from 2.60 to 3.33 in case of XRD measurements, which well correspond to the values of n obtained from the DSC technique. It suggests the three-dimensional crystallites from instantaneous and sporadic nucleation.[27,28] The slight differences found between the values of n obtained from analysis DSC and XRD measurements can be related to a completely different geometry of the sample in these two experimental methods.

Analyzing the temperature behavior of the other parameter, τ_{cr}, it is obvious that the lowering of temperature of supercooled sildenafil leads to the slowing down of the crystallization process.

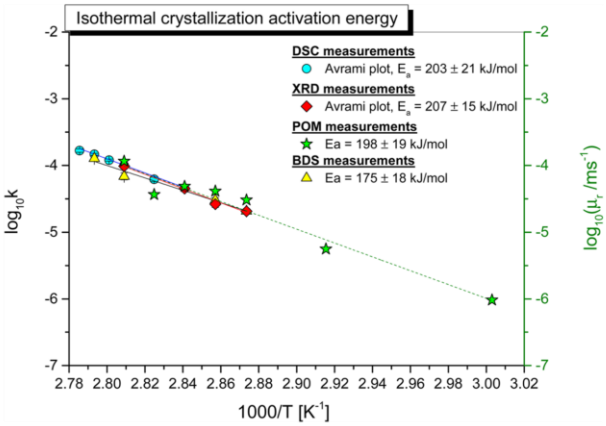

Figure 5. Plot of log k versus $1000/T$ from the Arrhenius plot for isothermal crystallization activation energy of sildeanfil. The plot compares values of the parameter k received from analysis based on the Avrami parameters obtained in studied methods. The line presents the Arrhenius fits.

The value of the constant k increases with increasing temperature of crystallization. Moreover, it turned out that the values of the rate constant k obtained from the above analysis agree reasonably well with the values found using DSC data. These results suggest that the crystallization process is dominated by the diffusion of molecules.[29]

Crystallization Activation Energy. Using the DSC and XRD data, we also determined the activation energy, E_a, of the crystallization of sildenafil by analyzing the temperature dependence of log k. As shown in Figure 5, the logarithm of the crystallization rate depends linearly on the inverse of temperature. It means that the experimental data obeys the Arrhenius law

$$\log k = \log k_0 - \frac{E_a}{RT}\log e \tag{11}$$

where k denotes the crystal growth rate, R is the gas constant, whereas k_0 and E_a are fitting parameters.

Thus, the crystallization activation energy can be estimated from the numerical fitting procedure of the Arrhenius law to the data in Figure 5. The evaluated values of E_a for sildenafil from applied models to DSC and XRD data are presented in Tables 1 and 2, respectively. We found that the values of the activation energy are very similar for both the experimental methods. The value of E_a for the isothermal crystallization process of sildenafil is close to 200 kJ/mol for both the DSC and X-ray measurements (Figure 5 and Tables 1 and 2).

For comparison, in Figure 5, we also show data recently reported by us in ref 15, where we discussed isothermal and nonisothermal crystallization kinetics of sildenafil monitored by using broadband dielectric spectroscopy (BDS) and differential scanning calorimetry, respectively. As can be seen in Figure 5, the value of E_a received previously from the analysis of the isothermal crystallization kinetics monitored by using BDS spectroscopy at similar temperatures is not significantly different from the value of the activation energy for the isothermal crystallization investigated herein by using DSC and XRD techniques. This result suggests that the barrier of the activation energy for the isothermal crystallization of sildenafil is not dependent on the measurement technique.

3.3. Optical Measurements. The polarized light microscopy studies (with 10× magnification) allowed to observe specific changes in the structure of the sample surface, which precede the crystallization process. The optical measurements revealed that the changes appears only above certain temperature and their character strongly depends on the temperature. As we can see in Figure 6, at lower temperatures, below T = 333 K, we do not observe any deformation of surface, while about 333 K there are 2-fold changes, domain-like structures (see violet arrow in Figure 6) and wrinkle-like spots (yellow arrow in Figure 6) on the surface of the sample. The domain-like structures on the surface occur merely in T = 333 K. To better illustrate the nature of the domain-like character, we drew a contours in Figure 6. On the basis of measurements, it was possible plotting the time-dependent occurrence between the length of roughness surface, as well as time of appearance's roughness surface from time of appearance's nuclei (Figure 6 and Table 3). The appearance domain-like structure can be simply explained by the ordering of molecules in pairs being parallel to each other.[30] On the other hand, the alterations above 333 K associated with roughness surface are harder to explain. It is also worth noting, that the length of deformation strongly depends on temperature. It is due to slower molecular dynamics which result in prolongation of time appearance of the nuclei as well as shortening the length of surface roughness (see Figure 6). It is also worth mentioning, that the temperature of T = 333 K in which the domain-like structures are observed correlates with a glass transition temperature for sildenafil determined from DSC and BDS methods (329 and 328 K, respectively).[15]

Additionally, observation under polarized light microscopy showed that in the first step of the process when the corrugations optically are visible, the sample still has amorphous structure.

The recorded optical images enabled also estimate number of the noncrystalline deformation centers per unit area. As a result, we found that it is approximately equal to 0.02 μm^2 and this number is constant and independent of temperature (Table 3).

In the second stage of the process the formation of small centers of crystallization and their growth with time are

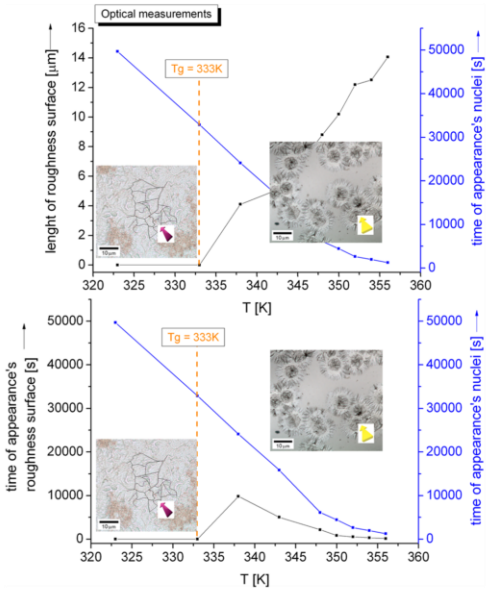

Figure 6. Temperature-dependent optical measurements between (a) length of roughness surface and time of appearance nuclei and (b) time of appearance roughness surface and time of appearance nuclei. The violet arrows points domain-like structures (T = 333 K) while yellow arrow indicate surface's roughness (after 333 K).

observed. The growing crystals take the form of needle and grow symmetrically from the center. Having these data, we estimated the number of nucleation centers, which is equal to 0.8 centers of nucleation per 1 μm^2.

To better illustrate this process one should delineate curves of the time dependence of the changes on the surface. As shown in Figure 7a, this dependence changes in specific way. Variations of the curves' slope indicate an appearance of nuclei on the roughness surface in the studied samples. Hence, it was possible to estimate an approximate time of the nuclei formation for each temperature (Table 3). These slopes of curves are strictly connected with new appending centers of the crystallization inside and on the corrugated surface. It has turned out that the time required for the formation of nuclei is comparable to the value of induction time t_0 estimated from Avrami−Avramov plot for DSC and XRD techniques.

The data from optical measurements of crystal growth process in time enable us to estimate activation barriers, E_{cg}. The length of the growing crystal is plotted as a function of the elapsed time in Figure 7b. The microscopic data allows also to estimate the value of the crystal growth rate, μ_r, in isothermal conditions. It was calculated from the slope coefficient of the linear regression of the length of the growing crystal as a function of time. Then μ_r was plotted as a function of inverse temperature and fitted to the Arrhenius equation (see Figure 5). Thus, we finally found the value of E_{cg} to be equal to 198 kJ/mol. It can be seen that this activation barrier is very similar to values of activation energy of total crystallization determined from DSC, XRD, and BDS.

3.4. Infrared Measurements and Theoretical Calculation. To shed more light on the unusual behavior of the quenched sildenafil sample during recrystallization, the theoretical calculations (Figure 7c) supported by infrared spectroscopy (IR) measurements were performed. The different molecular systems were theoretical optimized and used as input files for vibrational harmonic calculations. The theory predictions pointed to intermolecular H-bond formation between amide group of one molecule and amine group of the second one. It is due to shortening of the bond distance between O−H (−C═O−...−H−N−) from 4.1 (crystal) to 1.8 Å (supercooled sildenafil sample). The formation of the H-bond is reflected on the theoretical infrared spectra by blue shift of carbonyl and amine bands. To better illustrate theoretical predictions the IR spectrum of crystalline and glassy sildenafil was measured and presented in Figure 8. Experimental crystal spectrum shows two characteristic bands at 1682 and 1649 cm^{-1} originated from stretching vibration of carbonyl υ(C═O) group while two bands at 3106 and 3310 cm^{-1} are associated with symmetric and antisymmetric stretching vibrations of amine NH group. The transition process from crystal to glass state leads to the reduction in the intensity of two bands (3106, 1649 cm^{-1}), while the other two are shifted about 10 cm^{-1} toward higher wavenumber. Thus, we observe the main bands at 3320, 1696 cm^{-1}. The experimental data are in good agreement with theoretical calculations which showed that this shift is due to reciprocal pyrimidine rings rotation and formation of H-bond between NH and C═O group. These data also suggest that as a result of vitrification forms the system of n-molecules linked by hydrogen bond. To explain kinetics of

Table 3. Comparison of Isothermal Cold Crystallization Kinetics Parameters of Sildenafil Obtained from Optical Measurements

	optical measurements[a]				
crystallization temperature, T_c [K]	size of crystal, s [μm]	time of appearance's nuclei [min]	time of length of crystal [min]	number of deformation centers per area (0.3 mm × 0.3 mm) [$n/\mu m^2$]	number of nucleation/nuclei per area (0.3 mm × 0.3 mm) [$n/\mu m^2$]
323	5.25	828	12 667	0/670	28/140
333	3.21	548	6667	0/670	59/140
343	9.70	264	3375	7/670	71/140
348	6.66	102	750	14/670	96/140
350	11.56	74	600	14/670	110/140
352	5.14	44	431	14/670	118/140
354	12.50	33	376	13/670	118/140
356	6.80	21	240	14/670	120/140

[a] E_{cg} = 198 ± 19 kJ/mol.

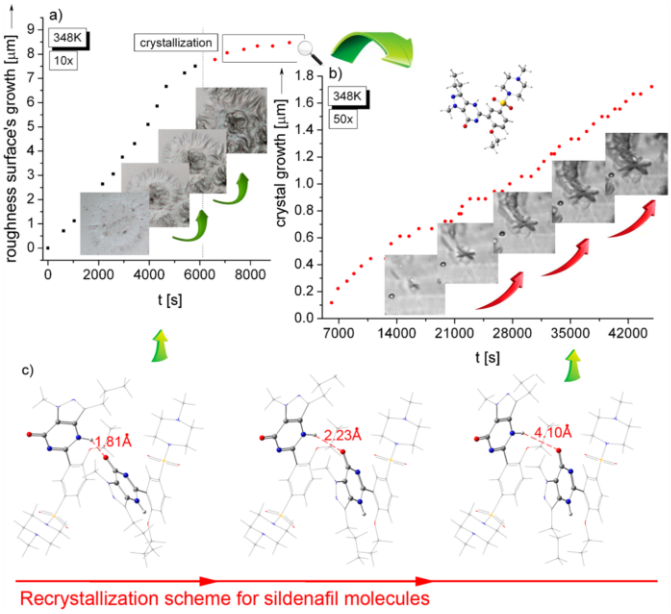

Figure 7. Molecular dynamic of quenched sildenafil observed on the example of the optical data at 348 K. (a) Kinetics of the process associated with roughness surface's growth while (b) Nucleation and kinetics of the crystal growth. (c) Recrystallization scheme in a system of two molecules.

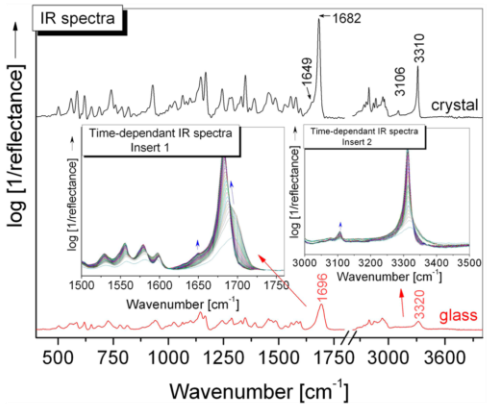

Figure 8. IR spectra of crystalline (black line) and quenched sample of sildenafil (red line). Insert 1 and 2 presents alternation in two spectral range during recrystallization of the sample at 348 K.

this process, we performed time-dependent IR spectra (see insets in Figure 8), which show an increase in the bands intensity at 3320 and 1696 cm^{-1} in the first stage of the process. These differences give us evidence that the equilibrium in supercooled sample changes and the population and strength of H-bond decreases over time. In the second part of the process, we observe an increase in two bands at 3106 and 1649 cm^{-1} and a gradual band shift of the other toward 3310 and 1682 cm^{-1} because of crystallization. Additionally, to better illustrate the changes in supercooled sildenafil we performed isothermal time-dependent integral intensity analysis for OH band at 3320 cm^{-1} as well as OH band position analysis at two different temperatures of 348 and 352 K (see Figure 9). The kinetics curves show an exponential increase in the values of integral intensity at the first stage which corresponds to the corrugation observed from optical data (see Figures 6b and 9). Similar behavior with exponential decrease in OH band position from 3320 to 3310 cm^{-1} is observed. It may point to stronger interaction between molecules. However, the theoretical

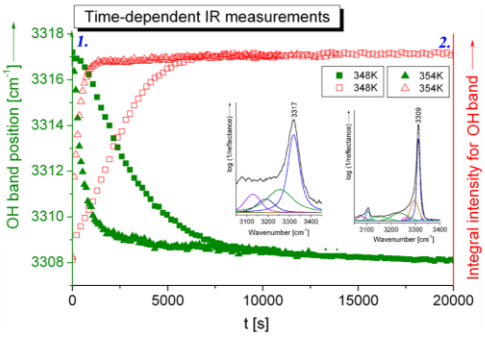

Figure 9. Kinetic curves obtained by OH band position, as well as integrate intensity analysis for OH band at 348 (rectangular) and 354 K (triangle). Lines 1 and 2 are associated with infrared spectra on the beginning and on the end of time-dependent IR measurements.

dx.doi.org/10.1021/cg401364e | Cryst. Growth Des. 2014, 14, 3199−3209

calculations show the band shift into lower wavenumber ~10 cm^{-1} is associated with atypical molecular structure where pyrimidine rings tend to be set parallel to each other forms system of two molecules as in crystal.[30] Thus, the corrugation observed in the first step on the optical data may be associated with reorganization of molecules which will be formed by a system of H-bond. This reorganization in the next stage provide to recrystallization process of sildenafil (see Figure 9).

■ CONCLUSIONS

The main objective of this work was to compare parameters characterizing isothermal cold crystallization process that were determined from different techniques, DSC, X-ray, and optical measurements. The Avrami and Avramov models were applied to describe crystallization curves obtained for sildenafil. As we found out there are no significant difference in crystallization kinetics of sample. We have shown that the mechanism of isothermal cold crystallization is similar: the value of parameter $n \approx 3$ in both considered models, Avrami and Avrami–Avramov plots. The results suggest that sildenafil can form coexistent three-dimensional crystallites from instantaneous and sporadic nucleation. What is more, the crystallization rate k gradually increases with the increasing T_c and is independent of the measurement method: this means that the crystallization process is dominated by the diffusion of molecules. Moreover, we calculated value of activation energy for the crystallization determined from DSC, XRD, and optical studies are very similar. Additionally, measurements with the use of the microscope revealed formation of wrinkle-like spots on the sample surface which preceded the crystallization process and shape of formed crystals. Finally, it was also shown that the specific behavior before crystallization may be associated with the phenomenon of intermolecular H-bond formation between molecules of sildenafil.

■ AUTHOR INFORMATION

Corresponding Author

*E-mail: kkolodziejczyk@us.edu.pl.

Notes

The authors declare no competing financial interest.

■ ACKNOWLEDGMENTS

The authors are grateful for the financial support received from the Polish National Science Centre within the program OPUS3 (decision no. DEC-2012/05/B/ST3/02837). K.K. is deeply thankful for support through a stipend received within the project "DoktoRIS–the stipend program for the innovative Silesia," which is cofinanced by the EU European Social Fund. This research was supported in part by PL-Grid Infrastructure.

■ REFERENCES

(1) Vázquez, J.; Wagner, C.; Villares, P.; Jiménez-Garay, R. A theoretical method for determining the crystallized fraction and kinetic parameters by DSC, using non-isothermal techniques. *Acta Mater.* **1996**, *44*, 4807–4813.

(2) Chen, J.; Sarma, B.; M. B. Evans, J.; Myerson, A. S. Pharmaceutical crystallization. *Cryst. Growth Des.* **2011**, *11*, 887–895.

(3) Rodríguez-Hornedo, N.; Murphy, D. Significance of controlling crystallization mechanisms and kinetics in pharmaceutical systems. *J. Pharm. Sci.* **1999**, *88*, 651–660.

(4) Fokin, V. M.; Zanotto, E. D.; Yuritsyn, N. S.; Schmelzer, J. W. P Homogeneous crystal nucleation in silicate glasses: A 40 years perspective. *J. Non-Cryst. Solids* **2006**, *352*, 2681–2714.

(5) Mubarak, Y.; Harkin-Jones, E. M. A.; Martin, P. J.; Ahmad, M. Modeling of non-isothermal crystallization kinetics of isotactic polypropylene. *Polymer* **2001**, *42*, 3171–3182.

(6) Kong, X.; Yang, X.; Li, G.; Zhao, X.; Zhou, E.; Ma, D. Nonistohermal crystallization kinetics: Poly(ethylene terephthalate)–poly(ethylene oxide) segmentem copoymer and poly(ethylene oxide) homopolymer. *Eur. Polym. J.* **2001**, *37*, 1855–1862.

(7) Bhardwaj, S. P.; Suryanarayanan, R. Molecular mobility as an effective predictor of the physical stability of amorphous trehalose. *Mol. Pharmaceutics* **2012**, *11*, 3209–17.

(8) Cabral, A. A.; Fokin, V. M.; Zanotto, E. D.; Chinaglia, C. R. Nanocrystallization of fresnoite glass. I. Nucleation and growth kinetics. *J. Non-Cryst. Solids* **2003**, *330*, 174–186.

(9) Abu-Sehly, A. A. Study of the kinetics of non-isothermal crystallization in $Ge_{20}Te_{80}$ chalcogenide glass. *Phys. B* **2003**, *325*, 372–379.

(10) Aldica, G.; Secu, M. Investigations of the non-isothermal crystallization of CaF_2 nanoparticles in Sm-doped oxy-fluoride glasses. *J. Non-Cryst. Solids* **2010**, *356*, 1631–1636.

(11) Cai, J.; Yu, Q.; Han, Y.; Zhan, X.; Jiang, L. Thermal stability, crystallization, structure, and morphology of syndiotactic 1,2-polybutadiene/organoclay nanocomposite. *Eur. Polym. J.* **2007**, *43*, 2866–2881.

(12) Adrjanowicz, K.; Kaminski, K.; Wojnarowska, Z.; Dulski, M.; Hawelek, L.; Pawlus, S.; Paluch, M.; Sawicki, W. Dielectric relaxation and crystallization kinetics of ibuprofen at ambient and elevated pressure. *J. Phys. Chem. B* **2010**, *114*, 6579–6593.

(13) Kaminski, K.; Adrjanowicz, K.; Wojnarowska, Z.; Dulski, M.; Wrzalik, R.; Paluch, M.; Kamińska, E.; Kasprzycka, A. Do intermolecular interactions control crystallization abilities of glass-forming liquids? *J. Phys. Chem. B* **2011**, *115*, 11537–47.

(14) Puel, E.; Verdurand, E.; Taulelle, P.; Bebon, C.; Colson, D.; Klein, J. P.; Veesler, S. Crystallization mechanisms of acicular crystals. *J. Cryst. Growth* **2008**, *310*, 110–115.

(15) Kołodziejczyk, K.; Paluch, M.; Grzybowska, K.; Grzybowski, A.; Wojnarowska, Z.; Hawelek, L.; Ziolo, J. D. Relaxation dynamics and crystallization study of sildenafil in the liquid and glassy states. *Mol. Pharmacol.* **2013**, *10*, 2270–2282.

(16) Becke, A. D. A new mixing of Hartree–Fock and local density-functional theories. *J. Chem. Phys.* **1993**, *98*, 5648–5652.

(17) Becke, A. D. Density-functional exchange-energy approximation with correct asymptotic behavior. *Phys. Rev. A* **1988**, *38*, 3098–3100.

(18) Lee, C.; Yang, W.; Parr, R. G. Development of the Colle–Salvetti conelation energy formula into a functional of the electron density. *Phys. Rev. B* **1988**, *37*, 785–789.

(19) Hehre, W. J; Radom, L.; Schleyer, P. R.; Pople, J. A. *Ab Initio Molecular Orbital Theory*; Wiley: New York, 1986; pp 20–29, 65–88.

(20) Parr, R. G.; Yang, W. *Density Functional Theory of Atoms and Molecules*; Oxford University Press: New York, 1989; pp 142–197.

(21) Burke, K.; Perdew, J. P.; Wang, Y. *Electronic Density Functional Theory: Recent Progress and New Directions*; Dobson, J. F., Vignale, G., Das, M. P., Eds; Plenum: New York, 1998.

(22) Frisch, M. J.; Trucks, G. W.; Schlegel, H. B.; Scuseria, G. E.; Robb, M. A.; Cheeseman, J. R.; Scalmani, G.; Barone, V.; Mennucci, B.; Petersson, G. A.; Nakatsuji, H.; Caricato, M.; Li, X.; Hratchian, H. P.; Izmaylov, A. F.; Bloino, J.; Zheng, G.; Sonnenberg, J. L.; Hada, M.; Ehara, M.; Toyota, K.; Fukuda, R.; Hasegawa, J.; Ishida, M.; Nakajima, T.; Honda, Y.; Kitao, O.; Nakai, H.; Vreven, T.; Montgomery, J. A., Jr.; Peralta, J. E.; Ogliaro, F.; Bearpark, M.; Heyd, J. J.; Brothers, E.; Kudin, K. N.; Staroverov, V. N.; Kobayashi, R.; Normand, J.; Raghavachari, K.; Rendell, A.; Burant, J. C.; Iyengar, S. S.; Tomasi, J.; Cossi, M.; Rega, N.; Millam, J. M.; Klene, M.; Knox, J. E.; Cross, J. B.; Bakken, V.; Adamo, C.; Jaramillo, J.; Gomperts, R.; Stratmann, R. E.; Yazyev, O.; Austin, A. J.; Cammi, R.; Pomelli, C.; Ochterski, J. W.; Martin, R. L.; Morokuma, K.; Zakrzewski, V. G.; Voth, G. A.; Salvador, P.; Dannenberg, J. J.; Dapprich, S.; Daniels, A. D.; Farkas, O.; Foresman, J. B.; Ortiz, J. V.; Cioslowski, J.; Fox, D. J. *Gaussian 09*, revision A.1; Gaussian, Inc.: Wallingford, CT, 2009.

(23) Avrami, M. Kinetics of phase change. I. General theory. *J. Chem. Phys.* **1939**, *7*, 1103.
(24) Avrami, M. Kinetics of phase change. II. Transformation−time relations for random distribution of nuclei. *J. Chem. .Phys.* **1940**, *8*, 212.
(25) Avramov, I.; Avramova, K.; Russel, C. New method to analyze data on overall crystallization kinetics. *J. Cryst. Growth* **2005**, *285*, 394−399.
(26) Foubert, I.; A.Vanrolleghem, p.; Vanhoutte, B.; Dewettinck, K. Dynamic mathematical model of the crystallization kinetics of fats. *Food Res. Int.* **2002**, *35*, 945−956.
(27) Shi, X. M.; Zhang, J.; Jin, J.; Chen, S. J. Non-isothermal crystallization and melting of ethylene-vinyl acetate copolymers with different vinyl acetate contents. *Express Polym. Lett.* **2008**, *2*, 623−629.
(28) Böhm, N.; Kulicke, W. M. Rheological studies of barley (1″3) (1″4)-*b*-glucan in concentrated solution: Mechanistic and kinetic investigation of the gel formation. *Carbohydr. Res.* **1999**, *315*, 302−311.
(29) Massalska-Arodz, M.; Williams, G.; Smith, I. K.; Conolly, C.; Aldridge, G. A.; Dabrowski, R. Molecular dynamics and crystallization behaviour of isopentyl cyanobiphenyl as studied by dielectric relaxation spectroscopy. *J. Chem. Soc., Faraday Trans.* **1998**, *94*, 387−394.
(30) Yathirajan, H. S.; Nagaraj, B.; Nagaraja, P.; Bolte, M. *Acta Crystallogr.* **2005**, *E61*, o489−o491.

3.2.1 Oświadczenia współautorów publikacji II

dr Katarzyna Grzybowska
Uniwersytet Śląski
Instytut Fizyki im. Augusta Chełkowskiego
ul. Uniwersytecka 4
40-007 Katowice

Katowice, 24 lutego 2016 r.

OŚWIADCZENIE

Oświadczam, że w pracy K. Kolodziejczyk, K. Grzybowska, Z. Wojnarowska, M. Dulski, L. Hawelek, M. Paluch, Crystal Growth & Design 2014, 14 (7), pp 3199-3209 zatytułowanej „*Isothermal Cold Crystallization Kinetics Study of Sildenafil",* mój udział polegał na weryfikacji przeprowadzonych analiz, dyskusji otrzymanych wyników oraz korekt tekstu manuskryptu.

dr Żaneta Wojnarowska
Uniwersytet Śląski
Instytut Fizyki im. Augusta Chełkowskiego
ul. Uniwersytecka 4
40-007 Katowice

Katowice, 24 lutego 2016 r.

OŚWIADCZENIE

Oświadczam, że w pracy K. Kolodziejczyk, K. Grzybowska, Z. Wojnarowska, M. Dulski, L. Hawelek, M. Paluch, Crystal Growth & Design 2014, 14 (7), pp 3199-3209 zatytułowanej *„Isothermal Cold Crystallization Kinetics Study of Sildenafil",* mój udział polegał na dyskusji wyników.

Żaneta Wojnarowska

dr Mateusz Dulski
Uniwersytet Śląski
Instytut Fizyki im. Augusta Chełkowskiego
ul. Uniwersytecka 4
40-007 Katowice

Katowice, 7 stycznia 2016r.

OŚWIADCZENIE

Oświadczam, że w pracy K. Kolodziejczyk, K. Grzybowska, Z. Wojnarowska, M. Dulski, L. Hawelek, M. Paluch, Crystal Growth & Design 2014, 14 (7), pp 3199-3209 zatytułowanej „*Isothermal Cold Crystallization Kinetics Study of Sildenafil",* mój udział polegał na wykonaniu pomiarów optycznych z wykorzystaniem standardowego mikroskopu świetlnego, pomiarów w podczerwieni oraz obliczeń kwantowo-mechanicznych pozwalających zobrazować zmiany zachodzące w materiale i wyjaśnić zmiany obserwowane na widmach w podczerwieni. Dodatkowo wszystkie wyniki zostały opisane, a opracowane rysunki posłużyły przyblizeniu procesu tautomerii zachodzącej w sildanafilu w fazie cieczy przchłodzonej.

Mateusz Dulski

dr Łukasz Hawełek
Instytut Metali Nieżelaznych
ul. Sowińskiego 5
44-100 Gliwice

Katowice, 7 stycznia 2016

OŚWIADCZENIE

Oświadczam, że w pracy K. Kolodziejczyk, K. Grzybowska, Z. Wojnarowska, M. Dulski, L. Hawelek, M. Paluch, Crystal Growth & Design 2014, 14 (7), pp 3199-3209 zatytułowanej „*Isothermal Cold Crystallization Kinetics Study of Sildenafil",* mój udział polegał na pomiarach i analizie danych szerokokątowej dyfrakcji rentgenowskiej.

prof. zw. dr hab. Marian Paluch
Uniwersytet Śląski
Instytut Fizyki im. Augusta Chełkowskiego
ul. Uniwersytecka 4
40-007 Katowice

Katowice, 24 lutego 2016 r.

OŚWIADCZENIE

Oświadczam, że w pracy K. Kolodziejczyk, K. Grzybowska, Z. Wojnarowska, M. Dulski, L. Hawelek, M. Paluch, Crystal Growth & Design 2014, 14 (7), pp 3199-3209 zatytułowanej *„Isothermal Cold Crystallization Kinetics Study of Sildenafil“,* mój udział polegał na polegał na nadzorowaniu przeprowadzonych analiz, dyskusji otrzymanych wyników oraz korekcie tekstu manuskryptu.

3.3 PUBLIKACJA III

BADANIE KINETYKI KRYSTALIZACJI SALOLU ZAMKNIĘTEGO W MEMBRANACH AAO. MANIPULACJA FORMĄ KRYSZTAŁU ZA POMOCĄ ZMIANY ŚREDNICY PORÓW.

Autorzy:

K. Kołodziejczyk, M. Tarnacka, E. Kamińska, M. Dulski, K. Kamiński, M. Paluch

Referencje:

Crystal Growth & Design, Publication Date (Web): January 13, 2016; Articles ASAP (As Soon As Publishable)

Skrót:

W artykule przedstawione zostały badania krystalizacji oraz temperatury topnienia salicylanu fenylu „w masie”(ang. *bulk*) oraz zamkniętego w porowatych matrycach wykonanych z tlenku glinu (AAO). Na podstawie analizy kinetyki krystalizacji wykazaliśmy, że uformowane kryształy salolu „w masie” oraz w układach zamkniętych różnią sią wymiarowością i szybkością wzrostu. Zauważyliśmy również, że szybkość krystalizacji salolu umieszczonego w membranach AAO jest zależna od rozmiaru porów i może przyspieszyć (d=150 nm) lub zostać całkowicie zahamowana (gdy średnica porów d<75 nm). Dodatkowo analiza temperatury topnienia uformowanych kryształów salolu „w masie” wykazała jednoznacznie, że salol występuje w dwóch formach polimorficznych. Co więcej, polimorfizm salolu ujawnił się również w układach zamkniętych. Opierając się na danych kalorymetrycznych oraz FTIR doszliśmy do wniosku, że salol umieszczony w porach o większej średnicy (d=150 nm) tworzy niestabilną formę, a w przypadku porów o mniejszej średnicy (d=100 nm) stabilną formę kryształu.

CRYSTAL GROWTH & DESIGN

Article

pubs.acs.org/crystal

Crystallization Kinetics under Confinement. Manipulation of the Crystalline Form of Salol by Varying Pore Diameter

Karolina Kołodziejczyk,[*,†,‡] Magdalena Tarnacka,[†,‡] Ewa Kamińska,[§] Mateusz Dulski,[†,‡,⊥] Kamil Kamiński,[†,‡] and Marian Paluch[†,‡]

[†]Institute of Physics, University of Silesia, ul. Uniwersytecka 4, 40-007 Katowice, Poland

[‡]Silesian Center for Education and Interdisciplinary Research, University of Silesia, ul. 75 Pulku Piechoty 1A, 41-500 Chorzow, Poland

[§]Department of Pharmacognosy and Phytochemistry, Medical University of Silesia in Katowice, School of Pharmacy with the Division of Laboratory Medicine, ul. Jagiellonska 4, 41-200 Sosnowiec, Poland

[⊥]Institute of Material Science, University of Silesia, 75 Pułku Piechoty 1a, 41-500 Chorzow, Poland

ABSTRACT: The crystallization and melting behavior of phenyl salicylate under confinement were studied by means of dielectric spectroscopy (BDS) and differential scanning calorimetry (DSC). From the analysis of the kinetics of crystallization we established that crystals formed in bulk and under confinement are characterized by varying the rate of growth, dimensionality, and crystal lattice. It was shown that depending on the degree of confinement the crystallization can be accelerated or suppressed completely. Interestingly, we also found that the activation barrier for the crystallization either increases or decreases with respect to the bulk conditions. Further investigation of the melting temperature of the formed crystals indicated unequivocally that it is connected to the formation of different polymorphic forms of salol. Additional FTIR measurements confirmed that thesis. Based on calorimetric data obtained for the confined samples, we concluded that at pores of higher diameter the unstable (monoclinic) form is preferred, while at lower pores the original stable (orthorhombic) crystal is formed.

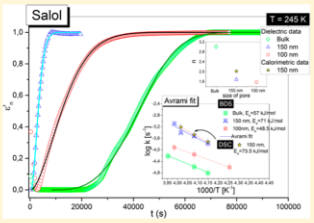

1. INTRODUCTION

The issue of crystallization in porous materials has attracted researchers for more than a decade. The first observation of this phenomenon was already noted in nature, mainly due to the destructive character of the crystal growth of ice[1,2] and salt[3,4] in pores of stones, masonry, and wall. The current development of technology, industry, and contemporary studies of the crystallization of ice,[2] solid organic,[5,6] and metals[7−9] in nanoporous matrices has revealed that spatial confinement has a huge impact on the physicochemical properties of such materials. However, the problem arises during attempts at characterization of new nanosystems. It is related to the fact that in various nanoporous matrices the same material may behave completely differently. What is more, despite numerous investigations, it is difficult to make any predictions about basic properties of compounds confined in matrices of varying internal structure, strength of interactions, geometry of pores, and so forth.

Melting temperature (T_m) and enthalpy of fusion (H_m) are most frequently analyzed quantities to detect the changes in properties of confined materials during crystallization. The observed changes in these two quantities are a direct consequence of the increasing surface-to-volume ratio when the crystal size is reduced.[10−12] Modification in T_m or H_m strongly depends on the size of confinement geometry. As shown in many studies, depression of the melting point and enthalpy of fusion is a function of crystal size as well as degree of confinement. In addition, a linear relationship between T_m and the pore diameter is reported.[7−9] To rationalize this dependency, the Gibbs−Thomson thermodynamic equation is usually applied.[13−15]

$$\Delta T_m = (T_m - T_m(d)) = \frac{4\sigma_{cl} T_m}{d\Delta H_m \rho_c} \quad (1)$$

where T_m is the melting point in bulk substance, $T_m(d)$ is a melting temperature of crystals formed in pores of diameter d, σ_{cl} is a surface energy between crystal and liquid, ΔH_m is the heat of melting, and ρ_c is the density of crystal. The obvious advantage of this approach is the possibility of calculating surface energy and critical radius of nucleation strictly from the data measured under confinement.

Another aspect related to this point is that the system spatially restricted can crystallize to different polymorphic forms. Polymorphism of crystal has a strong impact on the basic properties of a given compound. Hence, this issue seems to be of exceptional importance for the food and pharmaceutical

Received: August 17, 2015
Revised: January 5, 2016

DOI: 10.1021/acs.cgd.5b01181
Cryst. Growth Des. XXXX, XXX, XXX−XXX

industry, where different polymorphs might be characterized by various solubility, stability, bioavailability, compressibility, crystallization rates, and so forth.[16−20]

In this context one can mention anthranilic acid (AA). In bulk phase, the existence of three polymorphic forms has been reported.[21] On the other hand, by varying dimension of the pore size one can get control over the crystallization process and tune it toward formation of given polymorph.[22] As shown by the authors in ref 22, polymorphic III and II structures are formed in CPG pores of 55 and 7.5 nm diameter, respectively. Ha and co-workers claimed that stable III and metastable II forms are characterized by different critical nucleus size. Formation of the polymorph II in smaller pores was attributed to a lower critical nucleus size compared with the other forms, reflecting size-dependent polymorph stability.

Similar cases have been reported for glycine crystal in the CPG and p−PS-PDMA matrices.[23] The metastable form of bulk β-glycine becomes preferred when the crystal size is subjected to nanometer-scale restrictions. This is true when β-glycine is confined in pores having diameter 30 nm or lower.

In the literature there are only a few reports demonstrating that by an appropriate choice of pore size one can control crystal growth of the crystal of tailor-made morphology, structure, and properties. Moreover, it is also possible to suppress crystallization completely by varying the degree of confinement. This was well illustrated in the case of acetaminophen. Rangarajan et al.[24−27] proved that besides the formation of polymorphic forms (II and III, for pores of sizes ranging from 22 to 60 nm) being unstable in bulk, it is also possible to suppress crystallization of acetaminophen for the sample confined in CPG pores of diameter lower than 4.6 nm. These authors suggest that the inhibition of crystal growth could be caused by either critical size effects or a kinetic stabilization of the amorphous phase. Systematic studies of phase transitions between different acetaminophen polymorphs inside CPG revealed that the thermodynamic stability of the given polymorph depends on the crystal size, according to Ostwald's rule of stages.[28]

It is also worth mentioning crystallization of confined benzene which was thoroughly discussed in the literature. According to the reported results, it can be concluded that the crystallization process depends on the geometry of the pores. It should be added that the melting temperature of benzene confined in two different matrices having cylindrical and slit pores is different. It was proven that the melting point in slit pores occurs when its diameter is 0.7 nm,[29] whereas in the case of cylindrical pores the melting appears above 4.7 nm.[11] The effect of crystallization suppression can be related to the varying strength of interactions as well as internal surface area of nanoporous matrices which can be another important parameters and additional tool to control crystallization through heterogeneous nucleation on the pore walls.

The examples discussed above clearly demonstrate that the crystallization on the nanometer scale is a very complicated process. Therefore, the most important aim is to learn how to control crystal growth by manipulation of confinement degree to produce tailor-made crystals of desired properties.

In the present work, we focused on the crystallization process of salol and controlling its polymorphism by varying the degree of confinement. Consequently, we presented dielectric studies on crystallization kinetics of salol both in bulk sample and spatially restricted in AAO templates, whose pore diameter is in the range 13−150 nm. As a result, we have shown that the studied systems, bulk and confined, completely differ in rate of crystallization and mechanism of crystal growth. Additional measurements with the use of differential scanning calorimetry reveal that these differences can be attributed to the existence of two polymorphic forms of this compound. The stable crystal exists in an orthorhombic form and it is formed in pores of 100 nm diameter, while the metastable one (monoclinic form) is produced after cold crystallization and in pores of 150 nm diameter. This assignment was made based on the position of the melting temperature in the measured thermograms. Additional FTIR measurements showed that the structures of crystals formed at different pores differ, indicating formation of two different polymorphic forms of salol.

2. EXPERIMENTAL SECTION

2.1. Materials. The investigated drug, phenyl salicylate (salol) (99.8% purity) ($C_{13}H_{10}O_3$, M_w = 214.22 g/mol, IUPAC name: Phenyl 2-hydroxybenzoate) was delivered from Polpharma (Starogard Gdanski, Poland) as a white crystalline powder.

Amorphous samples were prepared by the quench-cooling technique. The crystalline form of salol was heated to the melting point (T_m = 315 K) and then rapidly cooled. The glass transition temperature of the amorphous salol is equal to 223 K.

Uniaxial anodic alumina oxide (AAO) membranes of very narrow distribution of the pore sizes were supplied by Synkera Technologies, Inc. from USA. All details concerning AAO can be found on the web page of the producer.

2.2. Sample Preparation/Infiltration Procedure. Prior to filling, AAO membranes were dried in an oven at 423 K under vacuum to remove any volatile impurities from the nanochannels. After cooling, they were placed in molten salol. Then, the whole system was maintained at T = 343 K in vacuum (10^{-2} bar) for 24 h to let salol flow into the nanocavities. After completing the infiltration process, the surface of AAO membrane was dried and the excess sample removed by use of sharp blades. In the experiment we used membranes with a different pores diameter: 150, 100, 73, and 13 nm. The fullness of the pores was estimated to be around 50%. We made a series of experiments to enhance this parameter. However, due to thermal decomposition of salol it was impossible to keep it longer than 24 h at melting temperature.

2.3. Methods. *2.3.1. Dielectric Spectroscopy (BDS).* Isobaric measurements of the complex dielectric permittivity $\varepsilon^*(\omega) = \varepsilon'(\omega) - i\varepsilon''(\omega)$ were carried out using the Novocontrol Alpha dielectric spectrometer over the frequency range from 10^{-2} to 10^6 Hz at ambient pressure. The temperature stability controlled by Quatro Cryosystem using a nitrogen gas cryostat was better than 0.1 K. Dielectric measurements of bulk salol were performed in a parallel-plate cell (diameter: 10 mm, gap: 0.1 mm) immediately after preparation of the amorphous sample. AAO membranes filled with salol were also placed in a similar capacitor (diameter: 10 mm, membrane: 0.005 mm).

Dielectric measurements were performed in the various crystallization temperatures, in the range 235−253 K for bulk and confined systems. Before measurement, each sample was annealed at T = 353 K for 5 min, then cooled to 173 K and heated up to crystallization temperature, T_c.

2.3.2. Differential Scanning Calorimetry (DSC). Calorimetric measurements were carried out by Mettler-Toledo DSC apparatus equipped with a liquid nitrogen cooling accessory and a HSS8 ceramic sensor (heat flux sensor with 120 thermocouples). Temperature and enthalpy calibrations were performed by using indium and zinc standards. First, crucibles with crystal samples were sealed and scanned at heating rates 10 K/min to melting point, then rapidly cooled to 173 K and reheated to selected crystallization temperature. Isothermal crystallization studies were carried out at various temperatures: 249, 245, and 241 K. After crystallization was finished, the sample was heated above the melting temperature. Each measurement at given heating rate was repeated 3 times.

2.3.3. Fourier Transform Infrared spectroscopy (FTIR). Infrared data for two anodic aluminum oxide membranes (AAO) filling out by salol as well as for bulk material were measured using Agilent Cary 640 FTIR

DOI: 10.1021/acs.cgd.5b01181
Cryst. Growth Des. XXXX, XXX, XXX−XXX

spectrometer equipped with a standard source and a DTGS Peltier-cooled detector. The spectra for AAO were accumulated between 4000 and 2500 cm^{-1} due to strong Al_2O_3 absorption in the low-frequency range while in the case of bulk material the range between 4000 and 400 cm^{-1} were measured. All spectra were recorded with a spectral resolution of 4 cm^{-1} and 16 scans.

3. RESULTS AND DISCUSSION

Salol confined in anodic alumina oxide membranes was a subject of our research in previous work.[30] In that paper, we focused mainly on the molecular dynamic and glass transition phenomenon. However, during these studies, we also observed that for lower cooling rate salol undergoes a crystallization process which can be well captured by dielectric as well as DSC techniques. Hence, herein we focused on the crystallization kinetics and properties of obtained crystals of bulk sample and salol confined in AAO membranes of varying diameter.

Crystallization Process. The isothermal crystallization kinetics of bulk and confined salol was investigated mainly by dielectric spectroscopy (BDS). This method is very sensitive to changes in the number of relaxing dipoles that freeze upon crystal growth. Hence, it is possible to follow and describe this process by monitoring time evolution of either permittivity located at low frequencies (static permittivity) or amplitude of the structural relaxation process. The isothermal cold crystallization of the bulk and confined salol has been investigated at a few different temperatures in the supercooled state, i.e., from 253 to 235 K in AAO membranes having different pore diameters (150, 100, 73, and 13 nm). One can add that due to shifting of the structural relaxation process out of the experimental window at higher temperatures, as well as very long time-consuming experiments at lower temperatures, the crystallization process was investigated only in the temperature range mentioned above.

The representative dispersion (ε') and loss (ε'') spectra measured during crystallization of bulk salol at 245 K are presented in Figure 1. As can be seen, both the static dielectric permittivity and the amplitude of the structural relaxation loss peak begin to rapidly decrease with time of measurement. It is due to freezing out internal degrees of freedom and increased immobilization of molecules. In Figure 2 we present the dielectric loss spectra obtained at T_c = 245 K upon time dependent measurements of salol confined in pores of varying diameter. It is seen that crystallization is observed in each case. However, for the salol confined in 73 nm pores this process is much longer and is far from completion (Figure 2c) after 3 days. In this case, the rate of crystal growth is too slow to be monitored in a reasonable time. It should also be stressed that crystallization of salol in 13 nm pores was not observed by us.

On the other hand, a completely different scenario is observed for salol confined in membranes of larger pore sizes, i.e., 150 nm, 100 nm, and also for bulk sample (Figures 1 and 2a,b). It is clearly visible that the amplitudes of structural relaxation loss peaks decrease with time, which is a clear indication of significant progress in crystallization of the sample.

In order to analyze the progress of crystallization, dielectric strength of the structural relaxation process, which was determined from fitting α-loss peaks to the HN function,[31] was renormalized by using the following formula:

$$\varepsilon'_n(t) = \frac{\Delta\varepsilon - \Delta\varepsilon(t)}{\Delta\varepsilon - \Delta\varepsilon(\infty)} \quad (2)$$

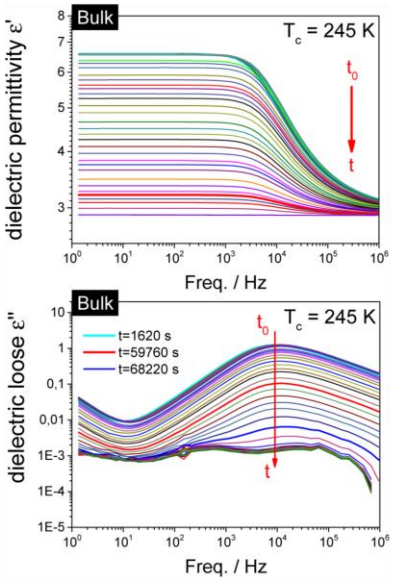

Figure 1. Dielectric spectra of the real (upper panel) and imaginary (lower panel) part of the complex dielectric permittivity collected during isothermal crystallization at T_c = 245 K for bulk salol.

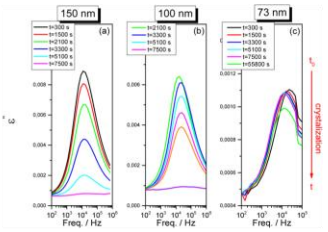

Figure 2. Comparison of the dielectric loss spectra collected during an isothermal crystallization at T_c = 245 K for salol confined in (a) 150 nm, (b) 100 nm, and (c) 73 nm AAO membranes.

where $\Delta\varepsilon$ is the dielectric strength of the structural process at the beginning of the crystallization, $\Delta\varepsilon(\infty)$ is the long-time limiting value, and $\Delta\varepsilon(t)$ is the value at a given time of crystallization, t.

In Figure 3 plots of ε'_n as a function of time for bulk and confined salol at each crystallization temperature are presented. At first sight it is easily seen that the shapes of the crystallization curves are slightly different for the studied samples. For the bulk salol a sigmoidal shape is observed, while for the confined compound more exponential kinetic curves are obtained. This indicates that nucleation step under confinement is strongly reduced with respect to the bulk conditions. Interestingly, in the kinetic curves obtained for the bulk sample some characteristic bumps can be observed. We suppose that it might be connected to the spontaneous interconversion between two polymorphic forms of salol, or to the nonperfection crystal growth.

The other observation is that crystallization measured in membranes having pore sizes 150 nm proceeds faster than the

DOI: 10.1021/acs.cgd.5b01181
Cryst. Growth Des. XXXX, XXX, XXX−XXX

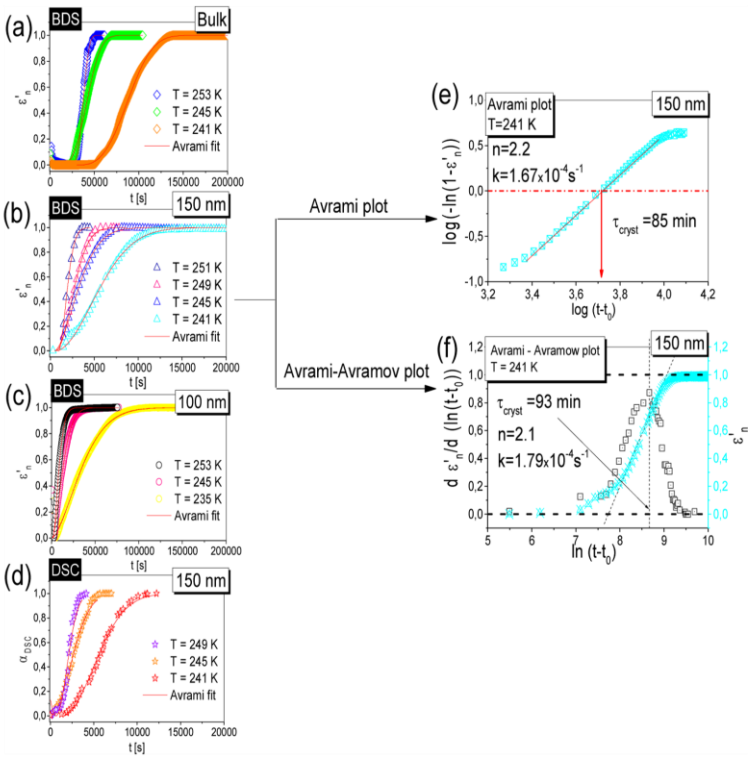

Figure 3. Time dependence of normalized real permittivity ε'_n(a–c) and relative crystallinity α_{DSC}(d) for salol during isothermal crystallization obtained from BDS and DSC measurements, respectively. Solid lines represent Avrami fits in terms of eq 3. (e) Avrami plot: The crystallization time τ_{cryst} was designated from $\log(-\ln(1-\varepsilon'_n(t))) = 0$. (f) Avrami–Avramov plot: time evolution of the normalized real permittivity and its first derivative with respect to the natural logarithm of the time at T_c = 241 K.

Table 1. Comparison of Parameters Estimated from Avrami Models for Kinetic of Isothermal Crystallization Obtained from BDS and DSC Measurements

	T [K]	n	k [1/s]	t_0 [min]	t_{cryst} [min]	E_a [kJ/mol]
			BDS			
Bulk	253	3.30 ± 0.30	(6.07 ± 1.68) × 10^{-5}	169 ± 4	275 ± 8	57 ± 3
	245	3.02 ± 0.30	(2.58 ± 1.28) × 10^{-5}	381 ± 3	646 ± 6	
	241	3.04 ± 0.30	(1.55 ± 1.26) × 10^{-5}	505 ± 3	1075 ± 9	
150 nm	251	1.85 ± 0.19	(8.06 ± 0.16) × 10^{-4}	15 ± 1	21 ± 2	71 ± 5
	249	1.93 ± 0.19	(3.94 ± 0.47) × 10^{-4}	10 ± 1	42 ± 4	
	245	1.69 ± 0.17	(2.96 ± 0.89) × 10^{-4}	8 ± 2	56 ± 5	
	241	1.90 ± 0.19	(1.67 ± 0.62) × 10^{-4}	10 ± 1	85 ± 6	
100 nm	251	1.87 ± 0.19	(1.21 ± 0.53) × 10^{-4}	25 ± 6	138 ± 4	49 ± 3
	245	1.73 ± 0.18	(6.89 ± 0.15) × 10^{-5}	12 ± 4	242 ± 7	
	235	1.63 ± 0.16	(2.48 ± 0.18) × 10^{-5}	7 ± 3	672 ± 9	
			DSC			
150 nm	249	2.00 ± 0.20	(5.71 ± 0.43) × 10^{-4}	10 ± 0.03	29 ± 0.03	73 ± 4
	245	2.02 ± 0.20	(3.11 ± 0.26) × 10^{-4}	0	54 ± 0.03	
	241	1.92 ± 0.19	(1.76 ± 0.33) × 10^{-4}	24 ± 0.03	95 ± 0.03	

bulk one (Figures 3a, b). Further reduction in pore diameter slows down and eventually suppresses the crystallization process completely (d = 13 nm). To quantify these obvious observations the Avrami model was used to describe kinetic curves presented in Figure 3

DOI: 10.1021/acs.cgd.5b01181
Cryst. Growth Des. XXXX, XXX, XXX–XXX

$$\varepsilon'_n(t) = 1 - \exp(-k(t - t_0)^n) \quad (3)$$

where k is a crystallization rate constant, which depends on a crystallization temperature and geometry of sample, n is the Avrami exponent that is related to the time dependence of the nucleation rate and to the dimensionality of the crystallization, and t_0 is the induction time of crystallization. As can be seen in Figure 3a–c, Avrami fit describes experimental data in a satisfactory way. All parameters characterizing the crystallization

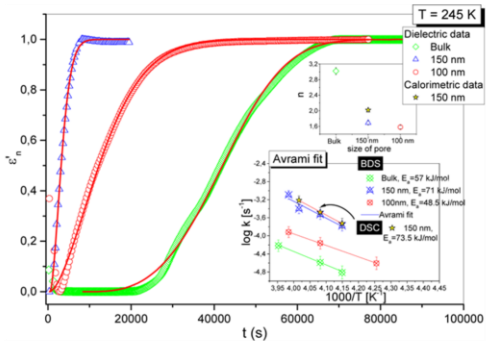

Figure 4. Progress of the crystallization process carried out for the bulk as well as confined salol, T = 245 K. Solid lines represent Avrami fits in terms of eq 3. Inset upper: dependence of Avrami exponent as a function of system size. Inset lower: Plot of log k versus $1000/T$ obtained from isothermal crystallization of salol. The plot compares values of the parameter k received from analysis. The line presents the Arrhenius fits (eq 8).

process obtained from Avrami equation are collected in Table 1 and depicted in Figure 4. The analyzed data show that although parameter n changes with temperature within the experimental uncertainty for a given geometry it varies between 3 and 2, for the bulk and confined system, respectively. According to the research published in the literature these results suggest that bulk-like salol can form three-dimensional crystallites whereas confined in AAO membrane it forms two-dimensional nucleus.[32−34] Hence, this simple comparison of Avrami exponent n indicates that the mechanism of crystallization is quite different for the bulk and confined sample.

In addition, we also performed complementary crystallization studies of salol confined in pores of 150 nm diameter by means of differential scanning calorimetry at three different temperatures: 249, 245, and 241 K. It should be mentioned that we also tried to carry out isothermal time dependent measurements for the AAO membrane with diameter 100 nm. However, the signal was too small and too noisy to get any reliable data.

Utilizing data obtained from DSC, it was possible to estimate the relative degree of crystallization α_{DSC}. In the case of DSC measurements, this parameter is defined as follows:

$$\alpha_{DSC} = \frac{\int_{t_0}^{t} \frac{dH}{dt} dt}{\int_{t_0}^{t_\infty} \frac{dH}{dt} dt} = \frac{A_t}{A_\infty} \quad (4)$$

where dH/dt is the rate of heat evolution, t_0 and t_∞ is the time when crystallization starts and ends and A_t and A_∞ are areas under normalized DSC curve for the partially and fully crystalline material, respectively.

The time evolution of the degree of crystallization α_{DSC} was determined from DSC measurements at different temperatures during isothermal crystallization. The kinetic curves were normalized by the maximum value of the parameter α_{DSC} measured when the crystallization was completed (see Figure 3d). In the next step, the time dependency values of the degree of crystallization obtained from DSC measurements were fitted by Avrami function (eq 3). As can be seen, the curves are shifted toward a shorter time with increasing T_c and this dependence is similar to data obtained from dielectric measurement for salol infiltrated into the AAO membrane with d = 150 nm. Remarkably, rates of crystallization obtained from dielectric and calorimetric studies (see inset to Figure 4) match each other almost perfectly for the measurements carried out in bulk and under confinement. Although some discrepancy in the shape of kinetic curves obtained from both techniques can be noticed.

Since the whole analysis of salol crystallization was carried out by fitting the data presented in Figure 3a–d by using eq 3, there might be some doubts raised about the precise determination of the constant rate k, Avrami exponent n, as well as t_0 or τ_{cryst}. Hence, to verify our results additional methods such as Avrami plot and Avrami–Avramov model were applied. One can add that Avrami plot is a method based on the conversion of eq 3 to its logarithmic form:

$$\log(-\ln(1 - \varepsilon'_n(t))) = \log k + n\log(t - t_0) \quad (5)$$

The above equation suggests that the dependence of $\log(-\ln(1 - \varepsilon'_n(t)))$ on $\log(t - t_0)$ should be a linear function. Consequently, one can estimate the values of n and log$k$ by using a simple linear regression. In Figure 3e, the Avrami plot constructed utilizing representative dielectric data obtained upon crystallization of salol confined in pores of d = 150 nm at T_c = 241 K is presented. Parameters n and k can be easily determined from the slope and the intercept of these curves, respectively. Also, the characteristic time of crystallization, τ_{cryst}, was calculated for each temperature. This time constant characteristic for the crystallization process was evaluated from the condition $\log(-\ln(1 - \varepsilon'_n((t)))) = 0$.

On the other hand, an additional tool proposed by Avramov et al.[35] was used to model data obtained during crystallization of salol.

$$\varepsilon'_n(t) = 1 - \exp\left(-\left(\frac{t - t_0}{\tau_{cryst}}\right)^n\right) \quad (6)$$

where τ_{cryst} is a characteristic time for the isothermal overall crystallization, which is related to the Avrami parameters as follows: $\tau_{cryst} = k^{-1/n}$. The parameters n and t_0 have the same meaning as the ones in the Avrami model (eq 3). All the parameters that characterize the crystallization process can be easily determined by plotting the first derivative of crystallization degree $d\varepsilon'_n(t)/d(\ln(t - t_0))$ versus $\ln(t - t_0)$. Additionally, in this case, the value of n can be calculated by using the following equation

$$n = \frac{(\varepsilon'_n(t))'_{max}}{0.368} \quad (7)$$

Such a typical plot, constructed for BDS data, is shown in Figure 3f.

DOI: 10.1021/acs.cgd.5b01181
Cryst. Growth Des. XXXX, XXX, XXX−XXX

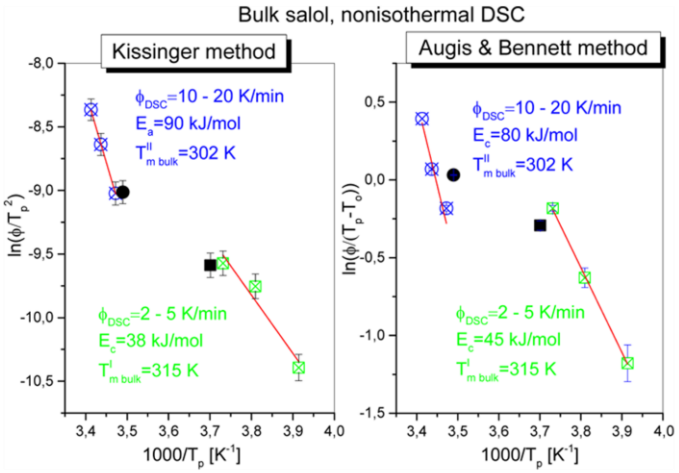

Figure 5. Kissinger and Augis and Bennett plots for exothermic crystallization peaks for bulk salol. The data was obtained from non-isothermal DSC published by Moura Ramos et al.[39] The solid lines indicate the linear fits to eqs 9 and 10, respectively. The black points, circles, and squares were calculated from our measurements for 10 and 5 K/min, respectively.

As can be seen, the values of crystallization parameters k, n, t_0, and τ_{cryst} estimated from these three different methods, i.e., Avrami equation, Avrami plot, and Avrami−Avramov model for salol confined in 150 nm (see Figure 3 and Table 1) are comparable. Therefore, in this paper we just focused on the results obtained from fitting the crystallization kinetics data to the Avrami model (see Table 1).

In the next step, activation energy E_a for the crystallization process was estimated. For this purpose constant rates determined from BDS and DSC studies were plotted as a function of inverse temperature. Furthermore, these dependencies were fitted to the Arrhenius law (see inset to Figure 4)

$$\log k = \log k_0 - \frac{E_a}{RT}\log e \tag{8}$$

where k is the crystal growth rate and R is the gas constant, whereas k_0 and E_a are fitting parameters.

We found that the values of the energy barrier are quite different for the studied samples (see Figure 4 and Table 1). For the bulk sample, the activation barrier is close to 60 kJ/mol, which is in quite good agreement with E_a provided by Hanaya et al.[36] On the other hand, the activation barrier for the crystallization of salol confined in pores of 150 and 100 nm diameter are equal to 71 kJ/mol and 49 kJ/mol, respectively. The variation in the value of activation barrier may suggest that this process is characterized by different tendency to crystal growth under spatial confinement. Alternatively, interaction between host matrix and guest molecules may significantly alter the results contributing to the development of the negative pressure in the confined systems. One can add that a few years ago Patkowski et al.[37] published an article on salol confined in CPG glasses, where they discussed the impact of negative pressure on the molecular dynamics and measured the glass transition temperature. By the analogy one can assume that a similar situation may occur in the investigated systems. In fact, our newest research indicated unquestionably that negative pressure plays a quite important role in controlling the dynamics of salol confined in alumina oxide membranes. It was well demonstrated by comparison of the data measured at high pressures with those obtained under confinement.[38] However, it should be added that this effect becomes significant below the temperature where vitrification of the interfacial molecules is observed. On the other hand, all crystallization studies were carried out above the temperature where the change in slope of the core molecules is observed.[30] Thus, it is justified to assume that the impact of negative pressure on the crystallization process in confined salol is negligible.

It should also be added that there might be another explanation of this non-monotonic change in activation barrier of crystallization of salol. We suppose that it can be due to formation of different polymorphic forms in pores of 150 and 100 nm diameter. One can mention that the phenomenon of polymorphism of bulk salol has been relatively well described in the literature. Therefore, to verify our hypothesis and to gain better understanding of various crystallization pathways of salol embedded in AAO matrices, we carried out additional non-isothermal DSC measurements and compared results to the data published earlier by Moura Ramos and co-workers.[39] It should be stressed that authors have studied the kinetics of non-isothermal crystallization of bulk salol, employing a series of experiments involving different heating rates, ϕ. The amorphous bulk salol was heated at various rates, from 2 to 20 K/min. They observed that the cold crystallization is strongly sensitive to heating rate and the position of the exothermic peak shifts to higher temperatures. Moreover, it was found that the melting temperature of salol after cold crystallization depends on heating rates—for low ϕ (lower than 6 K/min) the most stable polymorph with T_m^I = 315 K is obtained, whereas for the heating rates higher than 7 K/min cold crystallization leads to formation of other polymorph with melting point T_m^{II} = 302 K. In order to avoid repetition of non-isothermal DSC measurements, we performed only several scans to confirm the compatibility of presented results with those reported by Moura Ramos et al.

Based on the non-isothermal DSC thermograms published by Moura Ramos and co-workers, we estimated characteristic

DOI: 10.1021/acs.cgd.5b01181
Cryst. Growth Des. XXXX, XXX, XXX−XXX

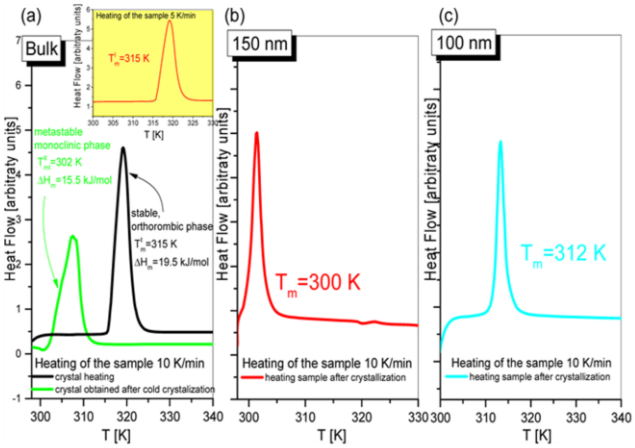

Figure 6. DSC heating scans for salol in (a) bulk state and confined in AAO pores, where diameters are (b) 150 nm and (c) 100 nm.

temperatures of crystallization, i.e., the onset temperature of crystallization T_o and the peak temperature of crystallization T_p (the temperature at the maximum crystallization rate). These parameters are useful to determine the activation energy of non-isothermal crystallization. To obtain the value of E_c, we used two different methods proposed by Kissinger[40] and by Augis and Bennett.[41] The approximation proposed by Kissinger takes into account only a variation of the maximum crystallization peak (T_p) with the heating rate (ϕ), according to equation

$$\ln\left(\frac{\phi}{T_p^2}\right) = C_K - \frac{E_c}{RT_p} \tag{9}$$

where C_K is a fitting parameter.

Another method commonly used to estimate activation energy of crystallization is the Augis and Bennett approach. This method considers the onset temperature of crystallization T_o and is given by the following equation:

$$\ln\left(\frac{\phi}{T_p - T_o}\right) = C_{AB} - \frac{E_c}{RT_p} \tag{10}$$

where C_{AB} is a fitting parameter.

The values of parameters T_o, T_p, and ϕ were digitized from the work by Moura Ramos et al. and were used to calculate E_c. The results of our studies with the use of both mentioned above approaches are shown in Figure 5.

Additionally, in Figure 5 we included black points (circle and square), which represent the data calculated from our measurements for two different heating runs (10 and 5 K/min). Interestingly, it was found that the rates obtained from our studies match almost perfectly the ones determined by Moura Ramos et al. In addition, it is seen that data presented in Figure 5 follow two different trends suggesting that crystallization of salol must be described with the use of two different activation barriers in the studied range of heating rates. It is undoubtedly related to the formation of two polymorphs of salol as discussed by Moura Ramos and co-workers. Utilizing data reported in ref 39 and applying approaches proposed by Kissinger and Augis and Bennett, we estimated activation barriers for the crystallization, which were approximately equal to 80 kJ/mol, 45 kJ/mol (Augis and Bennett) and 90 kJ/mol, 38 kJ/mol (Kissinger) for the metastable and stable polymorphic forms of salol, respectively.

However, what is meaningful for our discussion there are two activation barriers describing crystallization of stable and unstable forms of salol. Interestingly, E_c = 80 and 45 kJ/mol as obtained from Augis and Bennett approach corresponds quite well to the activation energies evaluated for the crystallization of salol infiltrated in 150 and 100 nm AAO membranes. It should also be pointed out that there are some small discrepancies between reported activation barriers. However, it can be due to the fact that both sets of activation barriers were obtained from isothermal and non-isothermal measurements. Moreover, the impact of confinement on the activation energy of crystallization cannot be neglected. Anyway, one concludes that quite good correspondence of E_c can be a good indicator that in fact depending on the degree of confinement, different polymorphic forms of salol are produced.

However, to fully address this issue we carried out further DSC measurements on the salol crystallized in AAO membranes.

Melting Behavior and Polymorphism. In order to identify the crystal form obtained after recrystallization, we investigated the thermal behaviors of salol. We have studied the melting of crystal by the DSC technique, employing a series of experiments carried out in bulk and confined salol at constant heating rates, ϕ = 10 K/min. Figure 6 shows the changes of melting point in crystal salol in a given system. In the case of bulk salol (Figure 6a) two very clearly visible endothermic peaks are recorded. The first one (black line) is related with the melting point of original crystal (T_m^I = 315 K), while the second line (green) shows the melting temperature (T_m^{II} = 302 K) obtained for sample after cold crystallization. As can be seen, melting temperatures of both samples differ significantly from each other. Differences in the melting temperatures in the same material are associated with the existence of two polymorphic forms. One can remind that the first, stable, phase is characterized by orthorhombic crystal system (T_m^I = 315 K) and second, metastable, is monoclinic with T_m^{II} = 302 K.[39,42−45] The form II is unstable and readily undergoes solid−solid monotropic transition to the stable phase during spontaneous transformation.[36,46]

DOI: 10.1021/acs.cgd.5b01181
Cryst. Growth Des. XXXX, XXX, XXX−XXX

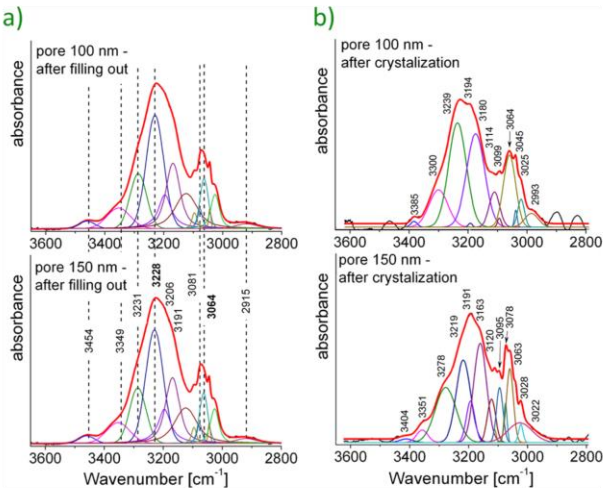

Figure 7. FTIR single spectra of salol inside the AAO membrane subtracted by pure membrane measured at the moment of filling out by substance (a) and after its crystallization in pores (b) (data for 100 and 150 nm pores).

The other characteristic property of the salol crystallization is melting enthalpy ΔH_m^{bulk}, which can be obtained by integrating the peak of crystallization as measured by DSC. We obtained ΔH_m^{bulk} to be equal to 19.5 and 15.5 kJ/mol for stable and metastable form, respectively. The estimated values agree very well with the reported ones by Moura Ramos et al.[39] and Hanaya et al.[36]

Hence, as discussed above one can use both parameters, i.e., melting temperature and heat of fusion, as quite reliable indicators to evaluate which kind of polymorph was produced upon crystallization of salol embedded into AAO templates.

In panels (b) and (c) of Figure 6, DSC curves obtained for salol crystallized in pores of 150 and 100 nm diameter are shown. As can be seen, the melting temperatures were shifted in comparison to the bulk material. According to the predictions and literature data,[7,10−12] the melting points of the given glass-former confined in the porous matrix should linearly decrease with the degree of confinement as it is predicted by the well-known Gibbs−Thomson relationship. However, we found out that in the case of salol this change is not monotonous. It is seen that for salol confined in pores of 150 and 100 nm diameter melting temperatures are equal to T_m = 300 and 312 K, respectively. Hence, breakdown of Gibbs−Thomson prediction is a clear indication of polymorphism of salol. Of course, it should be noted that melting temperatures of both forms are slightly shifted to lower temperatures (∼2−3 K) with respect to the bulk conditions. However, it is a natural consequence of the impact of confinement on the melting temperature. Thus, we conclude that the stable form of salol is preferred for the lower degree of confinement while the unstable one is preferred for the larger pores.

To confirm the various crystallization pathways of salol in pores of different diameters (d = 100 nm, d = 150 nm) additional FTIR measurements were carried out at the moment of filling out the membranes (t_0) as well as after crystallization (t_n) (see Figure 7). Unfortunately, we cannot compare directly confined and bulk samples due to (i) different geometry of both systems, (ii) strong interactions between template and salol, and (iii) impact of spatial confinement, which contribute to significant shift of the measured characteristic bands in FTIR spectrum.

The great similarity of both FTIR spectra at t_0 was observed. Two bands close to 3454 and 3349 cm^{-1} pointed to hydroxyl stretching vibrations of free OH group within the salol molecule. According to the literature data, the region between 3130 and 3070 cm^{-1} is determined by the aromatic CH stretching vibrations which are typically exhibited as a multiplicity of weak-to-moderate bands. Moreover, quite high complexity of infrared spectrum in the 3300−3000 cm^{-1} range might be strongly dependent on intramolecular interactions between two molecules as well as the presence of hydroxyl moieties attached to the pore walls which strongly interact with salol's hydroxyl and carbonyl moieties.

The character of the salol's FTIR spectrum in the 4000−2500 cm^{-1} region after crystallization in AAO pores (100 nm/150 nm) is quite different (see Figure 7b). This is particularly noticeable in the case of the number of bands observed in the spectrum, their intensity, and full width at half-maximum (fwhm). It is due to the different crystallization pathways of salol confined in AAO of varying pore diameter. In the case of salol embedded in 150 nm pores the character of the infrared spectrum after crystallization is close to data obtained at t_0. The main bands associated with H-bonds have similar intensity and fwhm (∼30 cm^{-1}). Molecular ordering and interaction changes between them influence the presence of bands at 3404, 3351, and 3278 cm^{-1}, which are associated with free hydroxyl stretching vibration taking place within salol molecules and due to hydroxyl units inside the pore walls. In the case of 100 nm pores, the infrared spectrum has completely different character with respect to t_0 and 150 nm pores. Free hydroxyl groups reflect at 3385 and 3300 cm^{-1}. The lower complexity of infrared spectrum between 3300 and 3000 cm^{-1} as well as different band intensity and higher fwhm (∼10 cm^{-1}) than for the 150 nm pore was observed. Interestingly, two very intense bands at 3239 and 3194 cm^{-1} detected in the case of the 100 nm pore are shifted about 20 cm^{-1} toward lower

DOI: 10.1021/acs.cgd.5b01181
Cryst. Growth Des. XXXX, XXX, XXX−XXX

wavenumbers with respect to the 150 nm pore. Additionally, the intensity of these bands is the opposite if we consider both membranes of different pore sizes. The similar behavior between infrared spectra was found in the case of bands at 3064 cm^{-1} (higher intensity in the case of 100 nm pores with respect to 150 nm).

Since the impact of confinement on the position of the characteristic bands captured by FTIR spectroscopy should be very similar for the salol confined in alumina oxide membranes in different pores sizes, one can certify that in fact the structure of crystals formed in both membranes must be different. In addition, with the other observations coming from the crystallization dielectric and calorimetric studies taken into account, it seems most probable that in fact in pores of higher diameter an unstable form of salol is formed, while at smaller nanochannels, orthorhombic crystals are preferred.

4. CONCLUSIONS

The opportunity to control the crystallization process of material in a confined nanosystem opens new ways to tailor the substance properties and to achieve property enhancements that are not possible with the bulk material. In this work we have shown that native nanoporous materials can be applied to tune the crystallization pathways toward formation of a given polymorphic form as well as to prevent the crystallization process as the pore size is significantly reduced. The size of confined spaces can greatly affect the value of the energy associated with nucleation, crystal growth, and orientation of the formed crystals. This way allows to control of the crystallization on the nanometer scale which in consequence may lead to formation of new crystalline forms characterized by completely different physicochemical properties.

Here, using different experimental techniques (BDS, DSC) we demonstrated that the tendency to crystallization of salol confined in AAO membranes depends on pore size and the morphology of formed crystal. All these factors have a significant impact on the kinetics of crystallization. As shown by BDS studies, dimension of formed crystal in confined system is reduced to two in comparison to the bulk-like salol (where $n \sim 3$). Moreover, it was observed that the increase of crystallization rate in 150 nm AAO membrane with respect to the bulk salol is directly connected to the different mechanism of crystallization. It was presented that crystallization is tuned toward formation of one well-defined polymorphic form of salol. However, at the same time we demonstrated that by reducing pore size one can suppress and avoid crystallization of this compound.

Moreover, thermal studies have shown that the melting point is shifted to lower temperature with decreasing pore diameter but the Gibbs−Thomson relation is not fulfilled. It is due to formation of various polymorphic forms of salol in pores of different diameter. Consequently, it is possible to obtain a stable form of salol in 100 nm with melting point T_m^I = 312 K, and metastable in 150 nm (T_m^{II} = 300 K). As evidence of the existence of two forms, we carried out infrared measurements for each membrane. FTIR spectra demonstrated differences in the number of bands, their intensity, and full width at half-maximum (fwhm).

In addition, activation energies calculated for two polymorphic forms in bulk salol (from nonisothermal DSC) agree quite well with the ones estimated from isothermal BDS and DSC measurements for salol confined in AAO membranes. The results presented in this paper show great potential of the nanoporous matrix to control crystal growth of a given polymorphic form. It may be useful in the future to develop new ways of producing crystals with tailor-made properties. Although one more important issue, i.e., the lifetime of a given polymorphic form under confinement, must also be addressed with special care.

AUTHOR INFORMATION

Corresponding Author

*E-mail: kkolodziejczyk@us.edu.pl.

Notes

The authors declare no competing financial interest.

ACKNOWLEDGMENTS

E.K. is thankful for financial support from the National Center of Science based on Decision No. DEC-2013/09/D/NZ7/04194. K.K. and M.T. acknowledge financial support by the Polish National Science Centre within OPUS Project (DEC 2015/17/B/ST3/01195). K.K. is deeply thankful for support through a stipend received within the project "DoktoRIS - the stipend program for the innovative Silesia", which is cofinanced by the EU European Social Fund.

REFERENCES

(1) Scherer, G. W. Crystallization in pores. *Cem. Concr. Res.* **1999**, *29*, 1347−1358.
(2) Rault, J.; Neffati, R.; Judeinstein, P. Melting of ice in porous glass: why water and solvents confined in small pores do not crystallize? *Eur. Phys. J. B* **2003**, *36*, 627−637.
(3) Unruh, K. M.; Huber, T. E.; Huber, C. A. Melting and freezing behavior of indium metal in porous glasses. *Phys. Rev. B: Condens. Matter Mater. Phys.* **1993**, *48* (12), 9021−9027.
(4) La Iglesia, A.; Gonzalez, V.; Lopez-Acevedo, V.; Viedma, C. Salt crystallization in porous construction materials I Estimation of crystallization pressur. *J. Cryst. Growth* **1997**, *177* (2), 111−118.
(5) Alcoutlabi, M.; McKenna, G. B. Effects of Confinement on Material Behaviour at the Nanometre Size Scale. *J. Phys.: Condens. Matter* **2005**, *17*, R461−R524.
(6) Park, J. Y.; McKenna, G. B. Size and confinement effects on the glass transition behavior of polystyrene/o-terphenyl polymer solutions. *Phys. Rev. B: Condens. Matter Mater. Phys.* **2000**, *61*, 6667.
(7) Jackson, C. L.; McKenna, G. B. Vitrification and crystallization of organic liquids confined to nanoscale pores. *Chem. Mater.* **1996**, *8*, 2128−2137.
(8) Buffat, P. H.; Borel, J.-P. Size effect on the melting temperature of gold particles. *Phys. Rev. A: At., Mol., Opt. Phys.* **1976**, *13*, 2287.
(9) Couchman, P. R.; Jesser, W. A. Thermodynamic theory of size dependence of melting temperature in metals. *Nature* **1977**, *269*, 481−483.
(10) Jackson, C. L.; McKenna, G. B. The melting behavior of organic materials confined in porous solids. *J. Chem. Phys.* **1990**, *93*, 9002−9011.
(11) Alba-Simionesco, C.; Dosseh, G.; Dumont, E.; Frick, B.; Geil, B.; Morineau, D.; Teboul, V.; Xia, Y. Confinement of molecular liquids: consequences on thermodynamic, static and dynamical properties of benzene and toluene. *Eur. Phys. J. E: Soft Matter Biol. Phys.* **2003**, *12*, 19−28.
(12) Jackson, C. L.; McKenna, G. B. The glass transition of organic liquids confined to pores. *J. Non-Cryst. Solids* **1991**, *131-133*, 221.
(13) Thomson, W. On the equilibrium of vapour at a curved surface of liquid. *Philos. Mag.* **1871**, *42*, 448−52.
(14) Gibbs, J. W. *Collected Works*; Yale University Press: New York, 1928.
(15) Defay, R.; Prigogine, I.; Bellemans, A.; Everett, D. H. *Surface Tension and Adsorption*; Wiley: New York, 1966.
(16) Garti, N.; Schlichter, J.; Sarig, S. Effect of food emulsifiers on polymorphic transitions of cocoa butter. *J. Am. Oil Chem. Soc.* **1986**, *63* (2), 230−236.

DOI: 10.1021/acs.cgd.5b01181
Cryst. Growth Des. XXXX, XXX, XXX−XXX

(17) Lopez, C.; Ollivon, M. Triglycerides obtained by dry fractionation of milk fat: 2. Thermal properties and polymorphic evolutions on heating. *Chem. Phys. Lipids* **2009**, *159*, 1−12.
(18) Yu, L. X.; Furness, M. S.; Raw, A.; Woodland Outlaw, K. P.; Nashed, N. E.; Ramos, E.; Miller, S. P. F.; Adams, R. C.; Fang, F.; Patel, R. M.; Holcombe, F. O., Jr.; Chiu, Y.; Hussain, A. S. Scientific Considerations of Pharmaceutical Solid Polymorphism in Abbreviated New Drug Applications. *Pharm. Res.* **2003**, *20*, 4.
(19) Bernstein, J.; Davey, R. J.; Henck, J.-O. Concomitant polymorphs. *Angew. Chem., Int. Ed.* **1999**, *38*, 3440−3461.
(20) Morissette, S. L.; Soukasene, S.; Levinson, D.; Cima, M. J.; Almarsson, O. *Proc. Natl. Acad. Sci. U. S. A.* **2003**, *100*, 2180−2184.
(21) Ojala, W. H.; Etter, M. C. Polymorphism in anthranilic acid: a reexamination of the phase transitions. *J. Am. Chem. Soc.* **1992**, *14* (26), 10288−10293.
(22) Ha, J.-M.; Wolf, J. H.; Hillmyer, M. A.; Ward, M. D. Polymorph selectivity under nanoscopic confinement. *J. Am. Chem. Soc.* **2004**, *126*, 3382−3383.
(23) Hamilton, B. D.; Hillmyer, M. A.; Ward, M. D. Glycine polymorphism in nanoscale crystallization chambers. *Cryst. Growth Des.* **2008**, *8*, 3368−3375.
(24) Rengarajan, G. T.; Enke, D.; Steinhart, M.; Beiner, M. Size-dependent growth of polymorphs in nanopores and Ostwald's step rule of stages. *Phys. Chem. Chem. Phys.* **2011**, *13*, 21367−21374.
(25) Rengarajan, G. T.; Enke, D.; Beiner, M. Crystallization behavior of acetaminophen in nanopores. *Open Phys. Chem. J.* **2007**, *1*, 18−24.
(26) Rengarajan, G. T.; Enke, D.; Steinhart, M.; Beiner, M. Stabilization of the amorphous state of pharmaceuticals in nanopores. *J. Mater. Chem.* **2008**, *18* (22), 2537−2539.
(27) Beiner, M.; Rengarajan, G. T.; Pankaj, S.; Enke, D.; Steinhart, M. Manipulating the Crystalline State of Pharmaceuticals by Nanoconfinement. *Nano Lett.* **2007**, *7*, 1381−1385.
(28) Ostwald, W. *Z. Phys. Chem.* **1897**, 289−330.
(29) Dosseh, G.; Xia, Y.; Alba-Simionesco, C. Cyclohexane and benzene confined in MCM-41 and SBA-15: confinement effects on freezing and melting. *J. Phys. Chem. B* **2003**, *107*, 6445−53.
(30) Adrjanowicz, K.; Kolodziejczyk, K.; Kipnusu, W. K.; Tarnacka, M.; Mapesa, E. U.; Kaminska, E.; Pawlus, S.; Kaminski, K.; Paluch, M. Decoupling between the Interfacial and Core Molecular Dynamics of Salol in 2D Confinement. *J. Phys. Chem. C* **2015**, *119* (25), 14366−14374.
(31) Havriliak, S.; Negami, S. A complex plane analysis of α-dispersions in some polymer systems. *J. Polym. Sci., Part C: Polym. Symp.* **1966**, *14*, 99.
(32) Shi, X. M.; Zhang, J.; Jin, J.; Chen, S. J. Non-isothermal crystallization and melting of ethylene-vinyl acetate copolymers with different vinyl acetate contents. *eXPRESS Polym. Lett.* **2008**, *2*, 623−629.
(33) Böhm, N.; Kulicke, W.-M. Rheological studies of barley (1″3) (1″4)-b-glucan in concentrated solution: mechanistic and kinetic investigation of the gel formation. *Carbohydr. Res.* **1999**, *315*, 302−311.
(34) Ha, J.-M.; Hillmyer, M. A.; Ward, M. D. Thermotropic Properties of Organic Nanocrystals Embedded in Ultrasmall Crystallization Chamber. *J. Phys. Chem. B* **2005**, *109*, 1392−1399.
(35) Avramov, I.; Avramova, K.; Russel, C. New Method to Analyze Data on Overall Crystallization Kinetics. *J. Cryst. Growth* **2005**, *285*, 394−399.
(36) Hanaya, M.; Hikima, T.; Hatase, M.; Oguni, M. Low-temperature adiabatic calorimetry of salol and benzophenone and microscopic observation of their crystallization: finding of homogeneous-nucleation-based crystallization. *J. Chem. Thermodyn.* **2002**, *34*, 1173−1193.
(37) Patkowski, A.; Ruths, T.; Fischer, E. W. Dynamics of supercooled liquids confined to the pores of sol-gel glass: A dynamic light scattering study. *Phys. Rev. E: Stat. Phys., Plasmas, Fluids, Relat. Interdiscip. Top.* **2003**, *67*, 021501.
(38) Adrjanowicz, K.; Kaminski, K.; Koperwas, K.; Paluch, M. Negative Pressure Vitrification of the Isochorically Confined Liquid in Nanopores. *Phys. Rev. Lett.* **2015**, *115*, 265702.
(39) Moura Ramos, J. J.; Correia, N. T.; Diogo, H. P. Vitrification, nucleation and crystallization in phenyl-2-hidroxybenzoate (salol) studied by Differential Scanning Calorimetry (DSC) and Thermally Stimulated Depolarisation Currents (TSDC). *Phys. Chem. Chem. Phys.* **2004**, *6*, 793−798.
(40) Kissinger, H. E. Variation of peak temperature with heating rate in differential thermal analysis. *J. Res. Natl. Stand.* **1956**, *57*, 217−221.
(41) Augis, J. A.; Bennett, J. E. Calculation of the Avrami parameters for heterogeneous solid state reactions using a modified the Kissinger method. *J. Therm. Anal.* **1978**, *13*, 283−292.
(42) Deffet, L. *Bull. Soc. Chim. Belg.* **1935**, *44*, 97−139.
(43) Michel, J. *Bull. Soc. Chim. Belg.* **1939**, *48*, 105−157.
(44) De Rooster, J. *Bull. Soc. Chim. Belg.* **1948**, *57*, 187−210.
(45) Hammond, R. B.; Jones, M. J.; Roberts, K. J.; Kutzke, H.; Klapper, H. A structural study of polymorphism in phenyl salicylate: determination of the crystal structure of a meta-stable phase from X-ray powder diffraction data using a direct space systematic search method. *Z. Kristallogr. - Cryst. Mater.* **2002**, *217*, 484−491.
(46) Bilgram, J. H.; Durig, U.; Wachter, M.; Seiler, P. Zone refining and structure determination of salol crystals. *J. Cryst. Growth* **1982**, *57* (1), 1−5.

DOI: 10.1021/acs.cgd.5b01181
Cryst. Growth Des. XXXX, XXX, XXX−XXX

3.3.1 Oświadczenia współautorów publikacji III

mgr Magdalena Tarnacka
Uniwersytet Śląski
Instytut Fizyki im. Augusta Chełkowskiego
ul. Uniwersytecka 4
40-007 Katowice

Katowice, 18 stycznia 2016 r.

OŚWIADCZENIE

Oświadczam, że w pracy K. Kołodziejczyk, M. Tarnacka, E. Kamińska, M. Dulski, K. Kamiński, M. Paluch opublikowanej na stronie internetowej czaspomisma Crystal Growth & Design (DOI**:** 10.1021/acs.cgd.5b01181) 13 stycznia 2016 r., a zatytułowanej „*Crystallization's Kinetic Under Confinement. Manipulation of the Crystalline Form of Salol by Varying Pore Diameter",* mój udział polegał na dyskusji wyników.

dr Ewa Kamińska
Śląski Uniwersytet Medyczny
Wydział Farmaceutyczny
z Oddziałem Medycyny Laboratoryjnej
ul. Jagiellońska 4
41-200 Sosnowice

Katowice, 24 lutego 2016 r.

OŚWIADCZENIE

Oświadczam, że w pracy K. Kołodziejczyk, M. Tarnacka, E. Kamińska, M. Dulski, K. Kamiński, M. Paluch opublikowanej na stronie internetowej czaspomisma Crystal Growth & Design (DOI**:** 10.1021/acs.cgd.5b01181) 13 stycznia 2016 r., a zatytułowanej „*Crystallization's Kinetic Under Confinement. Manipulation of the Crystalline Form of Salol by Varying Pore Diameter",* mój udział polegał na analizie części danych pomiarowych, uczestnictwie w dyskusji wyników oraz korekcie tekstu manuskryptu.

Ewa Ozimina-Kamińska

dr Mateusz Dulski
Uniwersytet Śląski
Instytut Fizyki im. Augusta Chełkowskiego
ul. Uniwersytecka 4
40-007 Katowice

Katowice, 18 stycznia 2016r.

OŚWIADCZENIE

Oświadczam, że w pracy K. Kołodziejczyk, M. Tarnacka, E. Kamińska, M. Dulski, K. Kamiński, M. Paluch opublikowanej na stronie internetowej czaspomisma Crystal Growth & Design (DOI**:** 10.1021/acs.cgd.5b01181) 13 stycznia 2016 r., a zatytułowanej *„Crystallization's Kinetic Under Confinement. Manipulation of the Crystalline Form of Salol by Varying Pore Diameter",* mój udział polegał na wykonaniu pomiarów w podczerwieni w przypadku związku umieszczonego w membranach Al_2O_3 o różnych średnicach porów oraz opracowaniu w postaci rysunków oraz tekstu, zarejestronwaych danych.

Mateusz Dulski

dr hab. Kamil Kamiński
Uniwersytet Śląski
Instytut Fizyki im. Augusta Chełkowskiego
ul. Uniwersytecka 4
40-007 Katowice

Katowice, 24 lutego 2016 r.

OŚWIADCZENIE

Oświadczam, że w pracy K. Kołodziejczyk, M. Tarnacka, E. Kamińska, M. Dulski, K. Kamiński, M. Paluch opublikowanej na stronie internetowej czaspomisma Crystal Growth & Design (DOI**:** 10.1021/acs.cgd.5b01181) 13 stycznia 2016 r., a zatytułowanej „*Crystallization's Kinetic Under Confinement. Manipulation of the Crystalline Form of Salol by Varying Pore Diameter",* mój udział polegał na dyskusji uzyskanych wyników eksperymentalnych oraz korekcie tekstu manuskryptu.

prof. zw. dr hab. Marian Paluch
Uniwersytet Śląski
Instytut Fizyki im. Augusta Chełkowskiego
ul. Uniwersytecka 4
40-007 Katowice

Katowice, 24 lutego 2016 r.

OŚWIADCZENIE

Oświadczam, że w pracy K. Kołodziejczyk, M. Tarnacka, E. Kamińska, M. Dulski, K. Kamiński, M. Paluch zaakceptowanej 13 stycznia 2016 r. do publikacji w czasopiśmie Crystal Growth & Design, a zatytułowanej „*Crystallization's Kinetic Under Confinement. Manipulation of the Crystalline Form of Salol by Varying Pore Diameter",* mój udział polegał na polegał na nadzorowaniu przeprowadzonych analiz, dyskusji otrzymanych wyników oraz korekcie tekstu manuskryptu.

Rozdział IV

4 OMÓWIENIE POZOSTAŁYCH OSIĄGNIĘĆ I WYNIKÓW PRAC BADAWCZYCH

Efektem realizacji tematu pracy doktorskiej są publikacje 1-3. Ponadto przyczyniłam się również do powstania dwunastu artykułów (4-15) opublikowanych w czasopismach z listy filadelfijskiej. W pracach tych moją główną rolą było wykonywanie analizy termicznej i/lub badań dynamiki molekularnej analizowanych substancji.

W artykule 4 opisana została analiza zależności pomiędzy ruchliwością molekularną a tendencją do rekrystalizacji amorficznego celokoksybu. Dane pokazują, że celokoksyb charakteryzuje się bardzo wysoką niestabilnością w szkle, co prawdopodobnie związane jest z dużą ruchliwością molekuł w tej fazie. Wykazano dużą rolę procesu *β*, który został zidentyfikowany jako *true*-JG, co świadczy o tym, że relaksacja ta jest prekursorem α-procesu.

Kolejna z prac, 9, ukazuje badania ruchliwości molekularnej amorficznego itrakonazolu przygotowanego za pomocą witryfikacji i kriomielenia. Badania kalorymetryczne, dielektryczne oraz obleczenia DFT ujawniają, że itrakonazol wykazuje ciekłokrystaliczny porządek oraz że podczas dewitryfikacji obserwowane jest przejście z fazy smektycznej do nematycznej. Ponadto przedstawiona została charakterystyka dynamiki molekularnej itrakonazolu w podwyższonym ciśnieniu. Wykazano, że kształt procesu relaksacji strukturalnej nie zmienia się podczas zmian ciśnienia, a także, iż podczas zwiększania ciśnienia proces ten staje się mniej wrażliwy na zmiany temperatury.

Niezwykle interesującym tematem jest również analiza dynamiki molekularnej cieczy w układach zamkniętych (ang. *confined*). Przedmiotem badań przedstawionych w publikacji 14 był salol umieszczony w porowatych matrycach wykonanych z tlenku glinu (AAO) oraz salol w „masie". Okazuje się, że własności salolu zamkniętego w membranach AAO różnią się drastycznie od tych zaobserwowanych w próbce makroskopowej. Zamiany te są widoczne

szczególnie w czasach relaksacji strukturalnej. Warto zauważyć, że w widmach dielektrycznych układów salol-membrany AAO oprócz relaksacji strukturalnej widoczny jest także dodatkowy proces - nazwany przez autorów - międzyfazowym (ang *interfacial*). Proces ten prawdopodobnie związany jest z oddziaływaniem molekuł substancji na ścianki porów. Ponadto zaobserwowano istnienie dwóch przejść szklistych w salolu zamkniętym w matrycach AAO. Istnienie podwójnego przejścia szklistego świadczy o tym, iż w układzie salol-membrana AAO istnieją dwa rodzaje ruchliwości molekuł - pierwsza - związana z molekułami znajdującymi się blisko ścianek porów ($T_{g,hi}$) oraz druga - z cząsteczkami będącymi w centrum (w rdzeniu porów, $T_{g,lo}$). Dodatkowo na podstawie danych kalorymetrycznych oszacowany został rozmiar warstwy centralnej.

Wiele związków farmaceutycznie czynnych występuje w postali soli. Należą do nich m.in. bursztynian lidokainy, chlorowodorek prokainy czy chlorowodorek prokainamidu, które bardzo często nazywa się tzw. protonowymi cieczami jonowymi (ang. *protic ionic liquids (PILs)*). W pracy 5 zostały zaprezentowany sposób monitorowania zmian dynamiki molekularnej fosforanu karwedilolu oraz chlorowodorku prokainy w stanie szklistym. Wyniki te pokazują, że obserwacja zmian czasów relaksacji przewodnictwa podczas fizycznego „starzenia" próbki może być sposobem na przewidzenie ruchliwości molekularnej w szkle, a co za tym idzie – stabilność fizycznej amorficznych farmaceutyków. Dodatkowo w praca 7 opisane zostały bardziej szczegółowo badania relaksacji przodownictwa substancji z grupy PILs w pobliżu przejścia szklistego. Zauważono istnienie silnego rozdzielenia (ang. *decoupling*) pomiędzy przewodnictwem jonowym a relaksacją strukturalną. Analiza widm dielektrycznych (w reprezentacji M', M''), pokazała, że zbliżając się do T_g, relaksacja jonów przewodnictwa staje się szybsza niż proces strukturalny, a w temperaturze zeszklenia czasy relaksacji strukturalnej są o trzy dekady dłuższe niż czasy relaksacji przodownictwa. Zachowanie to wydaje się być uniwersalne, ponieważ zostało zaobserwowane już w kilku protonowych cieczach jonowych opisanych w literaturze.

Ponadto rozważany w kontekście rekrystalizacji temat dynamicznej heterogeniczności układów został przedstawiony w publikacjach 6 i 10. W artykule 6 przedstawiona została analiza wypływu zmian temperatury i ciśnienia na stopień dynamicznej heterogeniczności. Analiza dotyczyła dwóch modelowych cieczy van der Waals'a; 1,1'-bis (*p*-metoksyfenylo) cykloheksan (BMPC) i o-terfenylu (OTP). Wyniki zaprezentowane w artykule pokazują, że zmiana temperatury wywiera znacznie większy wpływ na dynamiczną heterogeniczność niż ciśnienie, co ma swoje odzwierciedlenie w czasach relaksacji strukturalnej. Rezultat ten ujawnia, że temperatura i ciśniecie nie mogą być traktowane jako równorzędne parametry.

Dodatkowo, w artykule 10 zaprezentowano rozważania dotyczące stopnia dynamicznej heterogeniczności, relaksacji strukturalnej w kontekście skalowania gęstościowego. Związek pomiędzy czasami relaksacji strukturalnej i objętością korelacji (definiowanej jako maksimum czteropunktowej funkcji korelacji, $\chi_4^{\max}$) jest jedną z najbardziej spodziewanych relacji pomiędzy skalą długości i czasów dynamiki molekularnej w pobliżu T_g. Na podstawie analizy danych dielektrycznych otrzymanych z pomiarów wysokociśnieniowych wykazano, że czasy relaksacji strukturalnej nie mogą być tylko i wyłącznie funkcją stopnia dynamicznej heterogeniczności. Ponadto pokazano, że gdy potęgowe skalowanie gęstościowe jest słuszne, to parametr łączący $\chi_4^{\max}$ i τ_α powinien być potęgową funkcją gęstości.

W rozdziale III, punkcie 3.4 wspominałam o sacharydach jako o matrycach stabilizujących amorficzne substancje czynne farmaceutycznie. W publikacjach 8, 11, 13 i 15 temat stabilizacji fizycznej za pomocą cukrów tj. glukoza, sacharoza oraz maltoza, a także ich acetylowanych pochodnych został dogłębnie przedyskutowany. W artykule 11 przeanalizowana została stabilność indometacyny w mieszaninach z acetylowanymi mono- i disacharydami. Wyniki pokazują, że mieszanina indometacyny+acetylowana glukoza charakteryzuje się najmniejszą stabilnością fizyczną spośród badanych próbek (indomatacyna+acetylowana sacharoza oraz indometacyna+acetylowana maltoza). Badania dielektryczne sugerują, że tendencja do rekrystalizacji tego układu nie jest związana ani z globalną ani z lokalną ruchliwością molekuł. Dopiero badania przy użyciu spektroskopii w podczerwieni oraz metody oparte na teorii funkcjonałów gęstości (DFT) wykazały, że przyczyną niestabilności są słabe oddziaływania wodorowe pomiędzy cząsteczką indometacyny i acetylowanej glukozy. Ponadto wskazano, że rozpuszczalności indometacyny połączonej z acetylowanymi sacharydami poprawia się w nieznaczny sposób, a powodem tego są utworzone oddziaływania pomiędzy matrycą a substancją czynną. Podobną analizę stabilności przeprowadzono w pracy 15. W publikacji tej przedstawiona została analiza dynamiki molekularnej oraz kinetyki krystalizacji mieszanin nifedypiny i acetylowanych sacharydów. Udowodnione zostało, że w przeciwieństwie do acetylowanych monocukrów, zmodyfikowane disacharydy mają znaczący wpływ na rekrystalizację nifedypiny. Symulacje dynamiki molekularnej układów nifedypina+acetylowany cukier wykazują, że siła i struktura wiązań wodorowych w mieszaninach jest zależna od zastosowanego węglowodanu, co ma swoje odzwierciedlenie we wzroście wartości energii aktywacji rozpatrywanych mieszanin. Badania fizycznej stabilności wykazały, że użycie acetylowanej maltozy i sacharozy znacznie spowalnia lub nawet hamuje rekrystalizację nifedypiny, a efekt ten zależny jest od stężenia acetylowanego cukru w mieszaninie. Zahamowanie rekrystalizacji nifedypiny związane jest prawdopodobnie

z powstaniem dodatkowych oddziaływań międzycząsteczkowych, które powodują, że dyfuzja cząsteczek nifedypiny jest na tyle powolna, że nie zdoła wywołać krystalizacji.

Kolejna z opublikowanych prac, 13, dotycz wpływu acetylowanej maltozy na porządek ciekłokrystaliczny i dynamikę molekularną itrakonazolu. Jak już wcześniej wspomniałam (praca 9), itrakonazolu wykazuje ciekłokrystaliczny porządek molekuł, który zostaje zaburzony przez dodanie oktaacetylowanej maltozy. Dodatkowo zaobserwowano, że zmniejsza się szerokość piku α-procesu itrakonazolu po dodaniu pochodnej maltozy, a co za tym idzie – zmniejsza się również wartość parametru kruchości i układ staje się bardziej stabilny. Dodatkowo, acetylowana maltoza wpływa również na relaksacje drugorzędowe. Zmiany w procesach drugorzędowych dowodzą, że najprawdopodobniej globalna ruchliwość molekuł steruje krystalizacją itrakonazolu oraz że dodanie acetylowanej maltozy wpływa na lokalną dynamikę cząsteczek badanej substancji. Co więcej, dodanie acetylowanej maltozy do itrakonazolu znacznie poprawia jego rozpuszczalność.

Ostatni z artykułów poświęcony acetylowanym sacharydom, 8, potwierdza zastosowanie tych substancji jako stabilizatory fizyczne, ale również i chemiczne dla amorficznego furosemidu. Amorfizacja czystego furosemidu nie jest możliwa ani za pomocą witryfikacji ani kriomielenia, ponieważ substancja ta ulega degradacji. Jednakże dodanie acetylowanych cukrów powoduje utworzenie stabilnej jednorodnej mieszaniny charakteryzującej się jedną temperaturą zeszklenia. Co więcej, pomiary rozpuszczalności pokazały, że furosemid kriomielony z acetylowanymi cukrami (maltozą, glukozą oraz sacharozą) cechuje się znacznie większą rozpuszczalnością niż krystaliczna postać tej aktywnej farmaceutycznie substancji.

Rozdział V

5 PODSUMOWANIE

Niniejsza rozprawa doktorska prezentuje zbiór artykułów naukowych poświęconych tematyce rekrystalizacji amorficznych substancji czynnych farmaceutycznie (API), możliwych przyczyn tego zjawiska, jak i metod zapobiegania tego procesu.

Analizę zjawiska rekrystalizacji przedstawiłam na przykładzie dwóch substancji aktywnych farmaceutycznie, salolu i sildenafilu, które charakteryzują się wysoką niestabilnością fizyczną w fazie amorficznej. Do monitorowania procesu rekrystalizacji posłużyłam się wieloma różnorodnymi technikami badawczym, to jest: szerokopasmową spektroskopią dielektryczną (BDS), różnicową kalorymetrią skaningową (DSC), spektroskopią w podczerwieni (FTIR), rentgenografią strukturalną (XRD) oraz mikroskopią optyczną (OM). Mnogość zastosowanych metod badawczych zapewniła dogłębny wgląd w naturę tego procesu, a także pokazała spójność otrzymanych wyników. W celu jak najlepszego odzwierciedlenia warunków produkcji i przechowywania amorficznych substancji, badania rekrystalizacji prowadzone były w warunkach izotermicznych oraz nieizotermicznych. Opis danych eksperymentalnych za pomocą modelu Avramiego, Avramiego-Avramova oraz Ozawy pozwolił mi na uzyskanie parametrów kinetyki krystalizacji badanych substancji takich jak: wymiarowości zarodka kryształu (n), szybkość procesu (k), czas krystalizacji (τ_{cr}) oraz indukcji (t_0), a także wysokość bariery aktywacji (E_a) by zapoczątkowane zostało to zjawisko. Otrzymane wyniki pokazują, że zastosowane modele dają bardzo zbliżone wartości parametrów kinetyki krystalizacji i mogą być stosowane wymiennie do opisu mechanizmu tego procesu.

Powszechnie uznaje się, że głównym czynnikiem kontrolującym zjawisko rekrystalizacji ze stanu amorficznego jest ruchliwość molekularna. Świadczą o tym znalezione przeze mnie (artykuł 1) korelacje pomiędzy czasami relaksacji α-procesu (τ_α) a czasem krystalizacji τ_{cr} oszacowanym z modelu Avramiego-Avramova oraz pomiędzy liczbą skorelowanych molekuł N_c a czasem indukcji, t_0 jak i N_c a τ_{cr}. Dodatkowo wykazałam, że relaksacja β obserwowana

w sildenafilu nie jest procesem JG, co wyklucza ją jako prekursor procesu α, a tym samym jako przyczynę rekrystalizacji.

Dowiodłam również, że teoretyczne przewidywania stabilności w szkle (używając rozszerzonego modelu Adama – Gibbsa) nie są zgodne z przeprowadzonym eksperymentem.

W drugiej kolejności przedstawiłam możliwość stabilizacji fizycznej amorficznych układów. W tym celu użyte zostały nieorganiczne porowate matryce wykonane z tlenku glinu (membrany AAO). Wyniki pokazują (artykuł 3), że w przypadku salolu umieszczonego w membranach AAO, których średnica porów była mniejsza niż 73 nm, krystalizacja nie zachodziła. Co więcej, pokazałam, że matryce AAO mogą być również skutecznym narzędziem do wymuszania geometrii formowanych kryształów, tak by otrzymane zostały kryształy o pożądanych przez przemysł właściwościach fizykochemicznych.

Reasumując, cel badań przestawiony w niniejszej rozprawie doktorskiej jakim było znalezienie możliwych relacji pomiędzy rekrystalizacją a dynamiką molekularną, a także metod stabilizacji, został osiągnięty.

STRESZCZENIE ROZPRAWY DOKTORSKIEJ

Niniejsza rozprawa doktorska prezentuje zbiór artykułów naukowych (1-3) poświęconych tematyce rekrystalizacji amorficznych substancji czynnych farmaceutycznie (API), możliwych przyczyny tego zjawiska jak i metod zapobiegania tego procesu.

Analizę zjawiska rekrystalizacji przedstawiono na przykładzie dwóch substancji aktywnych farmaceutycznie: salolu i sildenafilu, które charakteryzują się wysoką niestabilnością fizyczną w fazie amorficznej. Do monitorowania procesu rekrystalizacji posłużono się wieloma różnorodnymi technikami badawczym, tj.: szerokopasmową spektroskopią dielektryczną (BDS), różnicową kalorymetrią skaningową (DSC), spektroskopią w podczerwieni (FTIR), rentgenografią strukturalną (XRD) oraz mikroskopią optyczną (OM). Ponadto, w celu jak najlepszego odzwierciedlenia warunków produkcji i przechowywania amorficznych substancji, badania rekrystalizacji prowadzone były w warunkach izotermicznych oraz nieizotermicznych.

Do opisu danych eksperymentalnych posłużono się modelami Avramiego, Avramiego-Avramova oraz Ozawy, które pozwoliły na oszacowanie parametrów kinetyki krystalizacji badanych substancji takich jak: wymiarowości zarodka kryształu (n), szybkość procesu (k), czas krystalizacji (τ_{cr}) oraz indukcji (t_0), a także wysokość bariery aktywacji (E_a) by zapoczątkowane zostało to zjawisko. Otrzymane wyniki pokazują, że zastosowane modele dają bardzo zbliżone wartości parametrów kinetyki krystalizacji i mogą być stosowane wymiennie do opisu mechanizmu tego procesu.

Powszechnie uznaje się, że główną przyczyną rekrystalizacji ze stanu amorficznego jest ruchliwość molekuł. Świadczą o tym przedstawione w artykule 1 i 2 korelacje pomiędzy czasami relaksacji α-procesu (τ_α) a czasem krystalizacji τ_{cr} oszacowanym z modelu Avramiego-Avramova oraz pomiędzy liczbą skorelowanych molekuł N_c a czasem indukcji, t_0, a także N_c i τ_{cr}. Dodatkowo stwierdzono, że proces β obserwowany w sildenafilu nie jest procesem JG, co wyklucza relaksację drugorzędową jako przyczynę rekrystalizacji.

Wykazano także, że teoretyczne przewidywania stabilności fizycznej fazy szklistej (używając rozszerzonego modelu Adama – Gibbsa) nie są zgodne z przeprowadzonym eksperymentem.

Dodatkowo zaprezentowano możliwość stabilizacji fizycznej amorficznych układów. W tym celu użyte zostały nieorganiczne porowate matryce wykonane z tlenku glinu (membrany AAO). Wyniki pokazują (artykuł 3), że w przypadku salolu umieszczonego

w membranach AAO, których średnica porów była mniejsza niż 73 nm, krystalizacja nie zachodziła. Co więcej, wykazano, że matryce AAO mogą być również skutecznym narzędziem do wymuszania geometrii formowanych kryształów, tak by otrzymane zostały kryształy o pożądanych przez przemysł właściwościach fizykochemicznych.

STRESZCZENIE ROZPRAWY DOKTORSKIEJ W JĘZYKU ANGIELSKIM

This dissertation presents a collection of scientific articles (1-3) devoted to recrystallization of the amorphous of pharmaceutically active ingredients (API), the possible causes of this phenomenon and methods of preventing recrystallization process.

The phenomenon of recrystallization is exemplified by two pharmaceutically active substances, salol and sildenafil characterized by a high instability in the amorphous phase. To monitoring process of recrystallization it was used a large variety of research techniques, that are: broadband dielectric spectroscopy (BDS), differential scanning calorimetry (DSC), infrared spectroscopy (FTIR), X-ray diffraction (XRD) and microscopy technique (OM). Moreover, in order to best reflect the conditions of manufacture and storage of amorphous material, the study of recrystallization were carried out in an isothermal and non-isothermal condition.

To describe the experimental data, it was used Avrami, Avrami-Avramov and Ozawa model, which allowed estimation of kinetics crystallization parameters, such as: dimensionality of crystal (n), rate of crystallization (k), time of crystallization (τ_{cr}) and induction time (t_0) and the barrier of activation (E_a) this process. The results show that the application of those models provide to obtain a very similar values of crystallization parameters and that the models can be used interchangeably to describe the mechanism of this process.

It is widely recognized that the main cause of recrystallization from an amorphous state is the a molecular mobility. This is evidence by data presented in Article 1 and 2, where it was found a correlation between the relaxation times of α-process (τ_α) and crystallization time τ_{cr} estimated from Avrami-Avramov model. Moreover, it was also discovery of relation between the number of dynamic correlated molecules, N_c and induction time, t_0 and also between N_c and τ_{cr}. It was shown, that the β-relaxation of sildenafil cannot be classified as the JG process, which is often expected to play a potential role in devitrification. Therefore, influence of secondary process on physical stability in case of amorphous sildenafil seem to be not significant.

It was also proved that the sildenafil is stable for 6 months during long-term storage. However, the theoretical prediction of physical stability in the glass state by using the Adam – Gibbs model extended does not confirm this results.

Additionally, it was presented the possibility of physical stabilization of amorphous system. To achieve this purpose it was used an inorganic porous matrix made of aluminum oxide (AAO

membrane). The results show (publication 3) that the crystallization of salol did not occur when the pores diameters of AAO membranes are less than 73 nm. Moreover, it was shown that the AAO templates can be an effective tool for manipulation of geometry formed crystals, what may be useful in the future to develop new ways of producing crystals with tailor-made physicochemical properties.

LITERATURA

[1] C. Lipiński, Am. Pharm. Rev. 2002, 5, 82-85

[2] D. Q.M. Craig, P. G. Royall, V. L.. Kett, M. L. Hopton, Int. J. Pharm. 1999, 179, 179-207

[3] S. B. Murdande, M. J. Pikal, R. M. Shanker, R. H. Bogner, Pharm Res. 2010, 27, 2704-14

[4] B. C. Hancock, M. Parks, Pharm Res. 2000, 17, 397-404

[5] B. C. Hancock, G. T. Carlson, D. D. Ladipo, B. A. Langdon, M. P. Mullame, Int. J. Pharm., 2002, 241, 73-85

[6] P. Gupta, A. K. Bansal, AAPS PharmSciTech 2005; 6 (2) Article 32

[7] M. Yoshioka, B. C. Hancock, G. Zografi, J. Pharm. Sci. 1994, 83, 1700

[8] M. Avrami, J. Chem. Phys. 1939, 7, 1103

[9] M. Avrami, J. Chem. Phys. 1940, 8, 212

[10] I. Avramov, K. Avramova, C. Russel, J. Cryst. Growth 2005, 285, 394-399

[11] T. Ozawa, Polymer 1971, 12, 150

[12] H.E. Kissinger, J. Res. Natl. Bur. Stand. 1956, 57, 217221

[13] J. A. Augis, J. E. Bennett, J. Therm. Anal. 1978, 13, 283-292

[14] S. Bhattacharya, R. Suryanarayanan, J. Pharm. Sci. 2009, 98 (9) 2935– 53

[15] K. Kothari, V. Ragoonanan, R. Suryanarayanan, Mol. Pharmaceutics 2014, 11 (9) 3048– 55

[16] I. Saika-Voivod, R. K. Bowles, P. H. Poole, Phys. Rev. Lett. 2009, 103, 225701

[17] T. Kawasaki, T. Araki, H. Tanaka, Phys. Rev. Lett. 2007, 99, 215701

[18] L. Berthier, G. Biroli, J.-P. Bouchaud, L. Cipelletti, D. El Masri, D. L'Hote, F. Ladieu, M. Pierno, Science 2005, 310, 1797

[19] C. Dalle-Ferrier, C. Thibierge, C. Alba-Simionesco, L. Berthier, G. Biroli, J.-P. Bouchaud, F. Ladieu, D. L'Hote, G. Tarjus, Phys. Rev. E 2007, 76, 041510

[20] K. L. Ngai, K. Y. Tsang, Phys. Rev. E 1999, 60, 4511

[21] K. L. Ngai, M. Paluch. J. Phys. Chem. B 2003, 107, 6865

[22] W. Kamysz, Laborant 7/2014

[23] G. Adam, J. H. Gibbs, J. Chem.Phys. 1965, 43, 139-146

[24] S. L. Shamblin, X. Tang, L. Chang, B. C. Hancock, M. J. Pikal, J. Phys. Chem. B 1999, 103, 4113-4121

[25] I. M. Hodge, J. Non-Cryst. Solids 1996, 202, 164-172

[26] B. C. Hancock, S. L. Shamblin, G. Zografi, Pharm. Res. 1995, 12 (6) 799– 806

[27] S. Vyazovkin, I. Dranca, J. Phys. Chem. B 2005, 109 (39) 18637– 44

[28] V. Caron, C. Bhugra, M. J. Pikal, J Pharm Sci. 2010 Sep; 99 (9), 3887-900

[29] C. L. Jackson, G. B. McKenna, Chem. Mater.,1996, 8, 128–2137

[30] W. Thomson, Philos. Mag. 1871, 42, 448-52

[31] J. W. Gibbs, Collected Works; Yale University Press: New York, 1928